Computational Modelling and Simulation of Heat Transfer during Steel Billet Reheating and Transport with Growth of Oxide Scale

THESIS

Submitted in partial fulfillment of the requirements for the degree of

DOCTOR OF PHILOSOPHY

by

SATISH KUMAR DUBEY

Under the Supervision of

Prof. P. SRINIVASAN

BITS Pilani
Pilani | Dubai | Goa | Hyderabad

BIRLA INSTITUTE OF TECHNOLOGY & SCIENCE

PILANI – 333 031 (RAJASTHAN) INDIA

2014

Computational Modelling and Simulation of Heat Transfer during Steel Billet Reheating and Transport with Growth of Oxide Scale

THESIS

Submitted in partial fulfillment of the requirements for the degree of

DOCTOR OF PHILOSOPHY

by

SATISH KUMAR DUBEY
(2009PHXF030P)

Under the Supervision of

Prof. P. SRINIVASAN

BITS Pilani
Pilani | Dubai | Goa | Hyderabad

BIRLA INSTITUTE OF TECHNOLOGY & SCIENCE
PILANI – 333 031 (RAJASTHAN) INDIA

2014

BIRLA INSTITUTE OF TECHNOLOGY & SCIENCE
PILANI – 333 031 (RAJASTHAN) INDIA

CERTIFICATE

This is to certify that the thesis entitled **"Computational Modelling and Simulation of Heat Transfer during Steel Billet Reheating and Transport with Growth of Oxide Scale"** submitted by SATISH KUMAR DUBEY, ID.No. 2009PHXF030P for award of Ph.D. Degree of the institute embodies original work done by him under my supervision.

Signature in full of the Supervisor _____

Name : **Dr. P. SRINIVASAN**

Designation : **Associate Professor, Department of Mechanical Engineering**
BITS-Pilani, Pilani Campus

Date _____

Dedicated to my beloved Parents

Acknowledgements

I wish to thank and express my heartiest gratitude to God, the almighty for his all kindness and blessings.

I wish to express gratitude and sincere thanks to my supervisor Prof. P. Srinivasan for his able guidance, active support, encouragement and suggestions during this thesis work. He has been an extremely patient and caring thesis supervisor. It has been a privilege for me to work under his guidance.

I thank our Vice Chancellor, Directors, Deputy Directors and Deans for giving me the opportunity to work as a faculty member in the Department of Mechanical Engineering of BITS-Pilani, Pilani Campus and allowing me to pursue my doctoral thesis by providing necessary facilities and financial support. I am also grateful to Prof. S.K. Verma, Dean, Academic Research Division (Ph.D. Programme), BITS-Pilani, and Prof. Hemant R. Jadhav, Associate Dean, Academic Research Division (Ph.D. Programme), for their constant official support and encouragement.

I would like to thank Prof. Sai Jagan Mohan (Head of Department) and to all past and present faculty and staff of the Department of Mechanical Engineering, BITS-Pilani, Pilani Campus for their all help and support.

I am happy to acknowledge thanks to the Departmental Research Committee (DRC) members for their all supports.

I wish to record my sincere thanks to the Doctoral Advisory Committee (DAC) members: Prof. M.S. Dasgupta and Prof. B.K. Rout, who spared their precious time to provide valuable suggestions that helped in improving the quality of my Ph.D. thesis. They have also provided motivation through their affectionate enquiries about the status of my thesis work.

I wish to thank Prof. N. N. Sharma, Prof. K. S. Sangwan, and Prof. Srikant Routroy for their all supports.

My other colleagues at BITS Pilani and outside have also provided constant inspiration. In particular, I wish to thank, Prof. T.V.V.L. Rao, Dr. Manoj Soni, Dr. Sharad Shrivastva, Dr. A.K. Digalwar, Dr. Amit Singh, Dr. K. Vinayak, Dr. Arun Jalan

and Dr. Murali Palla. I also thank to Mr. Sachin U. Belgamwar, Dr. J.S. Rathore, Dr. Navneet Khanna, Mr. Anil Jindal and Mr. Grish Kant for all those open talks.

I am indebted to Dr. Maheshwar Dwivedy for his timely advice and great companionship. Special thanks to Mr. Arshad Javed and Dr. Dileep Kumar Gupta for always being with me. I will always cherish enjoyable moments, discussions and the great time we had together.

I express my thanks to Mr. Santosh Kumar Saini (ARC Division) for word-processing of the thesis.

I woe the greatest gratitude to my parents for all their incredible efforts and unconditional support for making all my dreams come true. I express my sincere thanks to my brother Mr. Ravindra Nath Dubey, Mr. Anil Dubey and sister Mrs. Asha Pandey for their loving support and motivation. I also wish to thank my friend and brother in law Mr. Mannu Tiwari, who always inspired me through his special interest in my work. Last but not least, my special loving thanks to my wife Ranjana and daughters Ayushi and Shubhi who have been very understanding and stood behind me with smiling faces.

SATISH KUMAR DUBEY

Abstract

The steel industry is one of the most energy intensive sectors and is therefore very vital for both national and international interests. The reheat furnaces are used in the steel industries for heating of steel billets before rolling processes. During reheating at high temperature, steel billet surfaces react with furnace gases, which are termed as oxidation reaction. The formation and growth of oxide scale affect the heat transfer characteristics to a great extent. Billets after heating in the reheat furnace are transported to the rolling mills, during this period temperature field in the billet changes considerably from reheat furnace discharge conditions.

Knowledge of transient temperature field in the billets is important for numerous reasons like energy efficiency, process optimization, roll force calculation, carbon segregation control, microstructure control, etc. However, it is almost difficult to obtain correct and complete transient temperature field in the billet through measuring instrument. Developing an analytical solution to the problem is also very difficult due to the complexities associated with the changing boundary conditions and large number of parameters affecting the process. In the recent past, more focus has been on improved furnace control and better temperature field predictions which are relying on numerical modelling. A suitable numerical model may offer a valuable tool for predictions of the temperature field with the growth of oxide scale.

Literature review suggests a need for numerical modelling and simulation considering the growth of oxide scale for predictions of 3D temperature field in the billet. Hence, this thesis work aims to address the need through development, validation and simulation of heat transfer numerical model for steel billet reheat and transport. The objective is not only to develop a numerical model for predictions of 3D temperature field in the billet with of growth of oxide scale, but also to keep model computationally efficient with reasonable accuracy, so that it can be used for online 3D temperature field monitoring and controls. In broader context, this thesis presents 3D transient heat conduction numerical modelling with consideration of oxide scale growth, model computer implementation and model simulation results along with the study of thermal characteristics of heating and cooling of the steel billet.

In the proposed model, the solution domain is the single billet which is divided into number of control volumes and follows its movement when it is travelling through different zones of the reheat furnace. The temperature history of the billet is carried forward from one position to other position along the length of the furnace and heat flux to the steel billet surface is assigned according to the billet positions. Heat flux calculation accounts radiation heat transfer from furnace walls and furnaces gases to billet surface. The emissive and absorptive behavior of reheat furnace combustion gas mixture is approximated through Weighted Sum of Gray Gases Model (WGGM). Whereas the convection heat transfer is included as heat flux on the steel billet surfaces, using constant convection heat transfer coefficient.

The 3D transient heat conduction numerical model accounts for the growth of oxide scale and oxidation reaction heat. The oxide scale growth has been implemented through temperature dependent parabolic rate law. The model also accounts for radiation shielding of the billet bottom surface due to skid structure and contact conduction between billet bottom and skid. This study adopts a control volume approach with implicit scheme of Finite Difference Method (FDM) for development of discretization equations. Separate mesh for oxide scale and steel are considered during model development. The oxide scale layer is modeled as one separate control volume in thickness with node at the outer surface. The heat exchange between the oxide control volume and steel control volume is through the conduction. The thermal conductivity and specific heat of steel and oxide scale are calculated using temperature dependent expressions.

In this work, a MATLAB® computer code is developed for computer implementation and solution of proposed 3D numerical model. The framework adopted for the computer implementation is flexible enough, so that the scope of modification is easy. Temperature field calculations require solving of the system of matrices as obtained from discretization equations. This system of matrices is solved iteratively. The developed MATLAB® program implemented Gauss-Seidel (GS) algorithm and returns temperature and oxide scale thickness matrices for different time of heating. The model is validated with analytical and published experimental results.

Simulations are carried out for predictions of 3D temperature field in the billet and oxide scale growth on the billet surfaces. The results obtained through the model simulations have displayed expected behavior. It was found that the effect of oxide scale on billet heating is considerable.

In order to investigate the effect of zone temperatures on the responses of interests, a parametric sensitivity subject to different responses of interest is carried out using Design of Experiment (DOE) approach. The model simulation results corresponding to the DOE combination set are analyzed by statistical techniques. It is observed from the analysis that all selected responses of interest have strong interaction.

The generalized discretization procedure used for modelling and simulation of billet reheating successfully extended to billet cooling during transport. The model is capable of capturing actual non-uniform initial temperatures and oxide scale conditions and accounts for descaling process in heat transfer simulation during transport. It is found that the temperature field in the billet during transport is considerably influenced by oxide scale and initial temperature field.

The presented model is capable of predicting 3D temperature field in the billet and oxide scale growth, which can be implemented for online monitoring of 3D temperature field. The work presented and discussed in the thesis is beneficial and having relevance to the steel industry.

Keywords: *Thermal, Heat transfer, Transient, Conduction, Computational modelling, Numerical modelling, Simulation, Discretization method, Implicit scheme, Control volume, Finite difference method, Steel, Billet, Oxide scale, Reheating, Billet Transport.*

CONTENTS		Page No.

CONTENTS	Page No.

List of Tables

List of Figures

1D	One Dimensional
2D	Two Dimensional
3D	Three Dimensional
ANOM	Analysis of Mean
ANOVA	Analysis of Variance
CFD	Computational Fluid Dynamics
DEAS	Dynamic Encoding Algorithm for Searches
DTRM	Discrete Transfer Radiation Model
DOE	Design of Experiment
DOM	Discrete Ordinates Method
FDM	Finite Difference Method
FEM	Finite Element Method
FVM	Finite Volume Method
MACZM	Multiple Absorption Coefficient Zonal Method
PPDF	Prescribed Probability Density Function
SIMPLE	Semi Implicit Method for Pressure Linked Equations
WSGGM	Weighted Sum Gray Gases Model

Dimensionless Number

Bi	Biot Number
Fo	Fourier Number
Pr	Prandtl Number
Re	Reynolds Number

Symbols

A	Arrhenius constant
$\mathbf{A}$	Coefficient matrix in system of matrices
a	Skid contact width
a_n	Coefficient in series solution
$\mathbf{b}$	Column vector in system of matrices
c	Specific heat capacity (J/kgK)
c_{os}	Specific heat capacity of oxide scale (J/kgK)
c_{st}	Specific heat capacity of steel (J/kgK)
d	Skid button height (m)
d_n	Eigenvalues
F	Shielding factor
H	Heat of oxidation reaction (J/kg)
h	Heat transfer coefficient (W/m^2K)
h_c	Convection heat transfer coefficient (W/m^2K)
h_{ct}	Contact coefficient between skid and billet (W/m^2K)
h_{rg}	Radiation heat transfer coefficient for billet and furnace gas (W/m^2K)
h_{rw}	Radiation heat transfer coefficient for billet and furnace wall (W/m^2K)
h_w	Convective heat transfer coefficient in skid pipe (W/m^2K)
h_q	Quench heat transfer coefficient (W/m^2K)
I	Number of gray gas components
J	Number of temperature polynomial coefficients
K	Number of irradiation polynomial coefficients
k	Thermal conductivity (W/mK)
k_{os}	Thermal conductivity of oxide scale (W/mK)
k_{sk}	Thermal conductivity of skid button (W/mK)
k_{st}	Thermal conductivity of steel (W/mK)

L	Pressure path length (Furnace gas layer thickness)
m	Mass (kg)
p_a	Partial pressure of gas mixture component
p	Total pressure inside the furnace
Q	Activation energy (J/mol)
$\dot{q}$	Heat generated (W/m^3)
q	Heat flux (W/m^2)
q_t	Total heat flux (W/m^2)
$q_{bottom,1}$	Total flux for bottom billet surface, which is in contact with skid
$q_{bottom,2}$	Total flux for bottom billet surface, which is not in contact with skid
R	Gas constant (J/molK)
R_{bt}	Overall thermal resistance for skid contact
R_1, R_2, R_3	Skid pipe insulations radius (m)
r	Distance of skid from center of billet
s	Oxide scale thickness (m)
$\mathbf{T}$	Temperature column vector in system of matrices
T	Temperature (K)
T_g	Furnace gas temperature (K)
T_r	Conveyor rolls temperature (K)
T_s	Billet surface temperature
T_w	Furnace wall temperature (K)
T_{water}	Water temperature flowing through skid/ spray water
t	Time (s)
v_b	Billet velocity (m/s)
x, y, z	Axis of 3D Cartesian coordinate system
X, Y, Z	Steel billet dimension in x-, y-, z- direction
$\Delta x, \Delta y, \Delta z$	Steel billet control volume size in corresponding x-, y-, z-directions (m)
nx, ny, nz	Number of control volumes or nodes in corresponding x-, y-, z-directions

Greek Symbols

α	Absorptivity
α_{gs}	Gas absorptivity for radiation from the billet
α_{gm}	Mean gas absorptivity for radiation from billet and wall
α_{gw}	Gas absorptivity for radiation from the walls
a_{α}	Absorptivity weighting factors
a_{ε}	Emissivity weighting factors
b_{ε}	Emissivity polynomial coefficients
c_{α}	Absorptivity polynomial coefficients
ε_g	Emissivity of the furnace gas mixture
ε_s	Emissivity of the billet surface
ε_{g,CO_2}	Emissivity of the CO_2 gas component
ε_{g,H_2O}	Emissivity of the H_2O gas component
ε_{sw}	Direct exchange factor
ε_w	Emissivity of wall
$\Delta\varepsilon$	Correction factor for gas mixture emissivity
κ_i	Absorption coefficient $(\text{atm-m})^{-1}$
τ_{gm}	Mean gas transmissivity
λ	Parabolic oxidation rate (m^2/s)
σ	Stefan Boltzmann constant
ϕ_{sw}	View factor between billet surface and furnace wall
ρ	Density (kg/m^3)
ρ_{os}	Density of oxide scale (kg/m^3)
ρ_{st}	Density of steel (kg/m^3)
ρ_a	Density of surrounding air (kg/m^3)
μ_a	Dynamic coefficient of viscosity (Ns/m^2)
γ	Contact parameter (billet and skid) for a cell

Subscripts

av	Average
c	Convection
g	Gas of furnace
i, j, k	Node Index in corresponding *x*-, *y*-, *z*-directions for 3D grid data
L	Linear
max	Maximum
min	Minimum
n	Node index after mapping of 3D grid data into 1D array
os	Oxide scale
P	Parabolic
r	Radiation
s	Billet surface
sk	Skid
st	Steel
t	Total
w	Wall
∞	Ambient air

Superscripts

e, w	Control volume faces in *x*-direction
n, s	Control volume faces in *y*-direction
t, b	Control volume faces in *y*-direction
m	at time *t*
m+1	at time $t + \Delta t$
nx, ny, nz	Number of control volumes or nodes in corresponding *x*-, *y*-, *z*-directions

Chapter 1

Introduction

1.1 Introduction

Reheat furnaces are used in the steel industries for heating the steel billets before rolling process. Notwithstanding the considerable efforts to direct rolling of continuously cast slabs, reheating is still an essential process in the production of steel. For numerous reasons, such as the presence of defects from a continuous casting process, plant scheduling, etc. direct rolling is not a standard practice even in the most modern iron and steel plant. Direct rolling is likely to remain as an intangible goal. Thus reheating furnace will remain essential link between casting and rolling operations for at least several decades to come.

The reheat furnaces used in the modern steel industries are either of walking beam-type, in which steel billets are separated by a gap, moved from one location to the next location in the longitudinal direction of furnace by periodic movement of walking beams or of the pusher-type in which billets are placed close to one another without any gap, that are advanced by forcibly adding more billets at the entry side. The billets are advanced by the force, applied at the time of new entry of billets. The billets in the reheat furnaces rests over the water cooled skid pipes and other supporting structure. There are various burners located at different locations, where reheat furnaces burn hydrocarbon fuels, resulting in high temperature environment within the furnace.

In the reheat furnace, the heat transfer to billet surface is mainly through radiation from furnace gases, radiation from furnaces walls and convection from furnace gases. However, at high temperature conditions that exist in the furnaces, radiation remains the dominant mode, accounting for the majority of total heat transfer in the furnace. The heat reached to the billet surfaces are conducted to the billet materials.

During reheating at high temperatures, steel billet surfaces react with furnace gases to form oxide scale. Initially, when hot scale free steel is exposed to the furnace oxidizing environment, there diffusion of oxidizing species of bulk gas to gas scale

interface occurs, followed by diffusion of iron ions or vacancies through the growing oxide layer. Oxide scale, thus formed on the surfaces also starts growing with the time, resulting in an increase of thickness. The formation and growth of oxide scale affect the heat transfer characteristics to a great extent due to the poor thermal conductivity, poor emissivity and large specific heat of oxide scale in comparison to the steel billet. The oxidation reaction is exothermic in nature, which may also affect the heat transfer characteristics (Abuluwefa et al., 1997; Chen and Yuen, 2003; Marston et al., 2004; Jang et al., 2010).

Ideally the temperature of the billet is expected to be uniform throughout after reheating to facilitate better rolling process. However, it is widely observed that the temperature field in the reheated billet is not uniform and varies from the surface to the core. Hence it is the key prerequisite in reheat furnace that the temperature of billets should be close to a target temperature. The furnace operations need to be designed and performed in such a way that the temperature variation within the billet does not vary beyond permissible limits.

The operation of reheating furnace is very much linked to various downstream activities of a rolling mill. Heated billets from the reheat furnace are transported to the rolling mills. When the billets discharge from the furnace, after some time it passes through descaler and then further transported to the rolling mills. Heat loss from the billet during transport significantly influences the temperature field in the billet. The prediction of temperature field will be of immense help to downstream activities of rolling mills such as roll force calculations, product quality and micro structural control of product.

Knowledge of transient temperature field in the billets at various stages; such as during reheat, end of reheat, during transport and end of transport to rolling mills, are vital for numerous reasons like energy efficiency, process optimization, roll force calculation, carbon segregation control, microstructure control of the product, etc. However, it is almost a difficult proposition to obtain correct and complete transient temperature field in the billet through measuring instruments. Developing an analytical solution to the problem is very difficult due to the complexities associated with the changing boundary conditions and large number of parameters influencing the processes. A suitable numerical model may offer a valuable tool for the temperature field predictions

Steel industry reheating process and transport systems has received very little attention until the early 1970s, prior to which only a few works related to numerical modelling were reported. Need for billet temperature field, energy efficiency, reducing the energy intensity in steel manufacturing, sustainable development and quality has attracted a great deal of attention towards the numerical modelling of processes in steel industries. These models range from simple one dimensional (1D) models to the complex two dimensional (2D) models and a few three dimensional (3D) models. However, some of these models tend to oversimplify or not, consider skid effect, formation and growth of oxide scale, etc.

Significant works have not been reported so far to predict the 3D temperature fields in the billet with growing oxide scale during reheat. The temperature field of the billets changes significantly, when it is transported to the rolling mill. All the previous billet transport simulations assume billet at uniform initial temperature. However, uniform initial temperature assumption makes temperature predictions erroneous because in actual situations, the billets coming out from the furnace by and large have a certain temperature gradient within material. Hence, it is essential for the model to capture non-uniform initial conditions for transport cooling simulation. An attempt has been made in the present work to fill the gaps by developing 3D numerical models considering formation and growth of oxide scale on the billet surfaces. The developed models are simulated for prediction of 3D temperature field in the billet and growth of oxide scale during reheating and transport. The model is validated with analytical results and published experimental results (Jang et al., 2010). Additionally the effects of furnace zone temperature on the responses of interest during steel billet reheat are investigated through a statistical based parametric study.

1.2 Computational Modelling

Increasing competition amongst steel manufacturers to bring down energy consumption, improved product quality and environmental concern have led to critically reexamine, knowledge and control of each stage during the steel making process. Any effort to reduce energy cost of billet reheating, control of the process or reliable temperature field predictions, etc. demands sophisticated furnace parameter measurement and experimentation. Experimental investigations may give more reliable information about the reheating process. However, experimental investigations involving full scale reheating

furnace tests are exorbitantly expensive and very often impossible. In addition to these difficulties, it must be remembered that there are various limitations and many potential difficulties of measurement in the context of reheat furnace heating and billet transport process. Modelling is one of the important steps in the study of any physical system. The model gives an alternate representation of physical systems. Theoretical temperature predictions of temperature field and oxide scale growth during billet reheating and transport process necessitates mathematical model, rather than the actual physical model.

For either study a new furnace or to optimize the heating process in existing ones, the heat transfer in the furnace has to be modeled as closely as possible to a real situation. The key aspects to be considered during modelling of a reheating furnace are oxide scale formation, skid system, different boundary conditions along the furnace length, variation of thermo-physical properties of billet materials, etc. The mathematical model for the physical processes of interests consists of a set of differential equations with large number of variables and time dependent boundary conditions. Development of analytical solutions for such mathematical models remains a difficult task.

Radiation heat transfer during reheat of a steel billet depends on the surface temperature of billet which varies with time, participating gas such as CO_2 and H_2O in the furnace, furnace wall temperature and other thermo physical properties of billet and furnace wall. Presence of skids, growth of oxide scale and many other complexities, necessitates a very comprehensive and computationally effective numerical model.

In recent years, fortunately the developments of numerical methods and the availability of high speed digital computers have brought back into focus the appropriateness of numerical models to simulate reheat furnace operations

The thesis work is based on developing numerical model for predicting 3D transient temperature field in the billet considering oxide scale. The steady state radiation heat transfer in the furnace was modeled, where the emissive and absorptive behavior of combustion gas is approximated by Weighted Sum Gray Gases Model (WSGGM) (Hottel and Sarofim, 1967; Smith et al., 1982). The transient heat conduction in the billet with oxide scale is modeled by the control volume approach of the Finite Difference Method (FDM) (Patankar, 1980; Ozisik, 1993). Implicit scheme is chosen for discretization. The radiation and transient heat conduction calculations were coupled via boundary conditions. This approach finds favor in computation to solve conduction heat

transfer with growth oxide scale during steel billet reheating in the reheating furnace and cooling during its transport from reheating furnace to the rolling mill. It can also be applied to a variety of geometry and boundary conditions.

1.3 Motivation

The outlined below have stimulated and inspired present study:

- Energy and steel have an overwhelming impact on human life, economy and environment; it should be dealt with effective and proper technology. India has approximately 11% of the Fe reserve of the world (Sinha et al., 2006). There are a large number of government-owned and private integrated steel plants in India, producing hot rolled coils, plates, sheets and wire rods with capacity of million tons per year. India could become pioneers of iron and steel sector provided it uses appropriate technology.
- In the international arena, recently there have been considerable interests in the development of a heat transfer model for heat transfer simulation during reheating of billets.
- 3D model with growth of oxide scale for steel billet reheating, and combined reheat and transport along with validation study have not been adequately reported so far.
- It is certain that 3D heat transfer model with growth of oxide scale for reheat and transport are desirable for a variety of reasons like energy efficiency, process optimization, roll force calculations, carbon segregation control, product microstructure control, etc.
- The proposed 3D model will be of immense help to the steel industry, especially for downstream activities like the development of reheating process control system and control strategy.
- The industrial motivation of using a 3D model is to obtain more precise temperature field in regions of interest like the corners, edges and the effect of skids. Additionally, 3D temperature field predictions are more useful in comparison to 2D predictions for metallurgical study and roll force calculations. For instance, 3D temperature difference within the billet affects the dynamic recrystallization and the dynamic recovery mechanism during the rolling of billet resulting in microstructure changes.

1.4 Objective of the Research

The research work in this doctoral thesis is aimed to develop a numerical heat transfer model to simulate steel billet reheating process in the reheat furnaces and cooling during transport from reheat furnace to rolling mills. The following objectives have been laid down for this research work:

- To develop a numerical model for predictions of the 3D temperature field in the steel billet with growth of oxide scale on the billet surface during reheating in the reheat furnace.
- To investigate the effect of different furnace zone temperature combinations on responses of interests during steel billet reheat, such as maximum temperature, minimum temperature, average temperature, maximum temperature difference, maximum oxide scale thickness and minimum oxide scale thickness.
- To develop a numerical model for prediction of the 3D temperature field in the billet with oxide scale during billet transport from reheat furnace to the rolling mills.
- To integrate the proposed reheat model and transport model, so that the numerical model can simulate heat transfer during transport with consideration 3D non-uniform initial temperature field of billet and oxide scale as obtained from the reheat model
- To study steel billet heating and cooling characteristics during reheating and transport respectively.

1.5 Scope of the Research

Steel billet reheating and transport simulation for the predictions of 3D temperature and investigation of heat transfer characteristics is vital for steel industry and it is difficult to find analytical solutions. So far the numerical heat transfer model with the growth of oxide scale for the prediction of 3D temperature field in the billet during reheating has not been developed and computer implemented. This research work deals with the necessary numerical modelling and heat transfer simulation. In addition to this, parametric studies have been carried out to investigate the effect of zone temperature on response of interests of reheating process.

1.6 Work Environment

In this thesis, all the numerical implementations of the proposed model and simulation studies are carried out using code developed in MATLAB®. The developed code contains generic MATLAB® functions which accommodates various practical aspects of the simulations. The developed generic code allows the user to conduct model simulations by defining the problem, billet dimensions, skid parameters, specific grid, material properties and boundary conditions.

1.7 Layout of Thesis

The work reported in this thesis has been divided into seven chapters. The content of each chapters are as described below:

Chapter 1 presents an introduction to the thesis. It introduces the need for computational modelling and various aspects considered during model development and simulations. Broad overview, general aspects of numerical model development and role of computational modelling are discussed. The objectives and scope of the present study along with the layout of the thesis are outlined.

Chapter 2 gives a brief introduction to the reheat furnaces, heat transfer in the reheat furnace, oxidation during reheat and phase change behavior during reheat. Literature review of various numerical models developed for billet reheat and transport simulations are presented. The reviewed literature has been analyzed to identify the gap in the research.

Chapter 3 is devoted to the numerical model development with the growth of oxide scale for heat transfer simulation during steel billet reheating. The detailed descriptions of boundary condition, formulations of discretization equations are presented.

Chapter 4 deals with computer implementation of numerical model and validation studies. The results of model simulations obtained during validation studies are presented.

Chapter 5 presents a reheat model simulation followed by an investigation on zone temperature sensitivity. The results of model simulation for the predictions of 3D temperature field in the billet and oxide scale thickness during reheating are summarized in this chapter.

Chapter 6 deals with the numerical model development and heat transfer simulation during billet transport from reheat furnace to the rolling mill. This chapter presents the billet transport simulation results.

Chapter 7 gives the overall conclusions of the thesis work along with future scope of work.

1.8 Closure

The quest of reduce energy consumption, sustainable development, product quality apprehension in the steel industry, demands suitable and cost effective means for billet temperature predictions. In this context, chapter introduces the motivation and need for computational modelling and simulation with growth of oxide scale for prediction of 3D temperature field of the steel billet during billet reheating and transport.. The literature on system descriptions, oxide scale growth and state of art of mathematical and numerical modelling are presented in the next chapter.

Chapter 2

Literature Review

2.1 Introduction

This chapter is organized into nine sections. The first part of chapter constitutes the preparatory phase. The first five sections describe steel reheat furnace, heat transfer in the reheat furnace, oxidation during reheat and phase change behavior. This is followed by a literature review. The literature review is presented in the sixth and seventh sections. The sixth section deals with literature review on the reheat modelling and simulation, gives an overall representation of the numerical models that have been developed for heat transfer simulations. The seventh section presents literature review on heat transfer modelling and simulations during billet transport, which is followed by discussions on the gaps in the research. The chapter ends with some closure remarks.

2.2 Reheat Furnace

Reheating is a process in which steel in the form of slabs or billets is placed into the furnace and heated before rolling. In the reheat furnaces, it is ensured that the steel billets are heated to an adequate and uniform temperature, so the rolling mills can deform billet into desired form with optimal roll force. The temperature field in the billet at the exit of the reheat furnace should ideally be uniform, but it is difficult to achieve uniform temperature of the billet in practical situations.

The reheat furnaces are classified according to the method of heating: electric type and combustion type. The combustion type reheat furnaces are fired by a range of hydrocarbon fuels, including natural gas, blast furnace gas and coke oven gas. The burners are installed in the roof and walls of the furnaces which inject fuel and air mixture for combustion. The reheat furnaces are also classified according to the method of charging: batch type and continuous type. The batch type of furnaces is the oldest type of furnaces which are used for heating of all grades and sizes of steel. In the batch type, large number of billets are simultaneously charged and taken out from the furnace. Continuous furnaces are further classified according to the movement of steel

billet inside the furnace as: roller hearth furnace, rotary hearth furnace, walking hearth furnace, pusher-type furnace and walking beam furnace (Krivandin and Markov, 1980).

Roller-hearth furnaces are continuous furnace with mechanized bottom, over which metal is transported. This type of furnaces can be successfully combined with production flow lines, in view of the fact that rollers hearth is an extension of the shop's roller table. The application of roller-hearth furnaces for high temperature heating of metal before rolling is limited due to low durability of rollers, particularly in wide furnaces, where they tend to bend in the absence of support and high loss of heat with cooling water.

Rotary-hearth furnaces are suitable for heating of shaped billets, for instance wheel rolling mills, as well as of round tube billets. Billets are placed on a rotary hearth, which carrying it through various heating zones of the furnace and discharged through the discharge door provided near the charging door. The charging and discharging of the billets is done simultaneously by two cranes. In the rotary-hearth furnace, burners are arranged evenly around circumference of a furnace. For zone less heating mode, all the burners can be of the same heating power. For zonal heating mode, which is commonly employed for steels, the power of the burner should be different in the various zones of the furnace in order to ensure the specified heating schedule. The rotary-hearth furnace can be easily switched over from zone to zone less heating mode and vice versa. The disadvantages of this furnace are high capital cost per unit of production, low hearth efficiency, less flexibility and limitation on length of pieces to be heated.

In walking hearth furnace, the steel stock rests on the fixed refractory hearth which is a combination of moving and stationary sections. The walking mechanism made up of a wheel and ramp or a bell crank mechanism depending on the mill requirement. The movement of the material toward the discharge end of the furnace is obtained from a series of working cycles: lift, traverse, lower, and return.

All contemporary reheating furnaces are either of pusher-type or walking beam-type. This classification of reheat furnaces is based on the methods by which slabs or billets, advance throughout the length of the furnace.

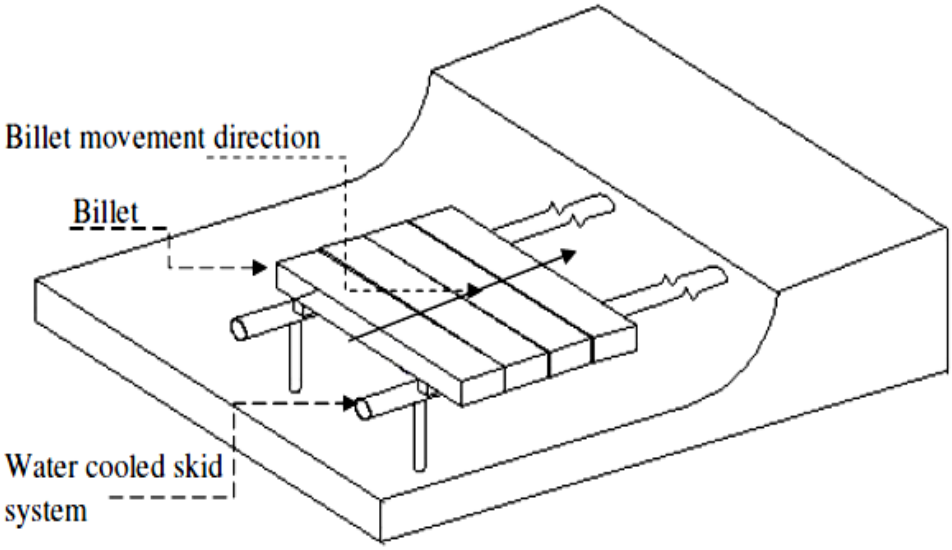

Fig. 2.1: Billets orientation within pusher-type reheat furnace

Pusher type furnaces are widely used for heating of rectangular slabs and billets. The billets are placed close to one another without any gap such as shown in Fig. 2.1. The billets are advanced by forcibly adding more billets at the entry side. The billets are advanced by the force applied at the time of new entry of billets. The magnitude of this force is just sufficient to avoid piling up of billets inside the furnace. Therefore, pusher type furnaces have a limited length and limited maximum throughput. Pushing the billets, cause rubbing of billets against each other and also significant frictional forces are transferred to the billet support structure. The billet can be discharged from the furnace through an end door or through a side door. The advantage of this furnace is the simplest and least expensive method of transferring billet through a furnace. The billet heating occurs only from four surfaces, as billets are placed close to one another without any gap. The billets slide over the fixed skid pipe (water cooled) lay along the furnace bottom. In order to retain low temperature strength against this frictional force, support structures are water cooled. Simplest and cost effective design and method of moving billets though a furnace are the major advantages of pusher-type furnaces. However, these advantages are offset by poor thermal efficiency and other disadvantages as mentioned earlier.

Walking beam furnaces avoids the inherent disadvantages of the pusher-type furnaces. The billets are advanced by motion of walking beam. The walking beams are periodically raised to lift billets and move it to the next position in the furnace.

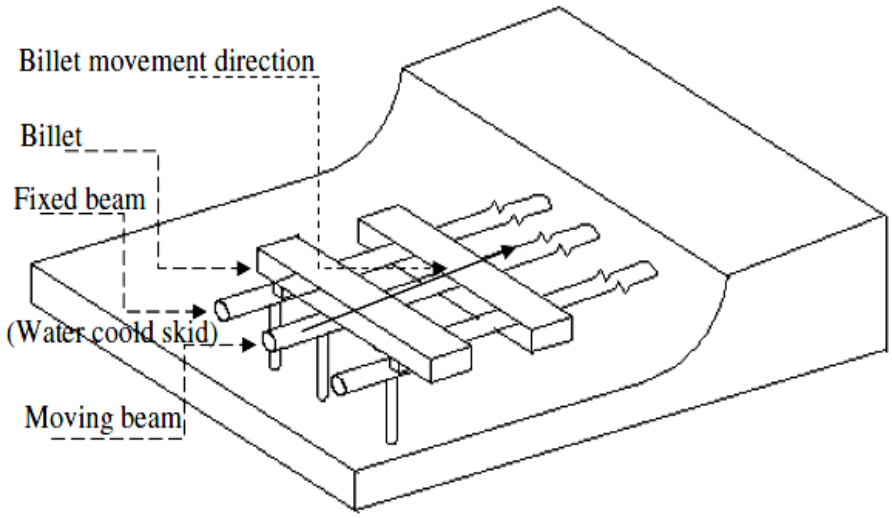

Fig. 2.2: Billets orientation within walking beam-type reheat furnace

The advantages of the walking beam furnace can be categorized into two groups: operational advantages; those due to higher intensity of metal heating. The operational advantages are as follows: easy scale removal from the furnace, easy billet removal through the furnace at the time of repair or standstill of the rolling mill, easy billet transfer rate control and lower surface damage. Additionally, in the walking beam-type of furnace a gap is present between the billets, such as shown in Fig. 2.2, ensuing all the six faces of the billet getting exposed to heat transfer as a result, intensity of heating can be increased appreciably. The billets rests on stationary and water cooled walking beams. Higher efficiency and other advantages of walking beam furnaces in comparison to pusher-type reheat furnaces are partially counterbalance by higher initial and maintenance cost of walking beam-type furnaces. Detailed descriptions on reheat furnaces construction and working can be referred from literatures (Krivandin and Markov, 1980; Brittain and Dales, 1988).

2.3 Thermal and Temperature Conditions

Reheat furnaces are used for heating of billets prior to plastic working in rolling mills. Billets must be heated to the required temperature with small permissible temperature gradient before discharging it from the furnace. Heated billet discharged from the furnace is transported to the rolling where its temperature changes considerably. A brief discussion on the thermal and temperature conditions during reheat and transport are given below.

2.3.1 Thermal and temperature conditions during reheat

The temperature in the reheat furnace can be either constant along the furnace length or vary considerably. The reheat furnaces in which the furnace temperature is almost constant along the furnace length are called a zoneless mode furnace. The furnaces with variable temperature along the furnace length are called a zonal mode furnace. The modes of heat transfer to the billets are through convection and radiation. The heat transfer in the furnaces occurs at high temperature; therefore the dominating mode of heat transfer is radiation, accounting for as much as 90 % of the total heat transfer. The heat transfer within the billet is through conduction mode. During reheating it is essential to maintain a specified billet average temperature, temperature distribution and acceptable temperature difference in the billet for correct performance of the downstream rolling activities and product quality. The thermal stresses developed in the billets are directly proportional to the temperature gradient in the metal.

In order to ensure requirements as discussed above, the temperature can vary substantially along the length of continuous furnace. Temperature variations along the length of the furnace, decide the number and purpose of the furnace zones. Continuous furnace may be of two-, three-, or multi-zone type and with one or two sided billet heating. Consider the purpose of furnaces zones, taking a three zone furnace as an example. The preheating zone is the first in the path of billet movement. In that zone, metal is gradually heated before entering the high temperature zone. Billet should be heated gradually in order to avoid excessive thermal stresses. The high temperature heating zone is the second zone in the path of billet. Here the surface of the billets is heated quickly to the final temperature. The soaking zone is the third one in the path of billet and serves to equalize the temperature over the cross- section of the billets. Sometimes while heating thin billet, the temperature gradient in the billet material after the heating zone is not significant, therefore soaking zone may not be required. In such cases the furnace has no soaking zone, only consisting of preheating and heating zone and is called a two-zone furnace. In the other cases, when heating thick section with requirement of smaller temperature before rolling mills, four- or five-zone furnaces are employed in order to increase the total temperature level and productivity.

In the reheat furnace formation and growth of oxides are usual, which is not only crucial from the heat, transfer point of view, but also involves huge intricacy in the billet reheating processes. Hence, it becomes essential to select temperature conditions, design and operation of the furnace so as to minimize the effect and losses of oxide scale formation and growth (Krivandin and Markov, 1980).

2.3.2 Thermal and temperature conditions during transport

During the transport, billets are placed on the conveyors and exposed to the surrounding air. The heat transferred from billet to conveyor is through thermal contact. The billet loses the majority of heat to the surrounding air by radiation. As billets are fast moving through the surrounding, some heat is lost by convection. The scale developed during reheating is largely removed through hydraulic descaling. When the billet gets discharged from the furnace, after the elapse of sometime it passes through a descaler. The billet surface temperature would be expected to be colder than the interior because of quenching caused by the descaler high pressure water jet.

2.4 Oxidation

The reheat furnaces combust hydrocarbon fuels, resulting in the product of combustion that includes CO_2, O_2, H_2O, etc. In the process of reheating, the steel billet is exposed to high temperature oxidizing gas environment. In the furnace the billet material (steel) undergoes chemical reaction with the surrounding oxidizing gases to form an oxide scale layer on the billet surfaces. The oxidation process may be affected by many factors, the most significant among them being billet surface temperature, residence time (time of heating), the hostility of oxidizing environment and steel composition, etc. The formation and growth of the oxide layer in the steel rolling industry give certain advantages. The advantages of oxide layer are: it reduces surface defect; oxidation is exothermic process which imparts heat to the billet; it reduces the heat loss from billet to the environment when the billets are transported to the rolling mill. The formation and growth of oxide scale also adversely affect the heat transfer characteristics to a great extent due to the poor thermal conductivity, less emissivity and large specific heat of oxide scale in comparison to steel billet. Additionally, oxide scale formation results in material loss. Hence, study and control of oxide scale formation and growth during reheating will be of immense help to the steel industry. Further details of oxidation of

metals can be referred from literature (Kofstad, 1966; Birks and Meier, 1983; Chen and Yuen, 2003; Lee et al., 2004).

Before proceeding further, an outline on oxidation mechanism and mathematical models for the growth of oxide scale is presented, so that oxidation can be better appreciated in the context of the present study.

2.4.1 Oxidation mechanism

The oxidation process is fundamentally a reverse of diffusion process in which oxygen diffuses from outside to deeper layers of steel and iron diffuses from the inside to the outer layer of scale. For the temperature range of steel reheating process, the oxide scale contains three distinct layers. It consists of an outer layer of haematite (Fe_2O_3), an intermediate layer of magnetite (Fe_3O_4) and an innermost layer of wustite (FeO). These iron oxides are formed at high temperature through following reactions (Abuluwefa, 1992, 1996):

$$3Fe + 2O_2 = Fe_3O_4 \tag{2.1}$$

$$2Fe + O_2 = 2FeO \tag{2.2}$$

$$6FeO + O_2 = 2Fe_3O_4 \tag{2.3}$$

$$4Fe_3O_4 + O_2 = 6Fe_2O_3 \tag{2.4}$$

Birks and Meier (1983) have proposed a simple mechanism of oxidation of iron, which is based on knowledge of diffusion properties of oxides.

The iron atoms at the of iron-wustite interface ionize in accordance with the following reaction

$$Fe = Fe^{2+} + 2e^{-} \tag{2.5}$$

The iron ions (cation) and electrons are transported through the wustite layer and reaching wustite-magnetite interface, which is mainly due to presence of cation vacancies and electron holes in wustite. Here, magnetite reduces to wustite according to the reaction

$$Fe^{2+} + 2e^{-} + Fe_3O_4 = 4FeO \tag{2.6}$$

The iron ions and electrons excess magnetite to wustite reaction are migrated through magnetite layer and reaching to magnetite- haematite interface which is again mainly due

to presence of cation vacancies and electron holes. The following reaction at the interface will lead to the formation of magnetite by reduction of haematite.

$$Fe^{n+} + n\,e^{-} + 4\,Fe_2O_3 = 3\,Fe_3O_4 \tag{2.7}$$

where the value of *n* is equal to 2 or 3 for Fe^{2+} or Fe^{3+} ions respectively.

The mobile iron ions and electrons are moved to the haematite-gas interface forming new haematite according to the reaction

$$2Fe^{3+} + 6e^{-} + \frac{1}{2}O_2 = Fe_2O_3 \tag{2.8}$$

The oxygen ionizes at the haematite-gas interface according to reaction

$$\frac{1}{2}O_2 + 2e^{-} = O^{2-} \tag{2.9}$$

The ionized oxygen reacts with iron ions in the haematite layer forming new haematite at magnetite haematite interface according to the reaction

$$2\,Fe^{3+} + 3O^{2-} = Fe_2O_3 \tag{2.10}$$

At elevated temperatures wustite layer thickness is considerably higher than the haematite and magnetite layers, which is primarily due to the higher mobility of the defects in the wustite layer in comparison to other two oxides. The percentage thicknesses of the three oxide layers wustite, magnetite and haematite are approximately 95, 4 and1 respectively (Briks and Meier, 1983).

2.4.2 Mathematical models of scale growth

A simple mathematical model of oxidation rate can calculate approximately the overall quantity of scale formed, and such mathematical model can assist steel industry numerical modelling for the prediction of the oxide scale growth and temperature field in the presence of oxide scale.

The oxidation rate equations: Kofstad (1966) and Marston, et al. (2004) discussed standard oxidation equations which suggest that the oxidation behavior of steel during reheat mainly depends on reaction rates, kinetics and temperature. Oxidation rate equations are based on the assumptions that the rate of reaction is controlled by diffusion process. The diffusion of species through the barrier process is governed by the concentration difference and the rate proportional to the concentration gradient. Here the

concentration gradient means: concentration difference divided by the thickness of the barrier. Two cases of scale growth model (Marston, et al., 2004) are possible: linear oxidation and parabolic oxidation which are explained below:

The linear oxidation is observed when scale free steel is heated and exposed to an oxidizing atmosphere; the metal consumes all the oxidizing species surrounding it. Oxygen potential at the gas scale interface is almost same at the interface of oxide scale and metal in the case of thin scale layers. The rate of reaction is therefore controlled by transfer of oxidizing species from bulk gas to the gas scale interface. Under such gas flow conditions, the rate of reaction will be constant, giving the linear oxidation rate equation as given by

$$\frac{ds}{dt} = \lambda_L \tag{2.11}$$

where *s* is the measure of oxidation (thickness of oxide scale), λ_L is linear oxidation rate constant and *t* is time. The linear oxidation rate constant will depend on the gas flow condition, gas compositions and the temperature.

At elevated temperatures, as the layer of scale thickens, the rate of further oxidation becomes limited by solid state diffusion through the scale. The oxygen potential at the gas-scale interface becomes significantly higher than at the scale-metal interface. The concentration gradient decreases with growth of scale. Hence, oxidation rate is inversely proportional to the scale thickness, and can be stated as:

$$\frac{ds}{dt} = \frac{\lambda}{s} \tag{2.12}$$

which on integration gives a parabolic rate equation rate equation as :

$$s^2 = 2\lambda t \tag{2.13}$$

The integration constant can be incorporated into the rate constant giving a customary parabolic oxidation rate constant given by

$$s^2 = \lambda_P t \tag{2.14}$$

where λ_p denote the parabolic rate constant. The high temperature parabolic oxidation signifies that a thermal diffusion process is rate- determining. Such a process may include a uniform diffusion of one or both of the reactants through a growing compact scale as discussed in the previous section. The oxidation rate can be represented by a

single parabolic rate constant, even if the scale has several layers, for example haematite magnetite and wustite, provided that the diffusion path is not broken by decohession (Marston, et al., 2004).

Taking the linear and parabolic scale growth equations, control of scale growth in the gas phase (the initial linear stage) and by ionic diffusion through the scale layer can be regarded as serial resistances. Hence, mixed (linear -parabolic) oxidation rate equation (Marston, et al., 2004) can be expressed as:

$$\frac{ds}{dt} = \frac{s}{\lambda} + \frac{1}{\lambda_L} \tag{2.15}$$

which on integrating give the mixed (linear-parabolic) oxidation

$$\frac{s}{\lambda_L} + \frac{s^2}{\lambda_P} = t \tag{2.16}$$

Abuluwefa et al. (1997) studied about the oxidation mechanism of low carbon steel during reheating and concluded that the initial rate of oxidation in CO_2 - N_2 and H_2O-N_2 atmosphere were found to be linear and proportional to the partial pressure of CO_2 and H_2O. It was observed that once the oxide scale reaches a certain thickness, the process of oxidation gradually changes to a parabolic rate. However, for oxidation in the high oxygen atmosphere, the transition occurs at a very fast rate.

The effect of temperature: The oxidation rate constants of discussed above are varying with the temperature. Numerous oxidation reactions have shown empirically that the temperature dependence of oxidation rate constants obeys an Arrhenius equation (Abuluwefa et al., 1997) i.e.,

$$\lambda = \lambda_0 \exp\left(\frac{-Q}{RT}\right) \tag{2.17}$$

where Q is the activation energy, R is the gas constant and T is the absolute temperature. The pre exponential factor λ_0, is within experimental accuracy, usually found to be independent of temperature. Using Equation (2.17), the activation energy Q can be determined by plotting, $\log_{10} \lambda$ as a function of $1/T$, in which case the slope of curve is given by $Q / 2.303R$.

2.4.3 Oxidation heat release

The oxidation reaction is exothermic in nature. Therefore, oxide formation increases the heat flow rate as given by

$$q_o = -\Delta H \frac{dm}{dt} \tag{2.18}$$

where, H is the oxidation reaction heat release (specific latent heat of oxide scale formation) expressed in J/kg. The rate of change of mass is calculated from oxide scale growth rate law as given by

$$\frac{dm}{dt} = \rho_{os} (\text{surface area}) \frac{ds}{dt} \tag{2.19}$$

where ρ_{os} is density of oxide scale and surface area refers to area on which oxide scale is growing. Thus, for parabolic oxidation rate the mass rate change can be expressed as:

$$\frac{dm}{dt} = \rho_{os} (\text{surface area}) \frac{\lambda}{s} \tag{2.20}$$

2.5 Phase Change Behavior

During reheating of steel billet when temperature reaches the lower critical temperature, ferrite will change to austenite. Such transformation will continue till steel billet reaches the upper critical temperature. Such transformation can be incorporated in the model of reheating through consideration of additional energy source term. Alternatively, energy source due to such structural changes of steel during reheating can be accounted by temperature dependent thermal conductivities and specific heat of steel.

Billets after heating in the reheat furnace are transported to the rolling mills. During transport, billets are exposed to the surrounding air, as a result the temperature field in the billet changes considerably from reheat furnace discharge conditions. In this entire range of temperature the steel is in Austenitic phase. As per the iron carbon diagram (Callister and Balasubramaniam, 2014) within this range of temperature that prevails during billet transport, there is no possibility of transformation into liquid or Ferritic phase.

With this brief background information relevant to reheat and transport study, next two sections discusses and reviews the contemporary literature pertaining to the heat transfer modelling and simulations of steel billet heating in the reheat furnace and cooling during transport process.

2.6 Literature Review on Heat Transfer Modelling and Simulation during Reheat

Reheating process has not received much consideration before 1970s, but the need for energy efficiency, sustainable development and qualities have attracted a great deal of attention towards the numerical modelling of processes in steel industries in the recent few decades.

There are some models, reported in the literature (Fitzgerald and Sheridan, 1970; Price, 1980; Hollander, 1983) which considers billet surface temperature as input and conduction in the billet solved as 1D semi-infinite conduction. These semi empirical models have been used to predict the billet center line temperature. These models were also applied to online control of reheating furnaces. However, these models did not account for the furnace conditions.

Pike and Citron (1970) reported lumped parameter model of reheat furnace. The developed lumped parameter model was combined with ordinary differential equation describing the heat transfer process for individual slab that has permitted the formulation of control problem of the system as lumped parameter dynamic optimization problem.

Gerasimov et al. (1984) performed some experiments monitoring the dimension of billet and thermocouple readings and supplemented them to a statistic based mathematical model. They have concluded that statistical model developed by them gives good results for the assumptions of constant temperature and uniform entry rate of billets into the furnace.

The early work on heat transfer modelling has been performed by Fontana et al. (1984). In this work they have developed a marching mathematical model to calculate the temperature profile in the billet during reheating. They have divided furnace into a number of transverse slices. Using estimated gas temperature profile slice wise calculations for the thermal energy distribution to slab and refectories were done. The slab temperature history was carried forward for next transverse slice calculations. After

doing similar calculations for a last transverse slice, a global energy balance was performed. The iterations were performed for convergence, using an improved estimate of the gas temperature profile.

Roth et al. (1986) reported a 1D transient heat conduction model for billet temperature and growing oxide scale predictions. The other model reported by them is in 2D for skid marks predictions.

Leden (1985, 1986) and Madsen. (1994) have developed model and computer code for 2D temperature analysis of steel billet heating. Their model was based on FDM.

Li et al. (1988) developed a steady state model for the pusher reheat furnace. Radiation heat transfer in the furnace was calculated using zone method with an assumed gas temperature profile in the furnace. The 2D transient heat conduction calculations within the slab were performed using explicit FDM. The model has been used for the predictions of 2D temperature profiles in the billet during reheat. In order to identify the mechanism of skid mark formation, they have examined skid rail and slab contact through radiation shielding factor concept, which account for the presence of the skid system structure. They have also examined the thermal behavior for various steel thicknesses, steel grades and push rates.

Yang and Lu (1988) proposed a dynamic model based optimization control for reheat furnaces. In this work they dealt with the development of an advanced computer control strategy and its application to reheating furnaces. They presented a dynamic model based optimization strategy that gives the optimal set points of the furnace zone temperatures and a related computer control system. They used a dynamic model based heuristic search algorithm to find the optimal furnace zone temperatures for minimal energy consumption under various operating conditions.

Rubini and Pollard (1990) developed a mathematical model designed to predict the flow and heat transfer within steel reheat furnaces is presented. Their numerical model employs Finite Volume Method (FVM). They modeled incompressible behavior and turbulence. The model calculations were verified by comparing the results with experimental measurements for a restricted but relevant isothermal problem. The Computational Fluid Dynamics (CFD) model is then applied to a representative full size reheat furnace. The model does not predict steel billet temperature.

Chapman et al. (1990, 1991) investigated the effects of non gray combustion products in the pusher type reheat furnace. The gas temperature in each zone of reheat furnace was calculated by zonal energy balance. They have modeled 1D heat conduction in the refractory wall and 2D heat conduction in the billet. The convective heat transfer coefficient was calculated using empirical correlations. They performed parametric investigations to establish operating characteristics that lead to optimum efficiency. They concluded that calculated slab temperatures were not very sensitive to refractory wall emissivities for typical values greater than 0.5.

Chapman et al. (1994) presented a 2D modelling and parametric studies of heat transfer in a direct-fired furnace with impinging jets. In this work, they have reported a steady state mathematical model of a direct-fired continuous reheating furnace, which was developed to identify the design and operating parameters that significantly affect furnace performance. The actual furnace was approximated in. The model was based on a turbulence model and a Discrete Ordinates Method (DOM) of the radiation field. In addition, the results of parametric studies, for the fuel firing rate and the load and refractory emissivities were reported. The main limitation of their model is that they have considered fixed billet surface temperature, in other words the heat transfer from combustion gas was not coupled to the temperature of the billet during reheating simulation.

Venturino and Rubini (1995) developed a computational methodology to predict 2D transient heat transfer of the billet in a continuous steel reheating furnace. The fluid dynamics and radiation heat transfer in the furnace was modeled using commercial CFD package FLUENT®. Radiation heat transfer was modeled by implementation of Discrete Transfer Radiation Model (DTRM) in FLUENT®. The specifically written transient conduction solver module of the steel billet was coupled to the FLUENT® fluid phase model. The transient heat transfer to the slab during the reheating operation is considered a heat flux boundary condition obtained from the CFD flow field calculation.

Barr (1995) developed a more detailed steady state thermal model for pusher type reheat furnace. Their model gives 2D thermal history of billet as it moves through the different zones of the reheat furnace. This model performs radiative heat transfer calculations using the zone method. In order to obtain 2D temperature profile in the billet, the transient heat conduction equation was solved by implicit FDM, employing

simple rectangular grids. An iterative scheme similar to that of Fontana et al. (1985) was used for solution model. The model was used to examine two skid designs and several placement strategies on skid mark severity and energy loss to the skid system.

Zhang et al. (1997) reported a combustion model for reheat furnaces. The combustion model was based on the assumption of instantaneous full chemical equilibrium. Numerical simulations of reactive turbulent flows and heat transfer in regenerative slab reheat furnaces have been carried out. A moment closure method with the probability density function for the mixture fraction was used to model the turbulent non premixed combustion process in the furnaces. They implemented combustion and P1 radiation model through commercial code FLUENT®.

Lindholm and Leden (1999), reported the finite element method (FEM) for solution of 3D transient heat conduction equation and its application for steel billet heating in the reheat furnace. In this model a FEM, where time integration was performed by exponential transformation of the heat combined with alternate direction implicit scheme. The validity of this model was investigated by comparing the results of simulation with limited condition analytical and experimental data.

Wick (1987, 1990) proposed Kalman Filter (Kalman, 1960) based model for estimation of the billet center temperature of steel slab by using a measured surface temperature of the billet.

Ko et al. (2000) reported modelling and predictive control of a reheating furnace. In this work, a dynamic model and multivariable controller design procedure of the reheating furnace was proposed, which was based on material and energy balances. They have calculated average temperature history of individual billet as it moves through the furnace during reheating.

Kim and Huh (2000) reported a heat transfer analysis, which was performed by the commercial code FLUENT®, for slabs heated in a walking beam type of a reheating furnace. Steady state, 3D analysis was performed for turbulent reactive flow and radiative heat transfer in the furnace. 2D transient heat conduction calculations in the slab were performed with the boundary condition given in terms of the calculated local heat flux in the furnace. A parametric study was also performed to examine the skid mark severity and energy loss to the skid system.

Kim et al. (2000) presented a heat transfer analysis for the walking beam reheat furnace, which was performed for the turbulent reactive flow and radiative heat transfer by FLUENT®. A simplified burner is validated against the results of the actual burner. They predicted temperature distribution in the furnace, heat flux to the slabs, velocity vectors and two dimensional temperature fields in the slab.

Marino et al. (2002) developed a numerical model of steel slab reheating in the pusher type reheat furnace. The model uses the temperature of hot gases inside the furnace, measured by thermocouples. It takes into account the radiative exchange between the gases, furnace refractory and billet. They have not considered fluid dynamics and combustion processes inside the furnace. Zone method was used to calculate radiative exchange among gases, billet and refractory elements. The heat fluxes obtained through zone method are used as boundary conditions to solve 2D transient heat conduction. The model predicts 2D temperature distribution of the billet.

Jiang et al. (2004) modeled the flue gas recirculation of an industrial reheat furnace by linear transfer function. The model was based on CFD simulation results where the inputs to the model were flow rate and temperature of combustion air and pressure head of the flue gas recirculation fan. The outputs were nitric oxide (NO) and oxygen (O_2) concentration.

Harish and Dutta (2005) reported a computational model for heat transfer in pusher type reheat furnaces for heating steel billets. Radiation heat transfer in the furnace and two dimensional transient conduction within the billets were modeled using the FVM. This model was used to predict the radiative heat flux distribution within the furnace, as well as the resulting 2D temperature distribution within the billets as they pass through various zones in the furnace.

Jaklic et al. (2005) studied the effect of the space between the billets on the walking beam type reheat furnace productivity. To perform this study, they have developed a model using Monte Carlo method for calculation of view factor matrix for radiation heat transfer. 3D transient heat conduction calculation within steel billet was performed using FDM.

Chen et al. (2007) developed an integrated reheat furnace optimization model. The model consist of six sub models: FEM thermal stress model, slab temperature model, furnace temperature profile model, micro alloy dissolution model, heating speed

model and residence time optimization model. The slab temperature model used a FDM with explicit scheme for analyzing 2D transient heat conduction calculations within the slab. The furnace temperature profile was generated through thermocouple measurements and weighted interpolation method. The 2D temperature field was input to the FEM thermal stress model.

Han et al. (2007) presented a simulation of transient heating characteristics of a slab inside bench scale reheating furnace. The bench scale reheating furnace is a test facility installed in POSCO Corporation. This model adopted a Semi Implicit Method for Pressure Linked Equations (SIMPLE) algorithm that includes a standard $k-\varepsilon$ model for turbulence, the eddy-dissipation model for combustion, and FVM for radiation heat transfer.

Jang and Kim (2007) proposed steel billet heat transfer model based on 2D FEM for estimation steel billet temperature. The heat flux boundary conditions for the billet heat conduction model was calculated by Stefan Boltzmann law using billet surface temperature, furnace gas temperature which is multiplied by spatial distributed emission factor. Emission factor used in this study was a tuning parameter. Optimal emission factors for the minimum difference between model output and measurements were searched through Dynamic Encoding Algorithm for Searches (DEAS) a non-gradient optimization method (Kim and Kim, 2005).

Kim (2007) reported a mathematical heat transfer model for the prediction of heat flux on the slab surface and 2D temperature distribution in the slab considering the steady state thermal radiation in the furnace chamber and transient heat conduction in the slab. Radiative heat flux was calculated through FVM radiation model where furnace radiative medium was assumed to have a constant absorption coefficient. They have also studied the effect of the variation of absorption coefficient and emissivity of the slab on heating characteristics.

Hsieh et al. (2008a &2008b) presented a 3D turbulent reactive flow and radiative heat transfer model for walking beam type reheating furnace by the commercial software STAR-CD®. The CFD simulation presented in this work considered single fuel by Prescribed Probability Density Function (PPDF) model for combustion study, Discrete Ordinates Method (DOM) with Weighted Sum of Gray Gases Model (WSGGM) for steady state radiation calculations in the furnace. The main limitation of their model is

that they have prescribed fixed billet surface temperature, in other words, the heat transfer from combustion gas is not coupled to the temperature of the billet during reheating simulation.

Huang et al. (2008) performed a coupled numerical study of slab temperature and gas temperature in the walking beam type slab reheating furnace. In this study, a 3D simulation is performed for the turbulent reactive flow and radiative heat transfer in the furnace using commercial software STAR-CD®. This model takes care of the skid system and other main components of the furnace. The slab movement was modeled as a laminar flow having a very high viscosity and moving at a constant speed. The heat flux on the slab surfaces, two dimensional temperature distributions of the slab and the gas mixture were predicted through a coupled simulation.

Han et al. (2009) presented a numerical model and simulation results for the study of transient radiative heating characteristics of slabs in a walking beam type reheating furnace. Transient radiative heating characteristics of slabs in a walking beam type reheating furnace were predicted by using FVM for radiation. The WSGGM was used for the calculation of furnace gas radiative properties. Entire domain was divided into eight sub-zones to specify the temperature distribution, and each sub-zone has been assumed at different temperatures and the same species composition. 3D temperature field of a slab was calculated by solving the transient heat conduction equation. The slab heating characteristics were studied for the various slab residence times.

Wild et al. (2009) presented a model for a pusher-type reheating furnace. In this model, reheat furnace was discretized into the control volume along the length using zone method. They have modeled the dynamics of furnace gases, where the mass and energy conservation principle were applied in each control volume. Their FDM based slab temperature prediction model was restricted to 1D.

Chen et al. (2010) investigated the optimal heating of slab in the reheat furnace. They have applied an arctangent function as the heating curves. In this work, they have predicted 2D temperature profile in the slab without skid cooling. They have developed an implicit scheme FDM model with arc tangent surface temperature boundary conditions In order to obtain optimal heating time for a fixed size slab with desired temperature uniformity, one extra boundary condition was introduced and solved by Newton scheme.

Ghannam et al. (2010) presented the application and validity of the Multiple Absorption Coefficient Zonal Method (MACZM) for the analysis of radiative heat transfer in multidimensional inhomogeneous non-gray media. MACZM is based on the concept of generic exchange factors The details of generic exchange factors can referred from Yuen W. W. (2006). The slab inside the furnace is divided into several 1D components and modeled with FEM.

Hsieh et al. (2010) studied skid marks on slabs in the walking beam furnace where they have simulated their previously developed numerical model (Hsieh et al., 2008). Their investigation shows that the skid mark is mainly caused by the radiation shielding effect of the static beams, which is further aggravated by the skid buttons which conduct heat to the cooling water.

Han et al. (2010) developed numerical model and simulated heat transfer using FLUENT®. They have modeled billet movement by transfer of temperature field of billet from one billet to another. To accomplish this task they have implemented user defined function in the FLUENT®.

Jang et al. (2010) carried out an investigation of the slab heating characteristics in the reheat furnaces with the growth of oxide scale. They have considered furnace as radiative medium with given furnace gas temperatures (constant in a zone). The radiation flux impinging on the slab surface was used for solution of 2D transient heat conduction equation. In this work they have used FVM for development of radiation and conduction model. Their model predicts 2D temperature field in the billet and growth of the oxide scale. They concluded that the effect of the oxide scale layer on the slab heating is considerable.

Han et al. (2011) proposed a model for the study of reheating furnace thermal efficiency. They have divided the entire furnace into fourteen subzones and calculated sub zone medium temperature and wall temperature on the basis of overall heat balance for all the subzones. To calculate the thermal efficiency of the furnace, they developed a model considering 3D radiation heat transfer in the furnace, 2D transient heat conduction in the slab and 1D conduction in the furnace walls, where the radiative heat transfer calculations were performed by FVM. Additionally, they have presented slab heating characteristics and thermal behavior of the furnace for various fuel feed conditions.

Han and Chang (2012a) carried out thermal analysis for walking beam furnace with combustion calculation using the commercial code FLUENT®. They performed simulations to obtain the optimal slab residence time for the required heating quality of a slab. In the other communication (Han and Chang, 2012b) they have predicted performance of walking beam furnace with different compositions of fuel gases.

Lee and Kim (2013) presented a mathematical model to calculate 2D temperature distribution of a slab in reheating furnace. They have modeled thermal radiation in the furnace and 2D transient conduction in the slab by FVM. Radiative heat flux calculations accounts the effects of the furnace walls, combustion gases, skid beams, and buttons. The weighted sum of gray gas model (WSGGM) was used for the calculation of furnace gas radiative properties. They considered two different charging and furnace gas temperature conditions for study of heating characteristics and residence time optimization.

Tan et al. (2013) presented 2D and 3D mathematical model for the study of reheat furnace behavior during unsteady and steady operation, their model is based on zone method of radiation heat transfer analysis. The exchange area was calculated through a Monte Carlo ray tracing computer program (RADEX) developed by Lwson and Ziesler (1996). The modelling approach accounts for the net radiation interchanges between the top and bottom firing sections of the furnace and also allow for enthalpy exchange due to the flows of combustion products between these sections. The inter zone mass flow rates are calculated by commercial code ANSYS FLUENT® CFD simulation. The transient radiation model is to calculate the heat flux for 1D and 2D explicit FDM conduction model for wall and bloom, respectively. They studied the feasibility of zone modelling for simulation of transient behavior of the furnace.

Singh and Talukdar (2013), compared four different models of the reheat furnace used for predicting heating characteristics of the slab. In model-1, steady state radiation was modeled by implementing the Discrete Ordinate Model (DOM) using commercial software FLUENT®. During this radiation simulation the slabs were assumed to be at 0 K. The heat flux from FLUENT® simulation results was used as boundary conditions for FVM based 3D heat conduction model which was solved using their self developed MATLAB® code. In model-2, radiation in furnace and 2D conduction in the slab was integrated as single problem and implemented in FLUENT®. The slab temperature data from one location to another in the furnace were transferred through user defined function. In model-3 they consider the skid system and

keeping the rest similar to the model-2. These three models used zone wise constant temperature of gas as input data for simulation. In model-4 both convection and radiation were considered. This model does not require temperature distribution as an input parameter and calculates its own temperature profile based on inlet conditions of hot gas input. They have concluded that model-1 was quite economical (from the computational time point of view) and reasonably accurate.

The following are the main observations of the present literature review of reheat models:

- The literature survey reveals that in the recent years, many numerical models have been developed and simulated for the study of billet heating in the reheat furnace.
- Few numerical models reported in the literature attempts to solve fluid dynamics and energy conservation equations governing hot gas flow and combustion in the reheat furnace for prediction of thermal, radiative and turbulent fluid characteristics of the reheating furnace and temperature analysis. The majority of these types of studies was done using commercial CFD code FLUENT®. However, few contributions with other commercial software like STAR-CD® cannot be ruled out. The advantages of these models are giving more accurate and elaborate thermal and fluid characteristics which, are offset by some disadvantages such as: (i) It involves many sub models which poses difficulty in implementation and their proper coupling. (ii) Excessive computational requirement. (iii) In many cases limited to 1D and 2D billet temperature predictions. (iv) In some cases heat transfer from combustion gas is not coupled to the temperature of the billet during reheating simulation. (iv) Non consideration of the oxide scale formation and growth. (v) In some cases, these models cannot be transferred out of the research environment partially to the fact that they require a very high computation resource and high ended research skills to assemble the sub models.
- Some of the numerical models have neglected furnace gas, fluid dynamics and modeled radiation, assuming isothermal gas zones using different radiation models with both gray and non gray gas radiations. These models calculated radiation heat flux impinging on the slab surfaces. These studies are mainly done by using in house developed codes. However, a significant number of studies are also done by

commercial CFD codes. The calculated heat fluxes were taken as boundary conditions for solutions in 1D, many cases 2D and in very few cases 3D transient heat conduction equation. The advantages of these models are that the simulations can be done with lower computational facilities in reasonable time; hence, these types of models are more suitable for industrial control use. These models also give reasonably accurate predictions of billet temperature field.

- The reported models differ in terms of prediction capabilities, accuracy, complexity and computational efficiency. There are no single numerical models that can takes-up all process parameters and situations encountered during the reheating. Therefore, it is important to select a suitable approach for modelling of reheating process depending upon the requirement and objective.

2.7 Literature Review on Heat Transfer Modelling and Simulation during Transport

Billets after heating in the reheat furnace are transported to the rolling mills. During the transport, billets are exposed to the surrounding air; as a result of this the temperature fields in the billet changes considerably from the reheat furnace discharge conditions. Knowledge of transient temperature field in the billets during transport and before rolling mills, are very important, especially for downstream activities like process optimization, roll force calculations, and microstructure control, etc. However, it is almost difficult to obtain correct and complete transient temperature field of the billet through measuring equipment. Numerical modelling may be a valuable tool for temperature predictions during billet transport. The reported literature explicitly dealing with numerical modelling and heat transfer simulation during transport is very limited.

Jaklic et al. (2002) developed a 3D transient heat conduction model for simulation of billet cooling during the transport from the reheating furnace to the rolling mills. FDM with the explicit scheme was used for discretization of 3D transient heat conduction equation. Their model takes into account effect of the constant thickness of oxide scale. They have presented a comparison of billet surface temperature with and without consideration of oxide scale. They concluded that the scale significantly affects the temperature field in the billet during transport and should not be neglected.

2.8 Gaps in the Research

The literature review suggests that the following significant issues still need to be addressed.

- The reviewed literature reveals that very few works have been reported so far to predict the 3D temperature fields in the billet. The detailed 3D transient heat conduction model and their computer implementation for steel billet reheating with the growth and formation of oxide scale have not been reported.
- Systematic parametric studies for investigating the effect of zone temperatures on various responses of interests like maximum temperature, minimum temperature, maximum temperature difference, average temperature, maximum oxide scale thickness and average oxide scale thickness have not been reported so far.
- The literature reviews of transport simulation suggest that numerical modelling and simulation for steel billet temperature prediction in the presence of oxide scale is very limited. The reported transient heat conduction models of billet transport simulations are based on explicit scheme of FDM, which assume billet at uniform initial temperature. However, the assumption of uniform initial temperature makes temperature predictions erroneous because in actual situations billet coming out from the furnace by and large have a certain temperature gradient within the material. Hence, it is essential to take up an approach, where the actual non- uniform temperature fields of billet after reheat is assigned as initial conditions for the modelling of transport simulation.
- The implicit transient heat conduction numerical model with oxide scale for the billet transport process has not been reported so far. Although, the explicit scheme solution procedure for transient heat conduction is computationally less complicated than that of the implicit; the maximum size of the time step restricted by stability criterion makes it inappropriate or complicated for simulation with thin oxide layer. Additionally, the explicit numerical model may be difficult to combine with reheat model.

2.9 Closure

In the recent past attention has been focused on steel industry processes for improved furnace control and billet temperature field predictions which are relying on appropriate numerical models. In this context the chapter introduced the reheat furnace, reheating, transport process and the associated phenomenon. The literature review on numerical models for reheat reveals that heat transfer modelling and simulation with the growth of oxide scale during reheat for predictions of 3D temperature field in the billet is not reported. Numerical heat transfer model and studies explicitly dealing with steel billet transport is also extremely limited. The present work aims to considerably bridge the gaps through heat transfer modelling and simulation with consideration of oxide scale, for predictions of 3D temperature field in the billet during reheating and transport. The next chapter provides a detail description for the development of 3D transient heat conduction model with growth of oxide scale for heat transfer simulation during reheating.

Chapter 3

Model Development for Steel Billet Reheat

3.1 Introduction

The literature reviewed in the previous chapter reveals that significant works have not been reported so far, for development of a numerical model to predict the 3D temperature fields in the billet with consideration of growing oxide scale during reheat.

This chapter presents the development of 3D transient numerical heat conduction numerical model for heat transfer simulation during steel billet reheating. The model considers temperature dependent material properties such as thermal conductivity and specific heat for steel and oxide scale. The model captures various time dependent boundary conditions corresponding to the billet reheat in the reheat furnace. Model also accounts for the growth of oxide scale layer on the billet surfaces, oxidation reaction heat source and skid effects. The discretization of governing equation is done by control volume approach and implicit scheme of FDM.

The chapter begins with the description of the overall modelling methodology, furnace radiative gas mixture property model and oxide scale growth model. This is followed by the descriptions of governing differential equation; initial conditions and boundary conditions for reheat simulation. The detailed procedure for formulations of discretization equations are presented in the subsequent sections.

3.2 Overall Modelling Methodology & Problem Descriptions

The model, which attempts to simulate entire reheating furnace and all billets simultaneously become computationally challenging. This type of model demands high end computing facility but also takes very high computation time. In order to develop a model that can operate with minimal computation facilities and solutions should be obtainable within reasonable running time, in the proposed model; the solution domain is the single billet. The billet is divided into number of control-volumes and follows its movement when it is travelling through different zones of the reheat furnace. The temperature history of the billet is carried forward from one position to another position along the length of the furnace and heat flux to the steel billet surface is assigned

according to the position of the billet. Heat flux calculation accounts radiation heat transfer from furnace walls and gases to the billet surfaces.

The proposed 3D transient heat conduction numerical model accounts for heat exchange from the interior of reheat furnaces which also include skid systems. The reheat furnace is divided into a number of zones such as: non firing, preheating, heating and soaking zones. The furnace gas and wall temperatures vary along the length of the furnace, but assumed to remain constant within a zone. The billets are placed in such a way that a gap is present between them ensuing each face is exposed to heat transfer. In the model billet orientation is transverse to the furnace longitudinal axis.

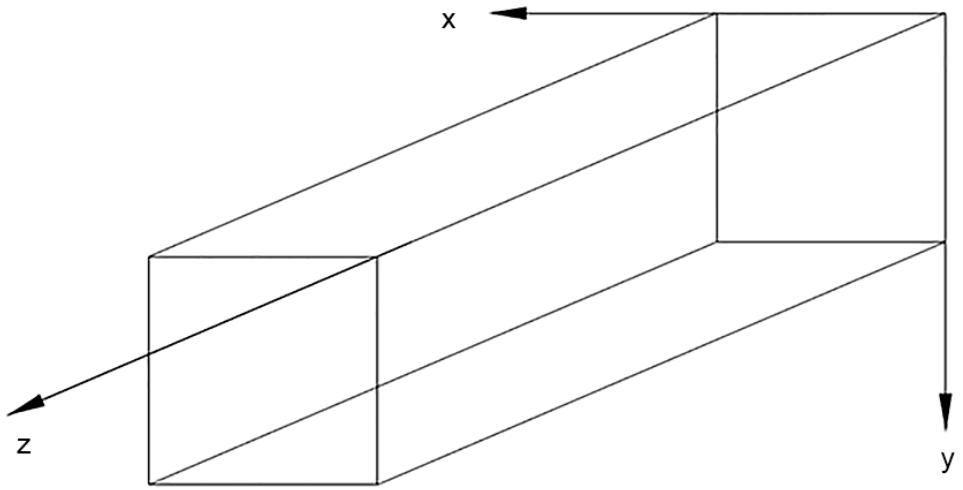

Fig. 3.1: Billet axis used in numerical model

In the 3D transient conduction model of billet: *x*, *y* and *z* directions are considered as billet width, billet height and billet length directions respectively as shown in Fig. 3.1. Billets are supported by static beams and moved by walking beams. Static beams are in contact with the billet through skid buttons. The walking beam is placed between two static beams which stay in lower elevation for most of the heating duration and comes into contact with the billet for a very small time (only during billet movement); therefore, present model considers contact of the billet with the only static beam. The beams are supported by pillars. The water cooled skid system over which the billet rests in the reheat furnace reduces heat transfer to the bottom surface of the billet. Fig. 3.2 shows the details of skid and billet contact.

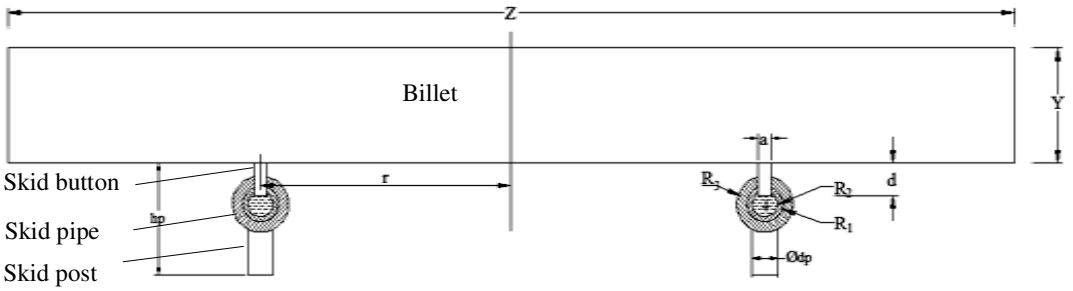

Fig. 3.2: Billet contact with water cooled skid system

3.3 Radiative Gas Mixture Property Model

Gas radiation is mainly relevant to heat transfer in furnaces and combustion chambers fired with hydrocarbon fuels. Reheat furnaces, mostly fired with hydrocarbon fuels are filled with the hot combustion gases that mainly consists of H_2O, CO_2, N_2 and O_2. The diatomic homonuclear molecules such as oxygen and nitrogen do not display any absorption properties and are considered to be infrared inactive. The polyatomic molecules such as CO_2 and H_2O vapor, etc. absorb and emit radiation. These gases in the furnace make gas absorption characteristics complicated because of their inherent non gray nature.

The radiative gas property models available in the literature can be categorized into four categories: narrow band models (Ludwig et al., 1973) exponential wide band models (Edwards, 1976; Modak, 1979) charts and correlations (Hottel and Sarofim, 1967; Leckner, 1972) and weighted sum of gray gases model (Hottel and Sarofim 1965, 1967; Smith et al., 1982). Some of these methods are interrelated and uses results of other model. Comparisons of these models are available in the literature (Modak, 1978; Farag et al., 1981; Smith et al., 1982)

The reheat furnace gas contains CO_2 and H_2O which are the major components that affect the emissivity and absorptivity of furnace gas. Hottel and Sarofim (1967) considered combustion gases and presented charts for total emissivity and absorptivity in the form:

$$\varepsilon = \varepsilon(p_a L, p, T_g) \tag{3.1}$$

$$\alpha = \alpha(p_a L, p, T_g, T_s) \approx \left(\frac{T_g}{T_s}\right)^{1/2} \varepsilon\left(p_a L \frac{T_g}{T_s}, p, T_s\right) \tag{3.2}$$

where T_s is temperature of hot surface and T_g is the gas temperature. Initially, the power T_g / T_s recommended was 0.65 for CO_2 and 0.45 for water vapor, but afterward the single value 0.5 was accepted (Hottel and Sarofim, 1967). Here p_a is partial pressure, p is the total pressure in the furnace and L is the pressure path length. Hottel and Sarofim (1967) also presented charts for pressure correction for overlap parameters. More recent correlations for above discussed emissivity are given by Leckner (1972). The further details about the correlations and the implementation procedure of this method can be referred from Modest (1993).

In order to account the emissive and absorptive behavior of reheat furnace combustion gases, Weighted Sum of Gray Gases Model (WGGM) (Hottel and Sarofim 1965, 1967; Smith et al., 1982) is adopted. Here the real gases behavior can be simulated by a weighted summation of a sufficient number of gases.

According to WGGM implementation procedure (Smith et al., 1982), the emissivity of gas mixture can be approximated as:

$$\varepsilon_g = \sum_{i=0}^{I} a_{\varepsilon,i}\ (T_g)(1 - e^{-\kappa_i PL}) \tag{3.3}$$

Here the absorption coefficient (κ_i) and weighting coefficient $(a_{\varepsilon,i})$. These coefficients are the function of gas temperature, but for mathematical simplicity, absorption coefficient (κ_i) is chosen to be a constant. Hence, temperature dependence is accounted only by weighting factor $(a_{\varepsilon,i})$. For the furnace gas mixture PL represents the pressure path length product, where P is the sum of the partial pressure of absorbing gases. In the Eq. (3.3) I is the number of gray gases and $i = 0$ is the clear gas. The total emissivity approaches unity. Hence, weighting factors subject to the conditions:

$$\sum_{i=0}^{I} a_{\varepsilon,i}(T_g) = 1 \quad \text{and} \quad a_{\varepsilon,i}(T_g) > 0 \tag{3.4}$$

The weighting factor for $i = 0$ is obtained as:

$$a_{\varepsilon,0} = 1 - \sum_{i=1}^{I} a_{\varepsilon,i} \tag{3.5}$$

The weighting factors are represented by $J-1$ order polynomial of furnace gas temperature, given as:

$$a_{\varepsilon,i} = \sum_{j=1}^{J} b_{\varepsilon,i,j} T_g^{J-1} \tag{3.6}$$

where $b_{\varepsilon,i,j}$ are emissivity gas temperature polynomial coefficients. A similar method can be applied for calculation of absorptivity of furnace gas, where absorptivity is function of both gas temperature (T_g) and surface irradiation temperature (T_s). Hence, the absorptivity of gas mixture can be approximated as:

$$\alpha_{gs} = \sum_{i=0}^{I} a_{\alpha,i}(T_g, T_s)(1 - e^{-\kappa_i PL}) \tag{3.7}$$

subject to the conditions:

$$\sum_{i=0}^{I} a_{\alpha,i}(T_g) = 1 \quad \text{and} \quad a_{\alpha,i}(T_g) > 0 \tag{3.8}$$

The absorptivity weighting factors are represented by polynomials of gas temperature (T_g) and surface irradiation temperature (T_s), given as:

$$a_{\alpha,i} = \sum_{j=1}^{J} \left[\sum_{k=1}^{K} C_{\alpha,i,j,k} T_s^{\kappa-1} \right] T_g^{J-1} \tag{3.9}$$

where $C_{\alpha,i,j,k}$ are the absorptivity gas temperature polynomial coefficients.

The absorption coefficient (κ_i) and emissivity gas temperature polynomial coefficients $(b_{\varepsilon,i,j})$ can be evaluated by fitting Eq. (3.3) to a table of total emissivity. Similarly absorptivity gas temperature polynomial coefficients $(C_{\alpha,i,j,k})$ can be evaluated by fitting Eq. (3.7) to a table total absorptivity. The data for a table of total emissivity and absorptivity for carbon dioxide, water vapor and mixtures of these gases can be generated from exponential wide band model (Edward, 1976; Modak, 1979).

In the proposed model the absorption coefficient (κ_i) emissivity gas temperature polynomial coefficients $(b_{\varepsilon,i,j})$ and absorptivity gas temperature polynomial coefficients $(C_{\alpha,i,j,k})$ were taken from Smith et al. (1982). These coefficients for a clear plus three gray gases model corresponding to $\frac{p_{H_2O}}{P_{CO_2}} \approx 2$, which is commonly the case for the gaseous combustion in the reheat furnace, are given in Tables 3.1 & 3.2. The results

obtained from this WSGGM were included in the proposed 3D transient heat conduction model to calculate radiative exchange in the reheat furnace.

Table 3.1: Coefficients used for evaluating the emissivity of gas mixtures in WSGGM (Smith et al., 1982)

i	κ_i	$b_{\varepsilon,i,1}\times10^{1}$	$b_{\varepsilon,i,2}\times10^{4}$	$b_{\varepsilon,i,3}\times10^{7}$	$b_{\varepsilon,i,4}\times10^{11}$
1	0.4201	6.508	-5.551	3.029	-5.353
2	6.516	-0.2504	6.112	-3.882	6.528
3	131.9	2.718	-3.118	1.221	-1.612

Table 3.2: Coefficients used for evaluating the absorptivity of gas mixtures in WSGGM (Smith et al., 1982)

k		1	2	3	4
i	j				
1	1	5.9324×10^{-01}	-6.1741×10^{-04}	2.9248×10^{-07}	-4.5823×10^{-11}
2	1	-3.5664×10^{-02}	2.1502×10^{-04}	-1.3648×10^{-07}	2.4284×10^{-11}
3	1	1.2951×10^{-01}	5.4520×10^{-05}	-8.0049×10^{-08}	1.7813×10^{-11}
1	2	3.5739×10^{-04}	2.2122×10^{-07}	-2.6380×10^{-10}	4.5951×10^{-14}
2	2	5.1605×10^{-04}	-7.0037×10^{-07}	3.8680×10^{-10}	-7.0429×10^{-14}
3	2	1.5210×10^{-04}	-3.7750×10^{-07}	2.1019×10^{-10}	-3.6011×10^{-14}
1	3	-7.1313×10^{-07}	4.6181×10^{-10}	-7.0858×10^{-14}	3.8038×10^{-18}
2	3	1.2245×10^{-07}	9.9434×10^{-11}	-1.5598×10^{-13}	3.73664×10^{-17}
3	3	-1.3165×10^{-07}	2.0719×10^{-10}	-9.6720×10^{-14}	1.4807×10^{-17}
1	4	1.7806×10^{-10}	-1.1654×10^{-13}	1.9939×10^{-17}	-1.3486×10^{-21}
2	4	-5.7563×10^{-11}	-1.0109×10^{-14}	3.5273×10^{-17}	-8.9872×10^{-21}
3	4	2.6872×10^{-11}	-3.4803×10^{-14}	1.4336×10^{-17}	-1.9754×10^{-21}

3.4 Oxide Scale Growth

During the reheating process, the steel billet is exposed to high temperature oxidizing gas environment. At such a high temperature in the reheat furnace, steel undergoes oxidation reaction to form oxide scale layer. The oxidation behavior and its kinetics have been analyzed in numerous studies (Kofstad, 1966; Mogan, 1999; Chen and Yuen, 2003; Marston et al., 2004; Jang et al., 2010) which gives an approach for modelling of oxide scale growth in the present work. For the entire temperature range of steel reheating process, the oxide scale contains three distinct layers: outer layer of haematite, an intermediate layer of magnetite and an innermost layer of wustite. However, at the elevated temperatures wustite layer thickness is considerably higher than the haematite and magnetite layers. The percentage thicknesses of the three oxide layers wustite, magnetite and haematite are approximately 95, 4 and 1 respectively. Since the wustite account for 95% of the oxide layer, the other two layer of oxide scale are neglected in the present modelling.

When hot steel is exposed to the furnace oxidizing environment, the rate of oxidation reaction is controlled by diffusion of oxidizing species from bulk gas to gas scale interface. For the above stated conditions, oxidation follows linear rate equation. As the oxide layer thickens, oxidation reaction is controlled by diffusion of iron ions or vacancies through the growing oxide layer. The concentration gradient decreases with the growth of oxide layer and gives parabolic rate equation for oxidation. Marston et al. (2004) suggest a combined linear plus parabolic model for the growth scale during reheat furnace application. However, there are certain inherent problems with the model as cited in their article. It is difficult to reproduce the conditions of sudden exposure to the scale free conditions for isothermal thermo balance tests. But, this is required for Arrhenius plot used for determination of linear rate constant. Since very small time durations are involved for the linear rate growth part and the difficulties associated with determination and availability of correct values of liner constant rate, there is a general consensus for selection of parabolic oxidation rate equation. Therefore, in the same line, the present study adopts the paraboilc rate equation for oxide growth modelling.

The change of oxide scale thickness with time according to parabolic rate law can be expressed as:

$$\frac{ds}{dt} = \frac{\lambda}{s} \tag{3.10a}$$

$$s^2 = 2\lambda t + s_o^{\ 2} \tag{3.10b}$$

where s is the oxide scale thickness, t is the oxidation time, s_o is initial scale thickness at time $t = 0$ and λ is the parabolic rate constant. The temperature dependent parabolic rate constant is expressed as:

$$\lambda = A \exp^{-Q/RT} \tag{3.11}$$

where A is Arrhenius constant, Q is activation energy for rate controlling, T is metal temperature (absolute) and R is the gas constant. In the present work the parabolic oxidation rate constant (m^2s^{-1}) (Mogan, 1999) at any metal temperature is calculated from:

$$\lambda = 7.1\times10^{-6} \exp^{\left[\frac{-16610}{T}\right]} \tag{3.12}$$

The oxidation reaction is exothermic in nature. Therefore, an additional heat source is included in the reheat model which accounts for oxidation reaction heat. The rate of heat release, during the oxidation reaction is given as:

$$q_o = -\Delta H \frac{dm}{dt} \tag{3.13}$$

where, H is the oxidation reaction heat release expressed in J/kg. The rate of change of mass is calculated from oxide scale growth rate law.

$$\frac{dm}{dt} = \rho_{os}\,(\text{surface area})\frac{ds}{dt} \tag{3.14}$$

where ρ_{os} is density of oxide scale and surface are refers to area on which oxide scale is growing.

Thus, for parabolic oxidation rate the mass rate change can be expressed as:

$$\frac{dm}{dt} = \rho_{os}\,(\text{surface area})\frac{\lambda}{s} \tag{3.15}$$

The oxidation heat release for 3D model cell is calculated as:

$$q_o = -\Delta H \rho_{os}\,(\text{cell surface area})\frac{\lambda}{s} \tag{3.16}$$

where cell surface area refers to the area of cell on which oxide scale is growing.

3.5 Governing Differential Equations

The numerical heat conduction model has been developed to obtain a solution of three dimensional transient heat conduction given as:

$$\frac{\partial}{\partial x}\left(k\frac{\partial T}{\partial x}\right)+\frac{\partial}{\partial y}\left(k\frac{\partial T}{\partial y}\right)+\frac{\partial}{\partial z}\left(k\frac{\partial T}{\partial z}\right)+\dot{q}=\rho c\frac{\partial T}{\partial t} \qquad (3.17)$$

where x, y and z directions are considered as billet width, billet height and billet length directions respectively, T is the temperature, ρ is the density, t is time, c is the specific heat, q is the source term. This study considers temperature dependent thermal conductivity and specific heat. The source term considered in this study accounts for the exothermic oxidation reaction heat of scale formation and growth of oxide scale on the billet surfaces.

3.6 Boundary Conditions

The billet is assumed to be at uniform temperature of 298 K, when charged to the reheat furnace. The surfaces of the billet are exposed to radiation and convection heat transfer. The total heat transfer flux (q_t) (Lindholm and Leden, 1999) can be expressed as:

$$q_t=\frac{\sigma\varepsilon_s}{\left[1-(1-\varepsilon_s)(1-\alpha_{gs})\right]}(\varepsilon_g T_g^4-\alpha_{gs}T_s^4)+h_c(T_g-T_s)+\sigma\varepsilon_{sw}(T_w^4-T_s^4) \qquad (3.18)$$

In Eq. (3.18), the first and second terms of RHS represent heat flux which accounts for heat exchange between the gas and billet by radiation and convection, respectively. The third term of RHS is the heat flux which accounts for heat exchange between furnace wall and the billet by radiation.

In the above Eq. (3.18), σ is the Stefan-Boltzmann constant having a value of $5.67\times10^{-8}\,\mathrm{W/m^2K^4}$; ε_s is the emissivity of billet surface; T_g is the furnace gas temperature; T_s is billet surface temperature; T_w is furnace wall temperature; ε_g is the emissivity and α_{gs} is the absorptivity of furnace gas mixture.

The emissivity and absorptivity of furnace gas are calculated by WSGGM as discussed previously. For calculation of radiation heat exchange between furnace wall and billet the direct exchange factor (ε_{sw}) (Lindholm and Leden, 1999) as stated in Eq. (3.18) is found using

$$\varepsilon_{sw} = \varepsilon_s \varepsilon_w \tau_{gm} \phi_{sw} \tag{3.19}$$

where τ_{gm} is mean transmissivity of the furnace gas which is expressed by

$$\tau_{gm} = \left(1 - \alpha_{gm}\right) \tag{3.20}$$

where $$\alpha_{gm} = \frac{1}{2}(\alpha_{gs} + \alpha_{gw}) \tag{3.21}$$

The view factors ϕ_{sw} used in Eq. (3.19) may be calculated prior to simulation. In the current form, this model does not include view factor calculations for the actual geometry of the furnace, and it is assumed that ϕ_{sw}=1 during the simulations.

The radiation heat transfer coefficient (h_{rg}), which accounts for the heat exchange due to radiation between steel billet and the furnace gas and can be expressed as:

$$h_{rg} = \frac{\sigma \varepsilon_s}{\left[1 - (1 - \varepsilon_s)(1 - \alpha_{gs})\right]} \frac{(\varepsilon_g T_g^4 - \alpha_{gs} T_s^{\,4})}{(T_g - T_s)} \tag{3.22}$$

The radiation heat transfer coefficient (h_{rw})which accounts for heat exchange due to radiation between billet and furnace wall can be expressed as:

$$h_{rw} = \sigma \varepsilon_{sw} (T_w^2 + T_s^{\,2})\,(T_w + T_s) \tag{3.23}$$

At higher temperature, the contribution of convection in total heat transfer is small and therefore, in present study convective heat transfer coefficient h_c is taken as 7.8 W/m^{2}K (Lindholm and Leden, 1999; Jang et al. 2010).

The combined heat flux can be expressed in terms of the heat transfer coefficient as:

$$q_t = h_{rg}\,(T_g - T_s) + h_{rw}(T_w - T_s) + h_c (T_g - T_s) \tag{3.24}$$

The boundary condition of Eq.(3.16) on the billet top and side surfaces is the total heat flux (q_t). which can be expressed as:

The boundary conditions at $x = 0$ and $x = X$ are expressed by as:

$$-k \left.\frac{\partial T}{\partial x}\right|_{surface} = q_t \tag{3.25}$$

The boundary conditions at $z = 0$ and $z = Z$ can be stated as:

$$-k\left.\frac{\partial T}{\partial z}\right|_{surface} = q_t \tag{3.26}$$

Similarly the boundary conditions at $y = 0$ are expressed are written as:

$$-k\left.\frac{\partial T}{\partial y}\right|_{surface} = q_t \tag{3.27}$$

The water cooled skid system over which the billet rests in the reheat furnace reduces heat transfer on the billet bottom surface. The fraction of direct radiation coming from an imaginary surface of furnace gas (between the skids) to the billet bottom surface is given by radiation view factor. The above said view factor is calculated by the Hottel cross string method (Hottel and Sarofim, 1967). The reflected and re-radiated radiations from skid structure were added to the direct radiation for calculation of the radiation shielding factor F. The boundary condition for the bottom surface of billet which is in contact with skid is the heat flux $q_{bottom,1}$

The boundary condition for the bottom surface of billet which is in contact with skid, at $y = Y$, can be expressed as:

$$-k\left.\frac{\partial T}{\partial y}\right|_{surface} = q_{bottom,1} \tag{3.28}$$

where $q_{bottom,1}$ is given as:

$$q_{bottom,1} = F(1-\gamma)\, q_t - \gamma\left(\frac{T_s - T_{water}}{R_{bt}}\right) \tag{3.29}$$

Here the contact ratio (γ) can be written as:

$$\gamma = \frac{\text{contact width}}{\text{gridspace}} \tag{3.30}$$

The overall thermal resistance R_{bt}, which accounts for contact resistance between billet and skid, the conduction resistance offered by skid button and convection resistance offered by water flowing through skid system. This can be expressed in the form:

$$R_{bt} = \frac{1}{h_{ct}} + \frac{d}{k_{sk}} + \frac{1}{h_w} \tag{3.31}$$

Contact coefficient (h_{ct}) between the skid and the billet can be calculated through temperature dependent co-relations (Howells et al., 1972, Ford et al., 1980). Convective heat transfer coefficient (h_w) in skid pipe is evaluated by Dittus-Boelter correlation (Cengel and Ghajar, 2011). Water flowing through the skid pipe has approximately constant temperature (Lindholm and Leden, 1999; Kim and Huh, 2000). In the present study water temperature, T_{water} is assumed to be at a constant temperature of 315 K. The boundary condition for surface which is not in contact with skid and situated between skid contact buttons, is the heat flux $q_{bottom,2}$.

Boundary condition for surface which is not in contact with skid and situated between skid contact buttons, at $y = Y$ on the bottom surface can be expressed as:

$$-k \left.\frac{\partial T}{\partial y}\right|_{surface} = q_{bottom,2} \tag{3.32}$$

where $q_{bottom,2}$ expressed as:

$$q_{bottom,2} = F \; q_t \tag{3.33}$$

3.7 Formulation of Discretization Equations

This study adopts a finite control-volume approach for development of finite difference discretized equations. In this approach, finite difference equations are developed by constraining the governing equation for finite control-volume and conserving the specific physical quantity of interest. This approach is suitable for multidimensional problems, complex boundary conditions and when there exists variable mesh and physical properties. The details of this approach can be referred from Ozisik (1993). In order to develop the finite difference equations, the finite difference nodes are established first, and then control-volumes are identified. The solution domain which in our case is the billet is divided into number of control-volumes (finite volumes). The integration of governing differential equation over the control volume about a node of interest and expressing the derivatives in the discrete form leads to the finite difference discretized equation. The basic idea is similar to heat balance over small volume surrounding a node of interest.

Implicit scheme is chosen for discretization in the present study, the rationale for this selection is to make model unconditionally stable. Although, the explicit scheme solution procedure is less computationally involved than that of the implicit; but the maximum size of the time step restricted by stability criterion (Ozisik, 1993), makes it inappropriate for reheat simulation with thin oxide layer where calculations are to be performed over a large time period.

3.7.1 Oxide scale discretization

The model considers the growth of oxide scale over the surface of steel billet. It is assumed that the oxide scale layer remains attached to the steel outer surface and the contact resistance between the two is neglected. The thicknesses of oxide scale are updated at the end of each iteration. For numerical modelling, oxide scale growth is approximated as:

$$s_{i,j,k}^{m+1} = \sqrt{(s_{i,j,k}^{m})^2 + 2\lambda\Delta t} \tag{3.34}$$

where superscript $m+1$ represents the index current iteration, m represents the index at the start of the current time step and Δt represents the time step.

The initial oxide thickness is approximated as:

$$s_{i,j,k}^{m} = \sqrt{2\lambda\Delta t} \tag{3.35}$$

The oxide scale layer is modeled as one separate finite volume with node at the outer surface. The oxide layer finite volume, thickness is equal to the variable oxide scale thickness. The cells (control volume) making up the oxide layer are termed as oxide cells. There can be ten basic types of nodal control volumes (cells) exist, out of which six different types of oxide cells and four different types of steel cells.

Fig. 3.3 shows basic oxide scale cells and nodal system, which is observed at the outer oxide scale surface. The third dimensions of different oxide cells (Fig. 3.3) along *z*- direction are equal to scale thickness. According to the position, such as those shown in Fig. 3.3, there are six basic oxide scale cells: oxide corner cell, oxide edge-1 cell, oxide edge-2 cell, oxide surface-1 cell, oxide surface-2 cell and oxide inner surface cell.

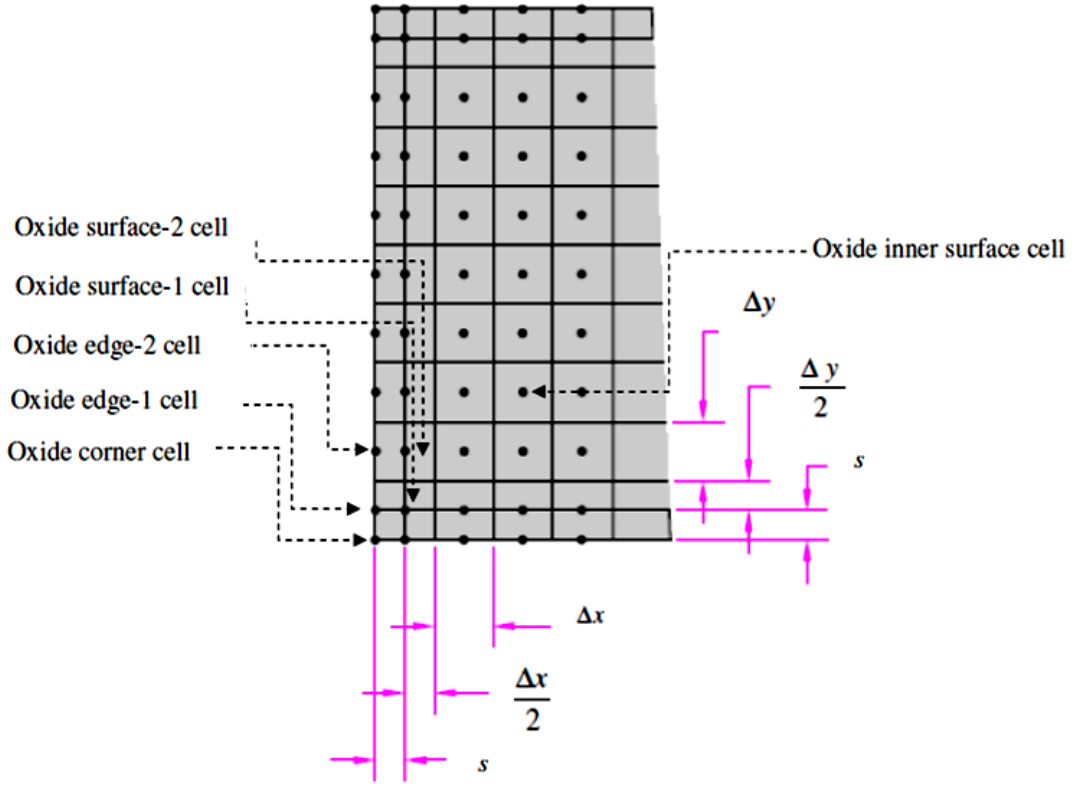

Fig. 3.3: Basic oxide scale cells and nodal system observed at outer oxide scale surface

Fig. 3.4 shows 3D view of the basic oxide corner, edge and surface cells, along with nodes of interest. The model oxide cell is shown in dark grey color. The oxide corner cell comprises of the intersection of three surface which are exposed to convection and radiation from hot gas which is maintained at temperature T_g, together with radiation from furnace wall which is at temperature T_w. On the contrary, for cells along the edges and plane surfaces are exposed to convection and radiation from two directions and one direction, respectively. The remaining faces are exposed to conduction heat transfer from surrounding oxide or steel cells. Discretization equations are derived for each type of oxide using control volume approach. The governing differential equation is integrated over the control volume and over the time interval from t to $t+\Delta t$ and derivatives are expressed the in the discrete form. It is assumed that the new value of nodal temperature prevails over the entire time step and such assumption leads to implicit scheme. The temperature derivative with space coordinate are evaluated by making assumptions of piecewise linear temperature profile between grid points. The basic idea is analogous to writing energy balance over the small volume.

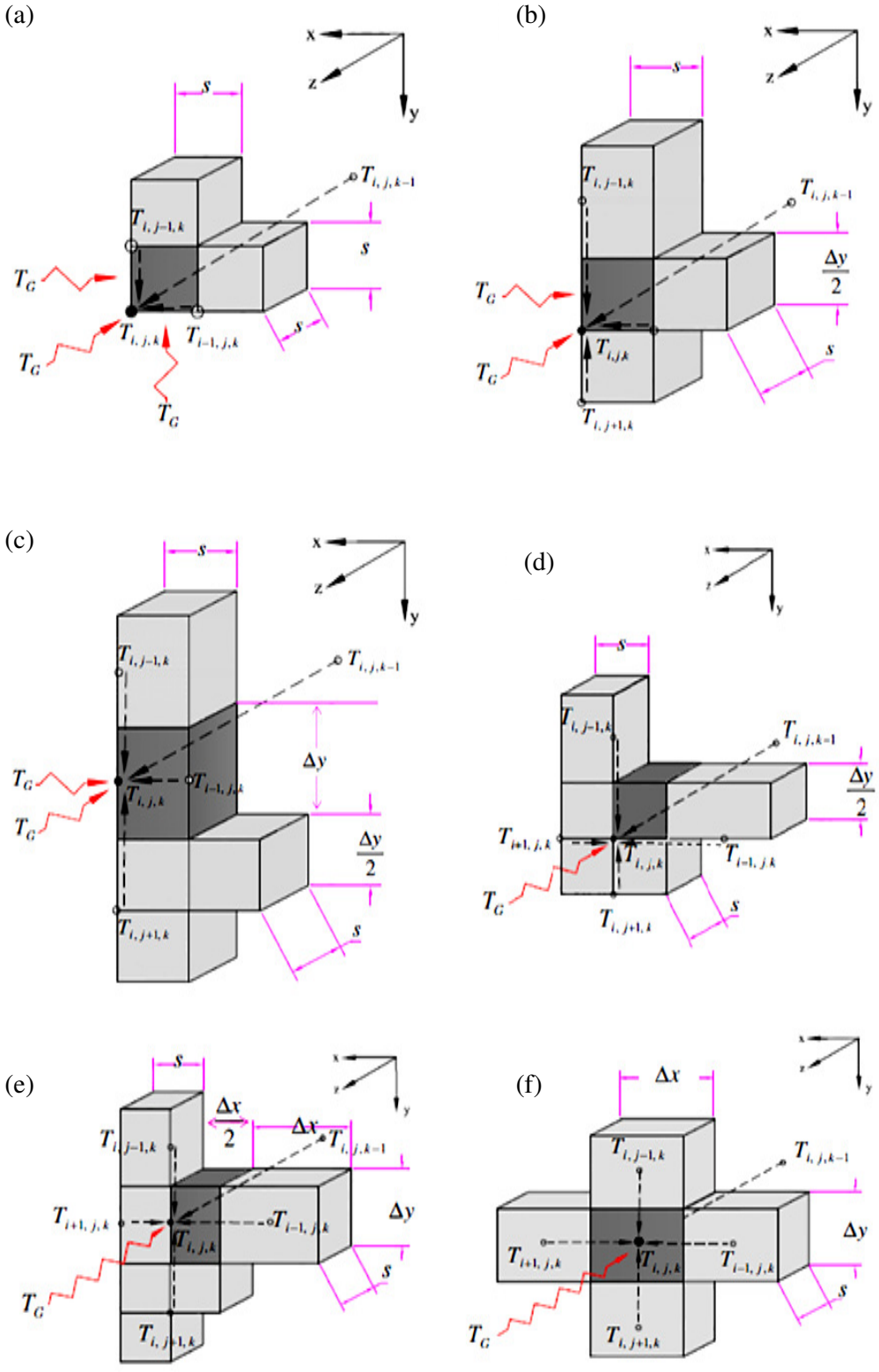

Fig. 3.4: Basic oxide scale cells: (a) oxide corner cell (b) oxide edge-1 cell (c) oxide edge-2 cell (d) oxide surface-1 cell (e) oxide surface-2 cell (f) oxide inner surface cell

Oxide inner surface cell:

For instance, for a given oxide inner surface cell, such as those shown in Fig. 3.4(f), the implicit finite difference equation, representing the instantaneous energy balance is expressed as:

$$\begin{aligned}\rho_{os}\, c_{os}\ \Delta x\Delta y\ s_{i,j,k}\frac{T_{i\,j,k}^{m+1}-T_{i,j,k}^{m}}{\Delta t} &= (k_{os})_{i+1/2,\ j,\ k}\ \Delta y\ s_{i,j,k}\frac{T_{i+1,jk}^{m+1}-T_{i,j,k}^{m+1}}{\Delta x}\\ &+(k_{os})_{i-1/2,\ j,\ k}\ \Delta y\ s_{i,j,k}\frac{T_{i-1,j,k}^{m+1}-T_{i,j,k}^{m+1}}{\Delta x}\\ &+(k_{os})_{i,\ j+1/2,\ k}\ \Delta x\ s_{i,j,k}\frac{T_{i,j+1,k}^{m+1}-T_{i,j,k}^{m+1}}{\Delta y}\\ &+(k_{os})_{i,\ j-1/2,k}\ \Delta x\ s_{i,j,k}\frac{T_{i,j-1,k}^{m+1}-T_{i,j,k}^{m+1}}{\Delta y}\\ &+(k_{os})_{i,j,k}\ \Delta x\Delta y\frac{T_{i,j,k-1}^{m+1}-T_{i,j,k}^{m+1}}{s_{i,j,k}}\\ &+(h_{rg}+h_{c})\Delta x\Delta y(T_{g}-T_{i,j,k}^{m+1})\\ &+h_{rw}\Delta x\Delta y(T_{w}-T_{i,j,k}^{m+1})+H\,\rho_{os}\frac{\lambda\Delta x\Delta y}{s_{i,j,k}}\end{aligned} \tag{3.36}$$

In the Eq. (3.36), the LHS represents an increase in internal energy within model cell volume. The first four terms of RHS are conduction into the model cell volume from surrounding oxide cells and the fifth term represents conduction into the model cell volume from surrounding steel cell. The sixth term represents convection and radiation across the one cell face from hot gas. The seventh term represents radiation across the one cell face - from furnace wall. The eighth term of RHS accounts for heat of oxidation reaction.

In the above Eq. (3.36), density of oxide scale is assumed constant, whereas oxide scale thermal conductivity (k_{os}), specific heat (c_{os}) and oxide scale thickness (s) are function of nodal temperature, which are evaluated at the temperature corresponding to the previous iteration.

The oxide scale thermal conductivities $\left((k_{os})_{i+1/2,\ j,\ k}\right)$ at the interface (representing face of model cell) placed midway and are the nodes i,j,k and $i+1,j,k$ are assumed to follow harmonic mean as discussed by Patankar (1980). Therefore, the thermal conductivity along x direction interfaces are expressed as:

$$\left(k_{os}\right)_{i+1/2,\ j,\ k}=\frac{2(k_{os})_{i,\ j,\ k}\,(k_{os})_{i+1,\ j,\ k}}{(k_{os})_{i,\ j,\ k}+(k_{os})_{i+1,\ j,\ k}} \tag{3.37}$$

$$(k_{os})_{i-1/2,\,j,\,k} = \frac{2(k_{os})_{i,\,j,\,k}\,(k_{os})_{i-1,\,j,\,k}}{(k_{os})_{i,\,j,\,k} + (k_{os})_{i-1,\,j,\,k}} \tag{3.38}$$

Similarly, the oxide scale thermal conductivity at the faces along y- and z -directions for model cell, can be found as:

along *y*-direction

$$(k_{os})_{i,\,j+1/2,\,k} = \frac{2(k_{os})_{i,\,j,\,k}\,(k_{os})_{i,\,j+1,\,k}}{(k_{os})_{i,\,j,\,k} + (k_{os})_{i,\,j+1,\,k}} \tag{3.39}$$

$$(k_{os})_{i,\,j-1/2,\,k} = \frac{2(k_{os})_{i,\,j,\,k}\,(k_{os})_{i,\,j-1,\,k}}{(k_{os})_{i,\,j,\,k} + (k_{os})_{i,\,j-1,\,k}} \tag{3.40}$$

along *z*-direction

$$(k_{os})_{i,\,j,\,k+1/2} = \frac{2(k_{os})_{i,\,j,\,k}\,(k_{os})_{i,\,j,\,k+1}}{(k_{os})_{i,\,j,\,k} + (k_{os})_{i,\,j,\,k+1}} \tag{3.41}$$

$$(k_{os})_{i,\,j,\,k-1/2} = \frac{2(k_{os})_{i,\,j,\,k}\,(k_{os})_{i,\,j,\,k-1}}{(k_{os})_{i,\,j,\,k} + (k_{os})_{i,\,j,\,k-1}} \tag{3.42}$$

In the similar way the discretization equation of other basic oxide such as those shown in Fig. 3.4 can easily be seen to be

Oxide corner cell [refer Fig. 3.4(a)]:

$$\begin{aligned}\rho_{os}\,c_{os}\;\; s_{i,\,j,\,k}\,s_{i,\,j,\,k}\,s_{i,\,j,\,k}\,\frac{T_{i\,j,\,k}^{m+1} - T_{i,\,j,\,k}^{m}}{\Delta t} &= (k_{os})_{i,\,j,\,k}\; s_{i,\,j,\,k}\; s_{i,\,j,\,k}\,\frac{T_{i-1,\,jk}^{m+1} - T_{i,\,j,\,k}^{m+1}}{s_{i,\,j,\,k}} \\ &+ (k_{os})_{i,\;j,\,k}\; s_{i,\,j,\,k}\;\; s_{i,\,j,\,k}\,\frac{T_{i,\,j-1,\,k}^{m+1} - T_{i,\,j,\,k}^{m+1}}{s_{i,\,j,\,k}} \\ &+ (k_{os})_{i,\,j,\,k}\; s_{i,\,j,\,k}\;\; s_{i,\,j,\,k}\,\frac{T_{i,\,j,\,k-1}^{m+1} - T_{i,\,j,\,k}^{m+1}}{s_{i,\,j,\,k}} \\ &+ (h_{rg} + h_c)(3\,s_{i,\,j,\,k}\; s_{i,\,j,\,k})(T_g - T_{i,\,j,\,k}^{m+1}) \\ &+ h_{rw}(3\,s_{i,\,j,\,k}\; s_{i,\,j,\,k})(T_w - T_{i,\,j,\,k}^{m+1}) + H\,\rho_{os}\,\frac{\lambda(3\,s_{i,\,j,\,k}\; s_{i,\,j,\,k})}{s_{i,\,j,\,k}}\end{aligned} \tag{3.43}$$

In the Eq. (3.43), the LHS represents an increase in internal energy within model cell volume. The first two terms of RHS are conduction into the model cell volume from surrounding oxide cells and the third term represents conduction into the model cell volume from surrounding steel cell. The fourth term represents convection and radiation across the three cell faces from hot gas. The fifth term represents radiation across the three cell faces from furnace wall. The sixth term of RHS accounts for heat of oxidation reaction for growth of oxide scale on the three cell faces.

Oxide edge -1 cell [refer Fig. 3.4(b)]:

$$\begin{aligned}\rho_{os}\, c_{os}\;\; s_{i,j,k}\,\frac{\Delta y}{2}\,s_{i,j,k}\,\frac{T_{i\,j,k}^{m+1}-T_{i,j,k}^{m}}{\Delta t} &= (k_{os})_{i,j,k}\;\frac{\Delta y}{2}\,s_{i,j,k}\,\frac{T_{i-1,j\,k}^{m+1}-T_{i,j,k}^{m+1}}{s_{i,j,k}} \\ &+ (k_{os})_{i,\;j,k}\;s_{i,j,k}\;\;s_{i,j,k}\,\frac{T_{i,j+1,k}^{m+1}-T_{i,j,k}^{m+1}}{s_{i,j,k}} \\ &+ (k_{os})_{i,\,j-1/2,k-1}\,s_{i,j,k}\;\;s_{i,j,k}\,\frac{T_{i,j-1,k}^{m+1}-T_{i,j,k}^{m+1}}{\Delta y} \\ &+ (k_{os})_{i,j,k}\;s_{i,j,k}\;\frac{\Delta y}{2}\,\frac{T_{i,j,k-1}^{m+1}-T_{i,j,k}^{m+1}}{s_{i,j,k}} \\ &+ (h_{rg}+h_c)(2\,s_{i,j,k}\,\frac{\Delta y}{2})(T_g-T_{i,j,k}^{m+1}) \\ &+ h_{rw}(2\,s_{i,j,k}\,\frac{\Delta y}{2})(T_w-T_{i,j,k}^{m+1})+H\,\rho_{os}\,\frac{\lambda(2\,s_{i,j,k}\,\frac{\Delta y}{2})}{s_{i,j,k}}\end{aligned} \tag{3.44}$$

In the Eq. (3.44), the LHS represents an increase in internal energy within model cell volume. The first three terms of RHS are conduction into the model cell volume from surrounding oxide cells and the fourth term represents conduction into the model cell volume from surrounding steel cell. The fifth term represents convection and radiation across the two cell faces from hot gas. The sixth term represents radiation across the two cell faces from furnace wall. The seventh term of RHS accounts for heat of oxidation reaction for growth of oxide scale on the two cell faces.

Oxide edge -2 cell [refer Fig. 3.4(c)]:

$$\begin{aligned}\rho_{os}\, c_{os}\;\; s_{i,j,k}\Delta y\,s_{i,j,k}\,\frac{T_{i\,j,k}^{m+1}-T_{i,j,k}^{m}}{\Delta t} &= (k_{os})_{i,j,k}\;\Delta y\,s_{i,j,k}\,\frac{T_{i-1,j\,k}^{m+1}-T_{i,j,k}^{m+1}}{s_{i,j,k}} \\ &+ (k_{os})_{i,\;j+1/2,k}\,s_{i,j,k}\;\;s_{i,j,k}\,\frac{T_{i,j+1,k}^{m+1}-T_{i,j,k}^{m+1}}{\Delta y} \\ &+ (k_{os})_{i,\;j-1/2,k}\,s_{i,j,k}\;\;s_{i,j,k}\,\frac{T_{i,j-1,k}^{m+1}-T_{i,j,k}^{m+1}}{\Delta y} \\ &+ (k_{os})_{i,j,k}\;s_{i,j,k}\;\;\Delta y\,\frac{T_{i,j,k-1}^{m+1}-T_{i,j,k}^{m+1}}{s_{i,j,k}} \\ &+ (h_{rg}+h_c)(2\,s_{i,j,k}\Delta y)(T_g-T_{i,j,k}^{m+1}) \\ &+ h_{rw}(2\,s_{i,j,k}\Delta y)\,(T_w-T_{i,j,k}^{m+1}) \\ &+ H\,\rho_{os}\,\frac{\lambda(2\,s_{i,j,k}\Delta y)}{s_{i,j,k}}\end{aligned} \tag{3.45}$$

In the Eq. (3.45), the LHS represents an increase in internal energy within model cell volume. The first three terms of RHS are conduction into the model cell volume from surrounding oxide cells and the fourth term represents conduction into the model cell volume from surrounding steel cell. The fifth term represents convection and radiation across the two cell faces from hot gas. The sixth term represents radiation across the two cell faces from furnace wall. The seventh term of RHS accounts for heat of oxidation reaction for growth of oxide scale on the two cell faces.

Oxide surface -1 cell [refer Fig. 3.4(d)]:

$$\begin{aligned}\rho_{os}\, c_{os}\ \frac{\Delta x}{2}\frac{\Delta y}{2} s_{i,j,k}\frac{T_{i\,j,k}^{m+1}-T_{i,j,k}^{m}}{\Delta t} &= (k_{os})_{i,j,k}\ \frac{\Delta y}{2} s_{i,j,k}\frac{T_{i+1,jk}^{m+1}-T_{i,j,k}^{m+1}}{s_{i,j,k}} \\ &+ (k_{os})_{i-1/2,j,k}\ \frac{\Delta y}{2} s_{i,j,k}\frac{T_{i-1,jk}^{m+1}-T_{i,j,k}^{m+1}}{\Delta x} \\ &+ (k_{os})_{i,\ j,k}\ \frac{\Delta x}{2} s_{i,j,k}\frac{T_{i,j+1,k}^{m+1}-T_{i,j,k}^{m+1}}{s_{i,j,k}} \\ &+ (k_{os})_{i,\ j-1/2,k}\ \frac{\Delta x}{2} s_{i,j,k}\frac{T_{i,j-1,k}^{m+1}-T_{i,j,k}^{m+1}}{\Delta y} \\ &+ (k_{os})_{i,j,k}\ \frac{\Delta x}{2}\frac{\Delta y}{2}\frac{T_{i,j,k-1}^{m+1}-T_{i,j,k}^{m+1}}{s_{i,j,k}} \\ &+ (h_{rg}+h_{c})\frac{\Delta x}{2}\frac{\Delta y}{2}(T_{g}-T_{i,j,k}^{m+1}) \\ &+ h_{rw}\frac{\Delta x}{2}\frac{\Delta y}{2}(T_{w}-T_{i,j,k}^{m+1}) \\ &+ H\,\rho_{os}\frac{\lambda\left(\frac{\Delta x}{2}\frac{\Delta y}{2}\right)}{s_{i,j,k}}\end{aligned} \tag{3.46}$$

In the Eq. (3.46), the LHS represents an increase in internal energy within model cell volume. The first four terms of RHS are conduction into the model cell volume from surrounding oxide cells and the fifth term represents conduction into the model cell volume from surrounding steel cell. The sixth term represents convection and radiation across the one cell face from hot gas. The seventh term represents radiation across the one cell face from furnace wall. The eighth term of RHS accounts for heat of oxidation reaction for growth of oxide scale on the one cell face.

Oxide surface -2 cell [refer Fig. 3.4(e)]:

$$\begin{aligned}\rho_{os}\, c_{os}\ \frac{\Delta x}{2}\Delta y\, s_{i,j,k}\frac{T_{i\,j,k}^{m+1}-T_{i,j,k}^{m}}{\Delta t} &= (k_{os})_{i,j,k}\ \Delta y\, s_{i,j,k}\frac{T_{i+1,jk}^{m+1}-T_{i,j,k}^{m+1}}{s_{i,j,k}} \\ &+ (k_{os})_{i-1/2,j,k}\ \Delta y\, s_{i,j,k}\frac{T_{i-1,jk}^{m+1}-T_{i,j,k}^{m+1}}{\Delta x} \\ &+ (k_{os})_{i,\ j+1/2,k}\frac{\Delta x}{2}s_{i,j,k}\frac{T_{i,j+1,k}^{m+1}-T_{i,j,k}^{m+1}}{\Delta y} \\ &+ (k_{os})_{i,\ j-1/2,k}\frac{\Delta x}{2}s_{i,j,k}\frac{T_{i,j-1,k}^{m+1}-T_{i,j,k}^{m+1}}{\Delta y} \\ &+ (k_{os})_{i,j,k}\frac{\Delta x}{2}\Delta y\frac{T_{i,j,k-1}^{m+1}-T_{i,j,k}^{m+1}}{s_{i,j,k}} \\ &+ (h_{rg}+h_{c})\frac{\Delta x}{2}\Delta y\,(T_{g}-T_{i,j,k}^{m+1}) \\ &+ h_{rw}\frac{\Delta x}{2}\Delta y\ (T_{w}-T_{i,j,k}^{m+1}) \\ &+ H\,\rho_{os}\frac{\lambda\left(\frac{\Delta x}{2}\Delta y\right)}{s_{i,j,k}}\end{aligned} \tag{3.47}$$

In the Eq. (3.47), the LHS and RHS energy terms refer to heat exchanges which are identical to the previous equation [Eq. (3.46)]. However, the terms differ because of different cell dimensions.

The nodal volume energy equilibrium equations are derived for all cells, where appropriately changed parameters are used for derivation corresponds to other directions.

3.7.2 Steel discretization

Fig. 3.5 shows the basic steel cells and nodal system, which is observed at the interface of oxide scale and steel surface. The third dimensions (along z-directions) of different cells (Fig. 3.5) are set equal to $\Delta z/2$.

Essentially four basic steel cells exist: steel corner cell, steel edge cell, steel surface cell and steel internal cell. Fig. 3.6 shows the 3D view of basic steel cells along with nodes of interest, wherein each cell is exposed to conduction from all six surrounding cells. In the Fig. 3.6, the model steel cells (shown in dark gray color) are surrounded by oxide cells (shown in light grey color) and steel cells (shown in white color).

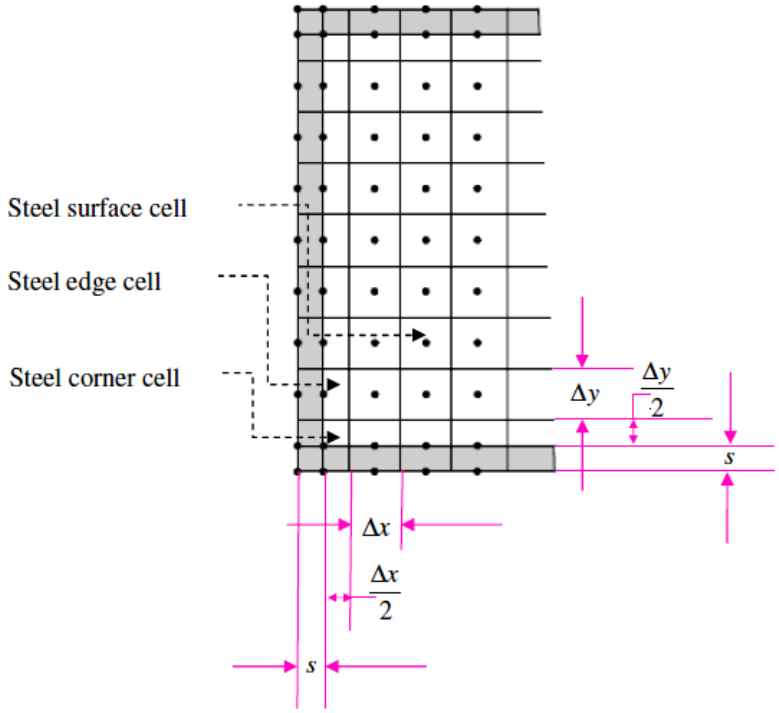

Fig. 3.5: Basic steel surface cells and the nodal system observed at the interface of oxide scale and steel

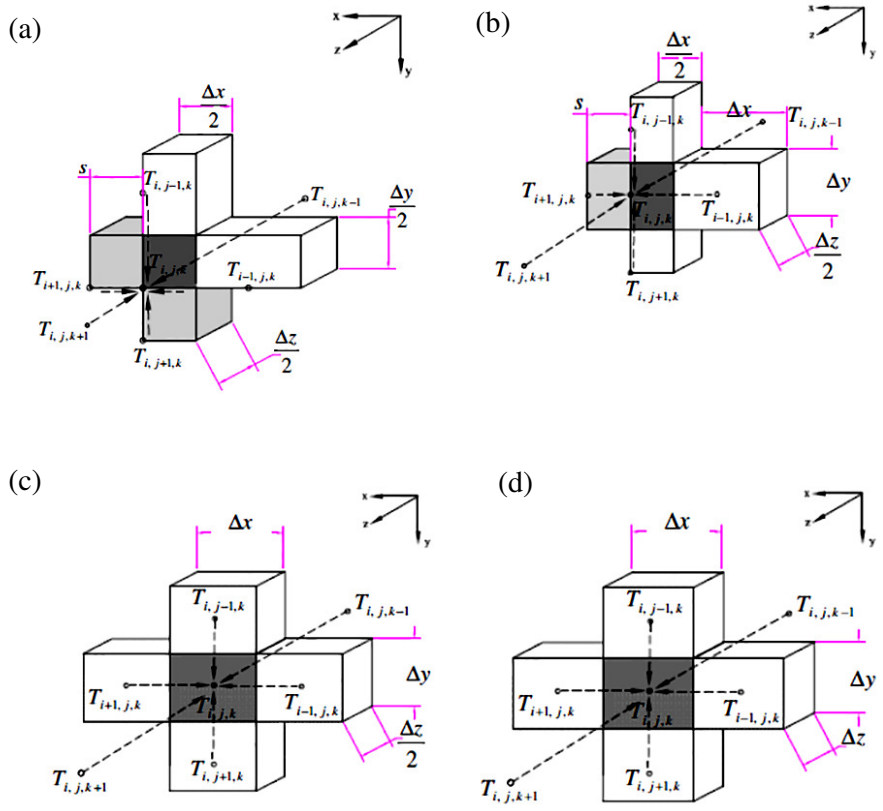

Fig. 3.6: Basic steel cells: (a) steel corner cell (b) steel edge cell (c) steel surface cell (d) steel internal cell

Steel corner cell: The steel corner cell, such as those shown in Fig 3.6(a) have half dimensions and exposed to conduction from three surrounding oxide cells, and three steel cells. The model cell as shown above is surrounded by three oxide cells (shown in gray color) representing the index $i+1, j, k$, $i, j+1, k$ and $i, j, k+1$. The implicit finite difference equation for this steel corner cell is expressed as:

$$\begin{aligned}\rho_{st}\, c_{st}\, \frac{\Delta x \Delta y \Delta z}{8} \frac{T^{m+1}_{i,\,j,\,k} - T^{m}_{i,\,j,\,k}}{\Delta t} &= (k_{os})_{i+1,\,j,\,k} \frac{\Delta y\ \Delta z}{4} \frac{T^{m+1}_{i+1,\,j\,k} - T^{m+1}_{i,\,j,\,k}}{s_{i,\,j,\,k}} \\ &+ (k_{st})_{i-1/2,\ j,\ k} \frac{\Delta y \Delta z}{4} \frac{T^{m+1}_{i-1,\,j,\,k} - T^{m+1}_{i,\,j,\,k}}{\Delta x} \\ &+ (k_{os})_{i,\ j+1,\ k} \frac{\Delta x \Delta z}{4} \frac{T^{m+1}_{i,\,j+1,\,k} - T^{m+1}_{i,\,j,\,k}}{s_{i,\,j,\,k}} \\ &+ (k_{st})_{i,\ j-1/2,k} \frac{\Delta x \Delta z}{4} \frac{T^{m+1}_{i,\,j-1,\,k} - T^{m+1}_{i,\,j,\,k}}{\Delta y} \\ &+ (k_{os})_{i,\,j,k+1} \frac{\Delta x \Delta y}{4} \frac{T^{m+1}_{i,\,j,k+1} - T^{m+1}_{i,\,j,\,k}}{s_{i,\,j,\,k}} \\ &+ (k_{st})_{i,\,j,k-1/2} \frac{\Delta x \Delta y}{4} \frac{T^{m+1}_{i,\,j,k-1} - T^{m+1}_{i,\,j,\,k}}{\Delta z}\end{aligned} \tag{3.48}$$

In the Eq. (3.48), the LHS represents increase in internal energy within model cell volume and first, third and fifth terms of RHS are conduction into the model cell volume from surrounding oxide cell. The second, fourth and sixth terms are conduction into the model cell volume from surrounding steel cell. In the above Eq. (3.48), density of steel is assumed constant, whereas steel thermal conductivity (k_{st}), specific heat (c_{st}) and oxide scale thickness (s) are function of nodal temperature, which are evaluated at the temperature corresponding to the previous iteration.

As discussed earlier thermal conductivities of oxide scale and steel at the interface (representing the face of model cell) placed midway between the nodes are calculated using the harmonic mean approach (Patankar, 1980). For instance, the steel thermal conductivity at the interfaces are expressed as:

$$(k_{st})_{i+1/2,\,j,\,k} = \frac{2(k_{st})_{i,\,j,\,k}\,(k_{st})_{i+1,\,j,\,k}}{(k_{st})_{i,\,j,\,k} + (k_{st})_{i+1,\,j,\,k}} \tag{3.49}$$

$$(k_{st})_{i-1/2,\,j,\,k} = \frac{2(k_{st})_{i,\,j,\,k}\,(k_{st})_{i-1,\,j,\,k}}{(k_{st})_{i,\,j,\,k} + (k_{st})_{i-1,\,j,\,k}} \tag{3.50}$$

$$(k_{st})_{i,\,j+1/2,\,k} = \frac{2(k_{st})_{i,\,j,\,k}\,(k_{st})_{i,\,j+1,\,k}}{(k_{st})_{i,\,j,\,k} + (k_{st})_{i-1,\,j+1,\,k}} \tag{3.51}$$

$$(k_{st})_{i,\,j-1/2,\,k} = \frac{2(k_{st})_{i,\,j,\,k}\,(k_{st})_{i,\,j-1,\,k}}{(k_{st})_{i,\,j,\,k} + (k_{st})_{i-1,\,j-1,\,k}} \tag{3.52}$$

$$(k_{st})_{i,\,j,\,k+1/2} = \frac{2(k_{st})_{i,\,j,\,k}\,(k_{st})_{i,\,j,\,k+1}}{(k_{st})_{i,\,j,\,k} + (k_{st})_{i-1,\,j,\,k+1}} \tag{3.53}$$

$$(k_{st})_{i,\,j,\,k-1/2} = \frac{2(k_{st})_{i,\,j,\,k}\,(k_{st})_{i,\,j,\,k-1}}{(k_{st})_{i,\,j,\,k} + (k_{st})_{i-1,\,j,\,k-1}} \tag{3.54}$$

Steel edge cell: The steel edge cell as shown in Fig. 3.6(b), is exposed to conduction from two surrounding oxide cells (shown in gray color) and four steel cells. The two oxide cells that surround model cell representing the index $i+1, j, k$ and $i, j, k+1$. The implicit finite difference equation for this steel edge cell is expressed as:

$$\begin{aligned}
\rho_{st}\,c_{st}\,\frac{\Delta x}{2}\Delta y\frac{\Delta z}{2}\frac{T^{m+1}_{i,\,j,\,k} - T^{m}_{i,\,j,k}}{\Delta t} = {} & (k_{os})_{i+1,\,j,\,k}\,\Delta y\frac{\Delta z}{2}\,\frac{T^{m+1}_{i+1,\,jk} - T^{m+1}_{i,\,j,k}}{s_{i,\,j,k}} \\
& + (k_{st})_{i-1/2,\,j,\,k}\,\Delta y\frac{\Delta z}{2}\frac{T^{m+1}_{i-1,\,j,\,k} - T^{m+1}_{i,\,j,k}}{\Delta x} \\
& + (k_{st})_{i,\,j+1/2,\,k}\,\frac{\Delta x}{2}\frac{\Delta z}{2}\frac{T^{m+1}_{i,\,j+1,\,k} - T^{m+1}_{i,\,j,k}}{\Delta y} \\
& + (k_{st})_{i,\,j-1/2,k}\,\frac{\Delta x}{2}\frac{\Delta z}{2}\frac{T^{m+1}_{i,\,j-1,\,k} - T^{m+1}_{i,\,j,k}}{\Delta y} \\
& + (k_{os})_{i,\,j,k+1}\,\frac{\Delta x}{2}\Delta y\frac{T^{m+1}_{i,\,j,k+1} - T^{m+1}_{i,\,j,k}}{s_{i,\,j,\,k}} \\
& + (k_{st})_{i,\,j,k-1/2}\,\frac{\Delta x}{2}\Delta y\frac{T^{m+1}_{i,\,j,k-1} - T^{m+1}_{i,\,j,k}}{\Delta z}
\end{aligned} \tag{3.55}$$

In the Eq. (3.55), the first and fifth terms of RHS represent conduction into the model cell volume from surrounding oxide cell. The second, third, fourth and sixth terms are conduction into the model cell volume from surrounding steel cell.

Steel surface cell: The steel surface cell as illustrated in Fig. 3.6(c) is exposed to conduction from one oxide cell and five steel cells. The index of oxide cell which surrounds model cell is $i, j, k+1$. The discretization equation for this steel surface cell is expressed as:

$$\begin{aligned}\rho_{st}\, c_{st}\ \Delta x\Delta y\frac{\Delta z}{2}\frac{T_{i,\,j,\,k}^{m+1}-T_{i,\,j,k}^{m}}{\Delta t} &= (k_{st})_{i+1/2,\,j,k}\,\Delta y\frac{\Delta z}{2}\,\frac{T_{i+1,\,jk}^{m+1}-T_{i,\,j,k}^{m+1}}{\Delta x}\\ &+(k_{st})_{i-1/2,\ j,\ k}\,\Delta y\frac{\Delta z}{2}\frac{T_{i-1,\,j,k}^{m+1}-T_{i,\,j,k}^{m+1}}{\Delta x}\\ &+(k_{st})_{i,\ j+1/2,\ k}\,\Delta x\frac{\Delta z}{2}\frac{T_{i,\,j+1,k}^{m+1}-T_{i,\,j,k}^{m+1}}{\Delta y}\\ &+(k_{st})_{i,\ j-1/2,k}\,\Delta x\frac{\Delta z}{2}\frac{T_{i,\,j-1,k}^{m+1}-T_{i,\,j,k}^{m+1}}{\Delta y}\\ &+(k_{os})_{i,\,j,k+1}\,\Delta x\Delta y\frac{T_{i,\,j,k+1}^{m+1}-T_{i,\,j,k}^{m+1}}{s_{i,\,j,\,k}}\\ &+(k_{st})_{i,\,j,k-1/2}\,\Delta x\Delta y\frac{T_{i,\,j,k-1}^{m+1}-T_{i,\,j,k}^{m+1}}{\Delta z}\end{aligned} \tag{3.56}$$

In the Eq. (3.56), the fifth term of RHS represents conduction into the model cell volume from surrounding oxide cell and other five terms are conduction into the model cell volume from surrounding steel cell.

Steel internal cell: A general interior steel cell, denoted as steel internal cell, such as those shown in Fig. 3.6(d), is exposed to conduction from all six surrounding steel cells. The energy equilibrium equation for steel internal cell is given as:

$$\begin{aligned}\rho_{st}\, c_{st}\ \Delta x\,\Delta y\,\Delta z\frac{T_{i,\,j,k}^{m+1}-T_{i,\,j,k}^{m}}{\Delta t} &= (k_{st})_{i+1/2,\,j,\,k}\,\Delta y\,\Delta z\,\frac{T_{i+1,\,j,k}^{m+1}-T_{i,\,j,k}^{m+1}}{\Delta x}\\ &+(k_{st})_{i-1/2,\,j,\,k}\,\Delta y\,\Delta z\frac{T_{i-1,\,j,k}^{m+1}-T_{i,\,j,k}^{m+1}}{\Delta x}\\ &+(k_{st})_{i,\,j+1/2,\,k}\,\Delta x\,\Delta z\frac{T_{i,\,j+1,k}^{m+1}-T_{ijk}^{m+1}}{\Delta y}\\ &+(k_{st})_{i,\ j-1/2,\ k}\,\Delta x\,\Delta z\frac{T_{i,\,j-1,k}^{m+1}-T_{i,\,j,k}^{m+1}}{\Delta y}\\ &+(k_{st})_{i,\,j,\,k+1/2}\,\Delta x\,\Delta y\frac{T_{i,\,j,\,k+1}^{m+1}-T_{i,\,j,k}^{m+1}}{\Delta z}\\ &+(k_{st})_{i,\,j,\,k-1/2}\,\Delta x\,\Delta y\frac{T_{i,\ j,\ k-1}^{m+1}-T_{i,\,j,k}^{m+1}}{\Delta z}\end{aligned} \tag{3.57}$$

In the Eq. (3.57), the LHS represents increase in internal energy within model cell volume and the all six terms of RHS are conduction into the model cell volume from surrounding steel cell.

The nodal volume energy equilibrium equations are derived for all basic types of cells. All basic cells equations with appropriately changed parameters are used for derivations of other corners, edges, surfaces and internal cells discretized equation.

3.8 Closure

This chapter described the development of 3D transient heat conduction model for reheat simulation. The model is based on control volume approach of FDM formulation and is considering growth of oxide scale, oxidation reaction heat, radiation from furnace walls and gases. It also considers skid cooling and radiation shadowing effect of skid structure. The model considers temperature dependent material properties such as thermal conductivity and specific heat for steel and oxide scale. The model captures various time dependent boundary conditions corresponding to the billet reheat in the reheat furnace. Computer implementation of developed model, solution methodology and validation studies of developed model will be presented in the next chapter.

Chapter 4

Computer Implementation and Validation of Reheat Model

4.1 Introduction

In the chapter 3, a numerical model was developed for solving the governing differential equation to predict the 3D temperature field and the growth of oxide scale applied to steel billet reheating. This chapter presents the computer implementation and validation study of the developed numerical model. The first section gives the computer implementation of numerical model which includes the procedure of MATLAB® code development. This includes discussions on mesh variables, data structure and functions. The remainder of this chapter is devoted for the validation study. In order to validate the proposed model, first the numerical results are compared with analytical solutions subjected to limited conditions. This is followed by second validation study, where results of proposed numerical model are compared with published experimental results. Finally some closure remarks are presented.

4.2 Computer Implementation

In describing the computer implementations for the developed numerical model for heat transfer simulation during steel billet reheat, the overall methodology for model solution using different module is first described. Next, the code development procedures are detailed.

4.2.1 Overall methodology of simulations

In order to simulate steel billet reheating, present study considers 3D transient heat conduction in the steel billet and oxide scale. The 3D transient heat conduction is modeled using control volume approach of FDM as detailed in the previous chapter. The radiation heat transfer is included as heat flux on the steel billet surfaces, where emissive and absorptive behavior of combustion gases is approximated by WSGGM (Hottel and Sarofim, 1967; Smith et al., 1982). The radiative heat fluxes on the billet surfaces are calculated based on billet surface, furnace gas and wall temperatures. Whereas the

convection heat transfer is included as heat flux on the steel billet surfaces, using constant convection heat transfer coefficient, furnace gas and billet surface temperatures. The radiative and convective heat transfer coefficients for heat flux on the billet surfaces are initially calculated considering assumed initial temperature field, furnace gas and furnace wall temperature. The flow chart shown in Fig. 4.1 presents outline of overall simulation process.

3D temperature field in the billet and oxide thickness on the billet surfaces are obtained by solving transient heat conduction discretized equations. The solution of equations set is obtained by an iterative process. The Gauss-Seidel (GS) algorithm is implemented through own developed MATLAB® code. The temperature dependent thermo-physical properties of steel billet and oxide scale are updated using time lag approach (Ozisik, 1993). The transient conduction solution is considered to have converged when fractional change of temperature that obtained from previous iteration satisfies the chosen convergence criterion. The heat transfer coefficients corresponding to the billet surface heat flux are then updated. The oxide scale thickness is also calculated and updated by parabolic oxidation growth rate equation as discussed in previous model development chapter.

At the early stages of simulations, the calculated oxide thickness (with 298 K initial temperature of billet and small time steps) is found to be much smaller than the steel cell dimensions. This results in a poor conditioned coefficient matrix and the 3D numerical model does not converge. In order to overcome this difficulty, simulations were performed with an initial assumed thickness of 0.01 mm. Oxide scale thicknesses computed from the model (with assumed small thickness at the beginning) are compared with the actual oxide thicknesses, calculated from rate law equations and in the event it exceeds the actual value, the assumed thickness is replaced by the actual calculated value. However, the reaction heat terms, are always calculated using the actual calculated scale thickness. It is obvious that the negligible initial thickness exercise made at the beginning of the simulation, have an almost negligible effect on the predicted temperature field and oxide scale thickness in succeeding iterations.

To facilitate the procedure discussed above for steel billet reheat numerical model solution a MATLAB® computer code has been developed. A short description of this code is given in the next sub section.

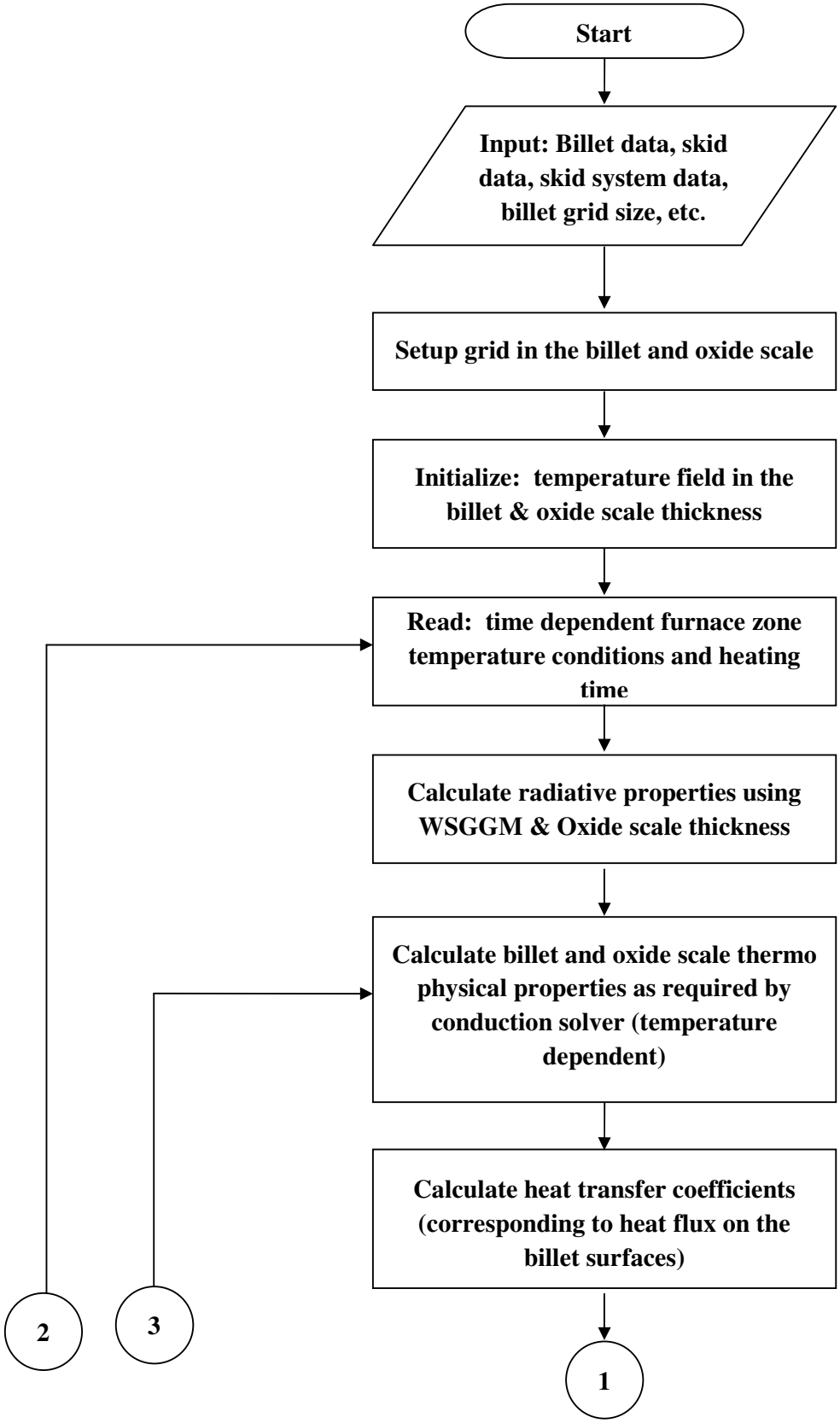
Start
Input: Billet data, skid data, skid system data, billet grid size, etc.
Setup grid in the billet and oxide scale
Initialize: temperature field in the billet & oxide scale thickness
Read: time dependent furnace zone temperature conditions and heating time
Calculate radiative properties using WSGGM & Oxide scale thickness
Calculate billet and oxide scale thermo physical properties as required by conduction solver (temperature dependent)
Calculate heat transfer coefficients (corresponding to heat flux on the billet surfaces)
2
3
1

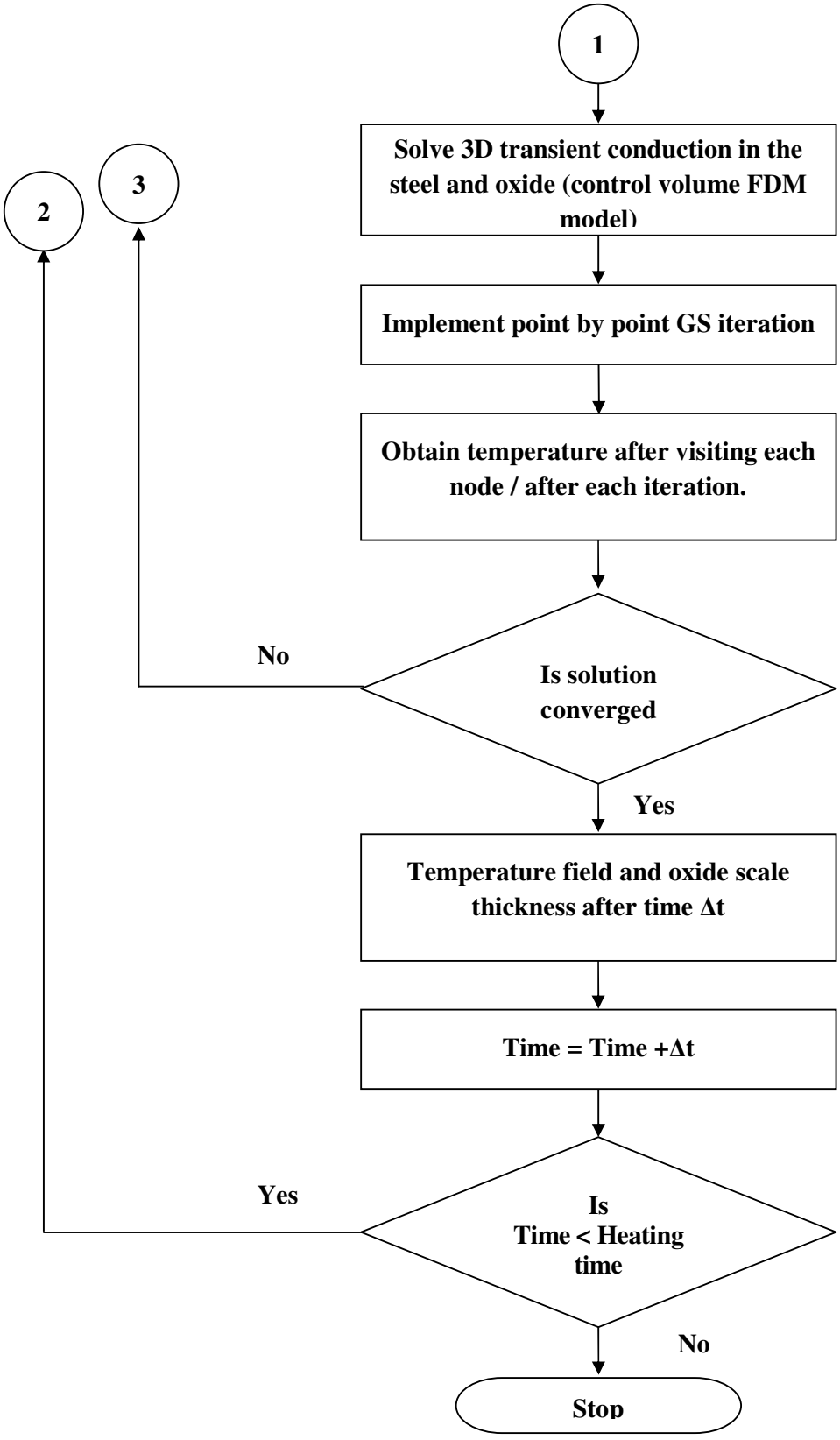

Fig. 4.1: Flow chart for the outline of the steel billet reheat simulation process

4.2.2 Mesh variable and data structure

MATLAB® is a high level scientific computing language, which is best suited for matrix operations (Hanselman and Bruce, 2011). In this work a MATLAB® computer code is developed for the solution of proposed 3D numerical model. This section gives details of routine designs employed for prescribing a range of boundary conditions and solution of discretized equations. The developed code is flexible enough to accommodate and simulate various aspects of practical situations.

The solution domain which in our case, the billet is divided into number of control-volumes (finite volumes). In the computer implementation, node of each control volume is numbered in a sequence which is based on billet dimension and grid size input. Here a mesh is defined for steel billet with oxide scale, which has uniform steel control volume size in a coordinate direction. The size of steel control volumes in different directions need not be same. In the computer implementation, the location of the node will be stored as variables. For the 3D solution domain with oxide scale the nodal values could be naturally stored in 3D array (*i, j, k*) where the indices *i*, *j* and *k* run for $1 \le i \le nx$, $1 \le j \le ny$, and $1 \le k \le nz$ respectively. Here *nx*, *ny* and *nz* are number of nodes, which are given as:

$$nx = \frac{X}{\Delta x} + 3 \tag{4.1}$$

$$ny = \frac{Y}{\Delta y} + 3 \tag{4.2}$$

$$nz = \frac{Z}{\Delta z} + 3 \tag{4.3}$$

In the above expressions *X*, *Y* and *Z* represent steel billet dimension in *x*-direction, *y*-direction and *z*-direction respectively. Whereas Δx, Δy and Δz represent space between two steel control volume nodes in *x*-direction, *y*-direction and *z*-direction respectively. There are $nx-2$ steel control volume nodes and 2 oxide control volume nodes are specified in the *x*-direction. Similar definitions are used for *y*- and *z*-directions. Alternatively, one can store the nodal values in a vector **n** where $n = 1,2,3,\ldots,N,$ where *N* is the total number of nodes. Considering the 3D domain with *nx*, *ny*, *nz* nodes in *x*-, *y*- and *z*-direction respectively, gives $nx \times ny \times nz$ the total number of nodes. Natural ordering approach, where the nodal values are stored in 1D vector is

chosen for computer implementations in the present study, the rationale for this selection is to make the program computationally efficient and fast. Although, with 3D data storage; it is easy to program, but it makes the program computationally less efficient. Further details about data structure in scientific computations are available in Golub and Ortega (1993).

The data of 3D grid can be mapped to 1D array using natural ordering, for example the typical node *(i, j, k)* is given by:

$$n = i + (j-1)\,nx + (k-1)\,nx \times ny \tag{4.4}$$

With this natural ordering scheme the neighbors of a typical node (*i, j, k*) as given in the model development section have indices:

$$(i+1, j, k) = n+1 \tag{4.5}$$

$$(i-1, j, k) = n-1 \tag{4.6}$$

$$(i, j+1, k) = n+nx \tag{4.7}$$

$$(i, j-1, k) = n-nx \tag{4.8}$$

$$(i, j, k+1) = n+nx \times ny \tag{4.9}$$

$$(i, j, k-1) = n-nx \times ny \tag{4.10}$$

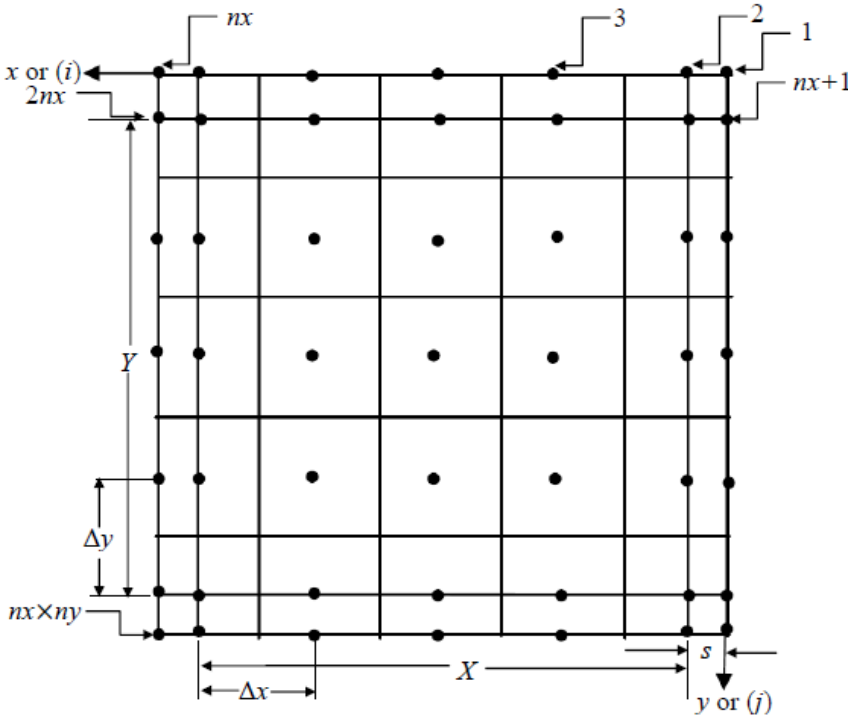

Fig. 4.2: Scheme for numbering of nodes shown on *x-y* plane: observed at outer oxide surface (at *k* = 1) in *z*-direction

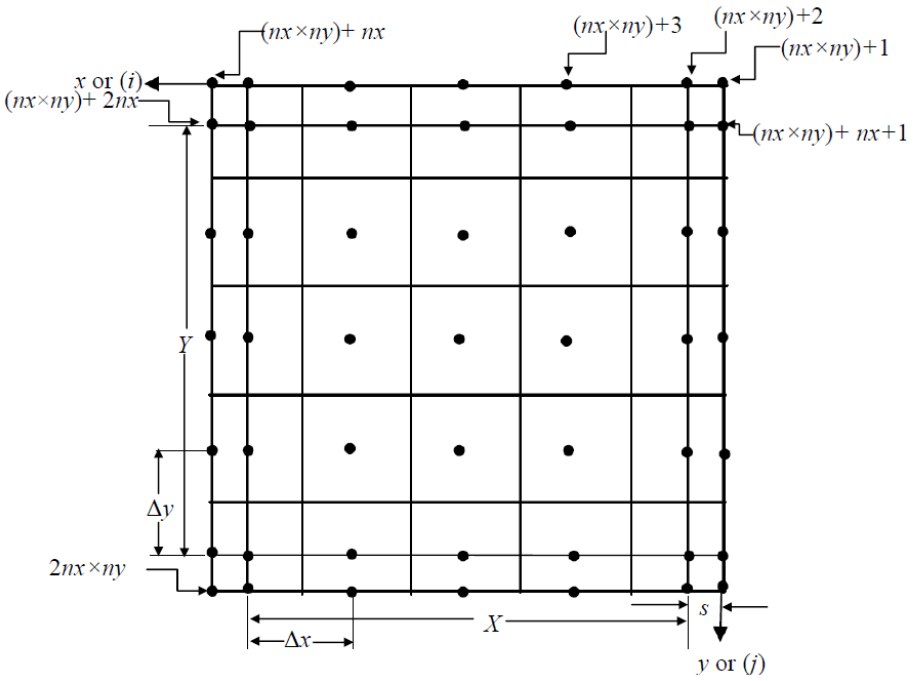

Fig. 4.3: Scheme for numbering of nodes shown on *x-y* plane: observed at the interface (*x-y* plane at *k* = 2) of oxide scale and steel surface in *z*-direction

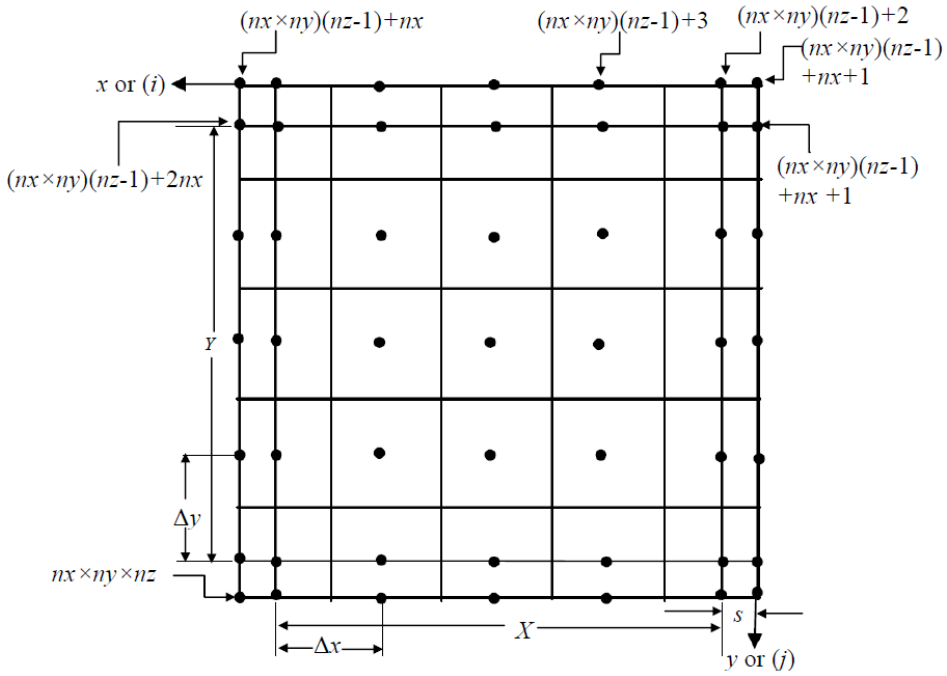

Fig. 4.4: Scheme for numbering of nodes shown on *x-y* plane: observed at outer oxide surface (at *k* = *nz*) in *z*-direction

Fig. 4.2 shows domain of width X in x-direction and height Y in y-direction, so that it represents an outer oxide surface on x-y plane of the steel billet. (The plane corresponds to k =1) The third dimension along z-direction is equal to the oxide scale thickness. The control volumes are depicted by the lines that define boundaries of the control volumes. These boundaries of control volumes are termed as interfaces of control volume. The nodes of each control volume are designated by black circles. The patterns created by the lines are termed as computational grids. The nodes in the computational domain are indicated by a single number (n) called as node indices. In the Fig. 4.2 nodes are indicated by number 1 to $nx \times ny$ according to Eqs. (4.4) to (4.8).

Fig. 4.3 shows computational grids, which is observed at the interface (x-y plane at k = 2) of oxide scale and steel surface in z-direction. The nodes are indicated by numbers from $(nx \times ny)+1$ to $(2 \times nx \times ny)$ according to Eqs. (4.4) to (4.10).

Fig. 4.4 shows computational grids, which is observed at the outer oxide surface (x-y plane at $k = nz$) in z-direction. Here, the nodes are indicated by numbers from $((nz-1) \times nx \times ny)+1$ to $(nx \times ny \times nz)$ according to Eqs. (4.4) to (4.10).

The nodal values of temperature, oxide scale thickness, etc., can be stored in a vector **n**, where **n** takes a positive value from 1 to N as discussed. Hence, values of unknowns ϕ (for example) with node index (i, j, k) of 3D array and corresponding ϕ with node index (n) of 1D vector with natural ordering can be represented as:

$$\begin{bmatrix} \phi_{1,1,1} \\ \phi_{2,1,1} \\ \vdots \\ \phi_{nx,1,1} \\ \phi_{1,2,1} \\ \phi_{2,2,1} \\ \vdots \\ \phi_{nx,ny,1} \\ \phi_{1,1,2} \\ \phi_{2,1,2} \\ \vdots \\ \phi_{i,j,k} \\ \vdots \\ \phi_{nx,ny,nz} \end{bmatrix} \Leftrightarrow \begin{bmatrix} \phi_1 \\ \phi_2 \\ \vdots \\ \phi_{nx} \\ \phi_{nx+1} \\ \phi_{nx+2} \\ \vdots \\ \phi_{nx \times ny} \\ \phi_{nx \times ny+1} \\ \phi_{nx \times ny+2} \\ \vdots \\ \phi_n \\ \vdots \\ \phi_N \end{bmatrix} \tag{4.11}$$

To accomplish this task a MATLAB® routine is developed. The developed routine transforms the node data specified by billet dimension and control volume width from 3D array to 1D vector. Additionally, the data of 1D vector can be mapped back to 3D array using developed routine. The 3D array was used to evaluate 2D and 3D plots at the end of computations.

4.2.3 Methodology for development of functions & routines

The outline below is generic MATLAB® functions developed for simulation:

4.2.3.1 Main program

The developed MATLAB® functions (routine) which are interacting with main program; functions for mesh generation and categorization of nodes, functions for system of matrices from discretized equations and function for the solution of the system of matrices (conduction solver). Main program that sends information such as input parameters to and receive information such as temperature field and oxide scale thickness data from above said routines. Additionally, this main program calls a routine that receives numerical model output data, further this 3D temperature field of the billet and oxide scale growth data stored in a matrix which were suitably utilized by 2D contour, surface and 3D slice plotting routines.

4.2.3.2 Functions for mesh generation and categorization of the nodes

This function is used for mesh generation as per procedure discussed earlier. Additionally, this function calls other subroutines which were developed to return groups of nodes such as oxide cell nodes and steel cell nodes, corner nodes, edge nodes, surface nodes and internal, nodes, etc. Similarly, there is a subroutine that returns information of the nodes which are in contact with skid and the nodes which in between the two skids beams.

Function for system of matrices from discretized equations

This function sends information such as system of matrices to the conduction solver function and main program. The function receives information such as: input parameters, node groups, surface and furnace gas radiative properties from main program, node categorization function and WSGGM function respectively. The temperature dependent expressions for billet and oxide thermo-physical properties are defined in the functions. The function also contains expressions for heat transfer coefficients and other temperature dependent expressions required for consideration of oxide scale growth and skid effect.

In order to determine temperature field form the discretized equations requires solving of the system of matrices as given by

$$\mathrm{A}\,T = b \tag{4.12}$$

where, **A** is $(N \times N)$ matrix and **T** and **b** are $(N \times 1)$ vector, N is total number nodes, which is equal to $nx \times ny \times nz$ as discussed previously. Here coefficient matrix ***A***, consists of the coefficients of discretized equations conduction, convection, radiation and storage terms which are calculated at the current temperature corresponds to the previous iteration. Whereas the RHS vector ***b*** consists of scale heat reaction, product of heat transfer coefficient and furnace gas temperature and storage terms. The storage term and furnace gas are considered at temperature corresponds to temperature at the beginning of the time step. The structure of matrix system is given as:

$$\begin{bmatrix} A_{1,1} & A_{1,2} & \cdots & \cdots & \cdots \\ A_{2,1} & A_{2,2} & A_{2,3} & \cdots & \cdots \\ \vdots & & \ddots & & \\ \vdots & & & \ddots & \\ \cdots & \cdots & \cdots & A_{N,N-1} & A_{N,N} \end{bmatrix} \begin{bmatrix} T_1^{m+1} \\ T_2^{m+1} \\ \vdots \\ \vdots \\ \vdots \\ T_N^{m+1} \end{bmatrix} = \begin{bmatrix} b_1 \\ b_2 \\ \vdots \\ \vdots \\ \vdots \\ b_N \end{bmatrix} \tag{4.13}$$

The coefficient matrix ***A***, is multiband for the present 3D solution domain. A MATLAB® function is developed that returns coefficient matrix ***A*** and vector ***b***. The developed routine evaluates each element of matrix ***A*** and vector ***b*** from energy balance equations and store it to the respective matrices. The procedure for evaluation of element of the matrix ***A*** and vector ***b*** from energy balance equations are illustrated through flowing two example cases.

Example case 1 (a), oxide inner surface node on *x-y* plane: For instance, if we consider an oxide inner cell, on *x-y* plane, such as those shown in Fig. 3.4(f), the elements of the matrix **A**, which correspond to its energy equilibrium equation (refer Eq. (3.36)) given in the previous chapter), are expressed as:

$$\begin{aligned} A_{n,n} = \rho_{os}\,(c_{os})_n \frac{\Delta x \Delta y\; s_n}{\Delta t} &+ (k_{os})_n^e \frac{\Delta y\; s_n}{\Delta x} + (k_{os})_n^w \frac{\Delta y\; s_n}{\Delta x} + (k_{os})_n^n \frac{\Delta x\; s_n}{\Delta y} \\ &+ (k_{os})_n^s \frac{\Delta x\; s_n}{\Delta y} + (k_{os})_n \frac{\Delta x \Delta y}{s_n} + ((h_{rg})_n + h_c)\Delta x \Delta y + (h_{rw})_n\; \Delta x \Delta y \end{aligned} \tag{4.14}$$

where, $A_{n,n}$ refers to the element in row n^{th} and column n^{th} of matrix $\boldsymbol{A}$. The other notations have usual meanings. In computing the thermal properties, the subscript n indicates properties that were evaluated at the previous iteration temperature values of the n^{th} node. The oxide scales thermal conductivities at the interface (representing the face of model cell) placed midway are represented by superscripts. Here superscripts: e and w denote faces of the chosen cell along the x-directions; n and s denote faces of the chosen cell along y-directions and t and b denote faces of the chosen cell along z-directions.

The following expressions are used to calculate the elements of $\boldsymbol{A}$, contributed by conduction from surrounding nodes:

$$A_{n,n-1} = -(k_{os})_n^e \frac{\Delta y \; s_n}{\Delta x} \tag{4.15}$$

$$A_{n,n+1} = -(k_{os})_n^w \frac{\Delta y \; s_n}{\Delta x} \tag{4.16}$$

$$A_{n,n-nx} = -(k_{os})_n^n \frac{\Delta x \; s_n}{\Delta y} \tag{4.17}$$

$$A_{n,n+nx} = -(k_{os})_n^s \frac{\Delta x \; s_n}{\Delta y} \tag{4.18}$$

For plane at $z = 0$

$$A_{n,n+nx*ny} = -(k_{os})_n \frac{\Delta x \; \Delta y}{s_n} \tag{4.19}$$

or for plane at $z = Z$

$$A_{n,n-nx*ny} = -(k_{os})_n \frac{\Delta x \; \Delta y}{s_n} \tag{4.20}$$

Similarly the elements of vector $\boldsymbol{b}$, which correspond to its energy equilibrium equation as referred above, can be expressed as:

$$\begin{aligned} b_n = \rho_{os} (c_{os})_n \; \frac{\Delta x \Delta y \; s_n}{\Delta t} T_n + ((h_{rg})_n + h_c) \Delta x \Delta y T_g \\ + (h_{rw})_n \Delta x \Delta y T_w + H \rho_{os} \frac{\lambda_n \; \Delta x \Delta y}{s_n} \end{aligned} \tag{4.21}$$

While computations of specific heat c_{os} and T_n of Eqn. 4.21 were evaluated at the temperature values of n^{th} node corresponds to the beginning of the time step.

Example case 1(b), oxide inner surface node on *y-z* plane: Similarly for oxide scale inner surface cell on *y-z* plane the elements of the matrix ***A*** which correspond to its energy equilibrium equation, are expressed as:

$$A_{n,n} = \rho_{os}\,(c_{os})_n\,\frac{\Delta y\,\Delta z\,s_n}{\Delta t} + (k_{os})_n^n\,\frac{\Delta z\;s_n}{\Delta y} + +(k_{os})_n^s\,\frac{\Delta z\;s_n}{\Delta y} + (k_{os})_n^t\,\frac{\Delta y\;s_n}{\Delta z} + (k_{os})_n^b\,\frac{\Delta y\;s_n}{\Delta z} + (k_{os})_n\,\frac{\Delta y\,\Delta z}{s_n} + ((h_{rg})_n + h_c)\,\Delta y\Delta z\; + (h_{rw})_n\,\Delta y\,\Delta z \tag{4.22}$$

Elements of **A,** contributed by conduction from surrounding nodes:

$$A_{\,n,n-nx} = -(k_{os})_n^n\,\frac{\Delta z\;s_n}{\Delta y} \tag{4.23}$$

$$A_{n,n+nx} = -\,(k_{os})_n^s\,\frac{\Delta z\;s_n}{\Delta y} \tag{4.24}$$

$$A_{n,n-nx*ny} = -\,(k_{os})_n^t\,\frac{\Delta y\;s_n}{\Delta z} \tag{4.25}$$

$$A_{\,n,n+nx*ny} = -\,(k_{os})_n^b\,\frac{\Delta y\;s_n}{\Delta z} \tag{4.26}$$

For plane at $x = 0$

$$A_{\,n,n+1} = -\,(k_{os})_n\,\frac{\Delta y\Delta z}{s_n} \tag{4.27}$$

or for plane at $x = X$

$$A_{\,n,n-1} = -\,(k_{os})_n\,\frac{\Delta y\Delta z}{s_n} \tag{4.28}$$

Elements of vector **b**:

$$b_n = \rho_{os}\,(c_{os})_n\,\frac{\Delta y\Delta z\;s_n}{\Delta t}\,T_n + ((h_{rg})_n + h_c)\,\Delta y\Delta z\,T_g + (h_{rw})_n\,\Delta y\Delta z T_w + H\;\rho_{os}\,\frac{\lambda_n\;\Delta y\Delta z}{s_n} \tag{4.29}$$

Example case 1(c), oxide inner surface node on *x-z* plane: Similarly for oxide scale inner surface cell on *x-z* plane the elements of the matrix ***A*** and ***b*** which correspond to its energy equilibrium equation are expressed as:

$$A_{n,n} = \rho_{os}\,(c_{os})_n\,\frac{\Delta x\Delta z\;s_n}{\Delta t} + (k_{os})_n^e\,\frac{\Delta z\;s_n}{\Delta x} + (k_{os})_n^w\,\frac{\Delta z\;s_n}{\Delta x} + (k_{os})_n^t\,\frac{\Delta x\;s_n}{\Delta z} + (k_{os})_n^b\,\frac{\Delta x\;s_n}{\Delta z} + (k_{os})_n\,\frac{\Delta x\Delta z}{s_n} + ((h_{rg})_n + h_c)\Delta x\Delta z + (h_{rw})_n\Delta x\Delta z \tag{4.30}$$

Elements of **A,** contributed by conduction from surrounding nodes:

$$A_{n,n-1} = -(k_{os})_n^e \frac{\Delta z \; s_n}{\Delta x} \tag{4.31}$$

$$A_{n,n+1} = -(k_{os})_n^w \frac{\Delta z \; s_n}{\Delta x} \tag{4.32}$$

$$A_{n,n-nx*ny} = -(k_{os})_n^t \frac{\Delta x \; s_n}{\Delta z} \tag{4.33}$$

$$A_{n,n+nx*ny} = -(k_{os})_n^b \frac{\Delta x \; s_n}{\Delta z} \tag{4.34}$$

For plane at y =0 $$A_{n,n+nx} = -(k_{os})_n \frac{\Delta x \Delta z}{s_n} \tag{4.35}$$

or for plane at $y = Y$ $$A_{n,n-nx} = -(k_{os})_n \frac{\Delta x \Delta z}{s_n} \tag{4.36}$$

Elements of vector **b**:

$$\begin{aligned} b_n = \rho_{os} (c_{os})_n \frac{\Delta x \Delta z \; s_n}{\Delta t} T_n \; + ((h_{rg})_n + h_c) \Delta x \Delta z T_g \\ + (h_{rw})_n \Delta x \Delta z T_w + H \rho_{os} \frac{\lambda_n \; \Delta x \Delta z}{s_n} \end{aligned} \tag{4.37}$$

As discussed in the earlier chapter, the oxide scale thermal conductivities at the interface (representing the face of model cell) placed midway are assumed to follow harmonic mean (Patankar, 1980). Therefore, the thermal conductivities at interfaces as used in the above equation are calculated as:

along x-direction interfaces:

$$(k_{os})_n^e = \frac{2(k_{os})_n (k_{os})_{n-1}}{(k_{os})_n + (k_{os})_{n-1}} \tag{4.38}$$

$$(k_{os})_n^w = \frac{2(k_{os})_n (k_{os})_{n+1}}{(k_{os})_n + (k_{os})_{n+1}} \tag{4.39}$$

along y-direction interfaces:

$$(k_{os})_n^n = \frac{2(k_{os})_n (k_{os})_{n-nx}}{(k_{os})_n + (k_{os})_{n-nx}} \tag{4.40}$$

$$(k_{os})_n^s = \frac{2(k_{os})_n (k_{os})_{n+nx}}{(k_{os})_n + (k_{os})_{n+nx}} \tag{4.41}$$

along z-direction interfaces:

$$(k_{os})_n^t = \frac{2(k_{os})_n (k_{os})_{n-nx*ny}}{(k_{os})_n + (k_{os})_{n-nx*ny}} \tag{4.42}$$

$$(k_{os})_n^b = \frac{2(k_{os})_n (k_{os})_{n+nx*ny}}{(k_{os})_n + (k_{os})_{n+nx*ny}} \tag{4.43}$$

Example case 2, General interior steel cell node: The second example case is general interior steel cell, denoted as steel internal cell, such as those shown in Fig. 3.6 (d), is exposed to conduction from all six surrounding steel cells. The elements of matrix **A** and b which correspond to its energy equilibrium equation (refer Eq. (3.57)), are expressed as:

$$\begin{aligned} A_{n,n} = \rho_{st}(c_{st})_n \frac{\Delta x \Delta y\ \Delta z}{\Delta t} + (k_{st})_n^e \frac{\Delta y\ \Delta z}{\Delta x} + (k_{st})_n^w \frac{\Delta y\ \Delta z}{\Delta x} + (k_{st})_n^n \frac{\Delta x\ \Delta z}{\Delta y} \\ + (k_{st})_n^s \frac{\Delta x\ \Delta z}{\Delta y} + (k_{st})_n^t \frac{\Delta x \Delta y}{\Delta z} + (k_{st})_n^b \frac{\Delta x \Delta y}{\Delta z} \end{aligned} \tag{4.44}$$

Elements of **A,** contributed by conduction from surrounding nodes:

$$A_{n,n-1} = -(k_{st})_n^e \frac{\Delta y\ \Delta z}{\Delta x} \tag{4. 45}$$

$$A_{n,n+1} = -(k_{st})_n^w \frac{\Delta y\ \Delta z}{\Delta x} \tag{4.46}$$

$$A_{n,n-nx} = -(k_{st})_n^n \frac{\Delta x\ \Delta z}{\Delta y} \tag{4.47}$$

$$A_{n,n+nx} = -(k_{st})_n^s \frac{\Delta x\ \Delta z}{\Delta y} \tag{4.48}$$

$$A_{n,n-nx*ny} = -(k_{st})_n^t \frac{\Delta x\ \Delta y}{\Delta z} \tag{4.49}$$

$$A_{n,n+nx*ny} = -(k_{st})_n^b \frac{\Delta x\ \Delta y}{\Delta z} \tag{4.50}$$

Elements of vector **b**:

$$b_n = \rho_{st}(c_{st})_n \frac{\Delta x \Delta y\ \Delta z}{\Delta t} T_n \tag{4.51}$$

The steel thermal conductivities of steel at the interface (representing face of model cell) placed midway are calculated as:

along x-direction interfaces:

$$(k_{st})_n^e = \frac{2(k_{st})_n (k_{st})_{n-1}}{(k_{st})_n + (k_{st})_{n-1}} \tag{4.52}$$

$$(k_{st})_n^w = \frac{2(k_{st})_n (k_{st})_{n+1}}{(k_{st})_n + (k_{st})_{n+1}} \tag{4.53}$$

along y-direction interfaces:

$$(k_{st})_n^n = \frac{2(k_{st})_n (k_{st})_{n-nx}}{(k_{st})_n + (k_{st})_{n-nx}} \tag{4.54}$$

$$(k_{st})_n^s = \frac{2(k_{st})_n (k_{st})_{n+nx}}{(k_{st})_n + (k_{st})_{n+nx}} \tag{4.55}$$

along z-direction interfaces:

$$(k_{st})_n^t = \frac{2(k_{st})_n (k_{st})_{n-nx*ny}}{(k_{st})_n + (k_{st})_{n-nx*ny}} \tag{4.56}$$

$$(k_{st})_n^b = \frac{2(k_{st})_n + (k_{st})_{n+nx*ny}}{(k_{st})_n + (k_{st})_{n+nx*ny}} \tag{4.57}$$

Similarly elements are obtained for all other types of cells from their energy equilibrium equations with appropriately changed parameters. The other cases are not reported here for the sake of brevity.

4.2.3.3 Functions for implementation of WSGGM

This function computes furnace gas mixture emissivity and furnace gas mixture absorptivity. Output of this routine is the desired furnace gas mixture emissivity and absorptivity. Furnace gas mixture emissivity depends on the gas temperature, but the absorptivity depends upon the furnace gas temperature and radiating surface temperature. The main steps for implementation of WSGGM are given below:

Step-1 **Input parameters:** The input parameters are: furnace gas temperature, radiating surface temperature (billet surface and furnace wall temperature), radiation path length, partial pressure of gases, absorption coefficients of individual gases of furnace gas mixture, emissivity gas temperature polynomial coefficients, and absorptivity polynomial coefficient. The furnace gas temperature and wall temperature is assumed to remain constant in a particular zone and updated with time that corresponds to the next zone. The billet surface temperatures are also updated at the end of each time step. The

polynomial coefficients are selected on the basis of the partial pressure ratio of H_2O vapor and CO_2 gas in the furnace gas mixture, which are taken from a previous study (Smith et al., 1982).

Step-2 **Calculation of weighting factors:** The emissivity and absorptivity weighting factors are evaluated from the temperature polynomial expression (Smith et al., 1982) as discussed in the chapter 3. Here the emissivity weighting factors are function of gas temperature. The absorptivity weighting factors are function of both furnace gas temperature and surface irradiation temperature.

Step-3 **Calculation of emissivity and absorptivity:** The total emissivity and absorptivity is evaluated from the WSGGM model expression (Smith et al., 1982) as discussed in the chapter 3.

Step-4 **Calculation of updated emissivity and absorptivity:** The surface irradiation temperatures are updated after each time step, and then the step 2 and 3 are repeated.

4.2.3.4 Functions for solution of system of matrix 'conduction solver'

The function receives information from function for 'system of matrices' and sends information such as 3D temperature field and oxide scale thickness to the main program. This function solves a system of matrix iteratively. The developed routine implements Gauss-Seidel (GS) algorithm and returns temperature and oxide scale thickness matrix at different time. The main steps for implementation of GS algorithm are given below:

Step-1 **Input parameters** The input parameters for this function are; coefficient matrix $\boldsymbol{A}$, and column vector $\boldsymbol{b}$, (Here matrices $\boldsymbol{A}$ and $\boldsymbol{b}$ are the output of 'Function for system of matrices from discretized equations' as discussed earlier in this chapter), billet initial temperature field, heating time (billet residence time).

Step-2 **Mesh initialization** To start computation the mesh of computational domain (steel billet with oxide) is initialized. This will define the initial temperature field and oxide scale thickness.

Step-3 **Furnace temperature conditions:** Define time dependent furnace zone gas temperature conditions, billet heating time, and time step.

Step-4 **Implementation of G-S iteration:** In order to solve the system of matrix, GS iteration is implemented. The temperatures are calculated by visiting each nodal point in an order. At the beginning, these nodal values represent the initial temperature or values from the previous iteration. Once the nodal point is visited, the corresponding value of temperatures is calculated and replaced by the newly calculated values in the computer storage. The temperature at the visited node is calculated by using surrounding nodal point temperatures. The surrounding nodes that have been already visited during the current iteration, temperature is the newly calculated value, for yet to be visited surroundings nodes the temperature is the value from previous iteration or initial value. In order to complete one iteration of GS method, all the nodal points have been visited in this manner. The further details about the GS method can be referred from Patankar, (1980).

Step-5 **Update coefficient matrix and column vector:** After each iteration with the new temperature field thermal conductivities, specific heat both for steel and oxide scale and oxide scale thickness are updated. This results in updating the entries of the coefficient in matrix $\boldsymbol{A}$. At the same time, the values of column vector $\boldsymbol{b}$, that includes scale heat of reaction and heat transfer coefficients are also updated with new temperature field after each of iteration. Whereas other values of column vector $\boldsymbol{b}$, such as storage terms and furnace gas temperature calculated corresponding to the temperature at the beginning of the time step.

Step-6 **Repeat the GS iteration:** After all these updating the sequence return to step 4 and 5. Solution procedure is repeated and iterations are carried out, till it reaches the convergence criterion.

Step-7 **Solution for the subsequent time step**: Furnace temperature conditions and radiative properties are updated. Step 4 to 7 are repeated till the total time approaches to the given billet heating time. When the total time becomes equal to the given billet heating time the temperature and oxide scale data are mapped back to 3D matrix using developed MATLAB® subroutines. This 3D array is used to evaluate function of three variables and to generate 3D volumetric plots.

The interactions among the different functions of developed code are illustrated by the flow chart shown in Fig. 4.5.

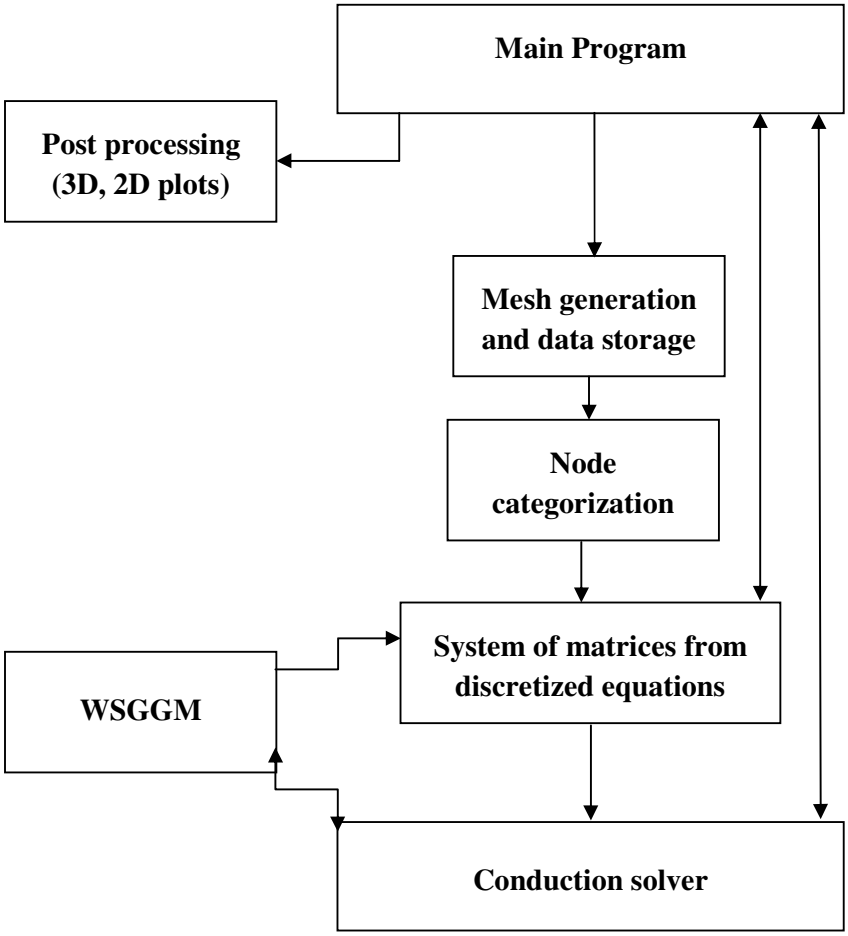

Fig. 4.5: Flow chart showing interaction among the different functions

4.3 Model Validation

In order to evaluate the accuracy of the developed numerical model and MATLAB® code, simulations were carried out with conditions for which the results are available in the existing literature. The proposed numerical model is validated with the analytical results and the published experimental results.

4.3.1 Validation with analytical results

The proposed numerical model has been validated with analytical results. However, the analytical results are available for simple cases and limited conditions. In order to validate the proposed model, the simulations are carried out in the conditions, for which analytical methods are available. The analytical results are obtained through the variable separation method which is available for one dimensional heat conduction with constant

heat flux and constant surrounding temperature as boundary conditions. The analytical solution available in the form of infinite series is expressed as:

$$\frac{T(x,t)-T_G}{T_i-T_G}=\sum_{n=1}^{\infty}a_n\exp^{-d_n^2 Fo}\cos\left(d_n\frac{x}{L}\right) \tag{4.59}$$

where Fo is Fourier number, dimensionless time ($Fo=\alpha t/L^2$) and coefficient a_n is expressed as:

$$a_n=\frac{4\sin d_n}{2d_n+\sin(2d_n)} \tag{4.60}$$

where eigenvalues d_n are the roots of characteristics equation or eigenfunction, expressed as:

$$d_n\tan d_n=Bi \tag{4.61}$$

where, Bi is Biot number, dimensionless heat transfer coefficient ($Bi=hL/k$). The infinite series term in summation of Eq. (4.59), decline rapidly as n increases, particularly for reheat problem where Fo number is large. Therefore only few terms are evaluated to determine the transient temperature. The same procedure is applied to other directions and 3D solution is obtained by using a product solution approach (Cengel and Ghajar, 2011; Ozisik, 1993). The conditions used in the present validation study are shown in Table 4.1.

Table 4.1: The input for validation simulation with analytical results

Billet dimension m $\times$ m $\times$ m	$0.3\times0.3\times0.3$
Initial temperature (K)	298
Surrounding heat transfer coefficient (W/m^{2}K)	112
Surrounding temperature (K)	1275
Thermal conductivity (W/mK)	31
Specific heat (J/kgK)	717.52

Present model has been validated by comparing the numerical model temperature predictions with analytical results. The comparison of nodal temperature, for node located at the corner of the billet and center of billet obtained through numerical model simulation and analytical method are shown in Fig. 4.6.

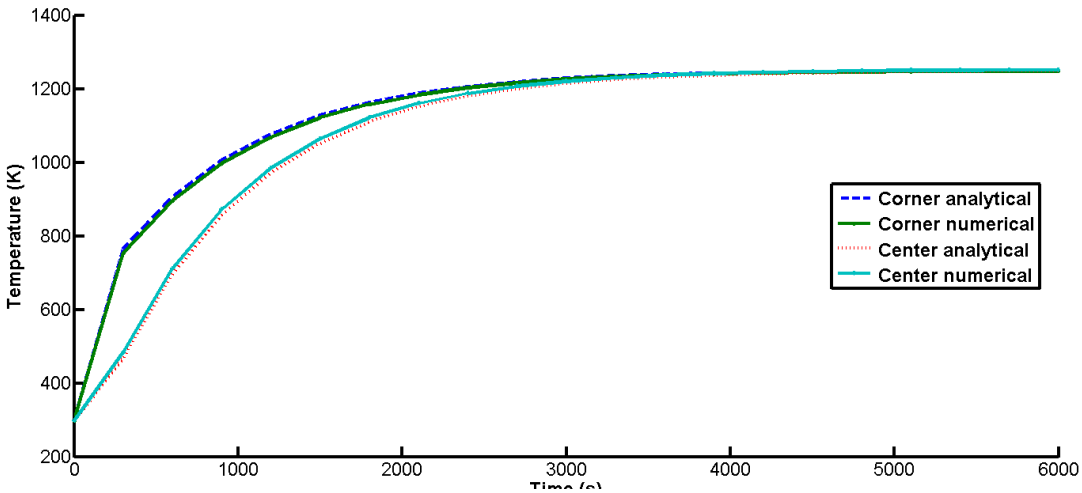

Fig. 4.6: Comparison of numerical and analytical results, temperature observed at the corner and center of the billet

It is observed that analytical results are very close to numerical results, especially the case when time is large. It is also observed that numerical model gives slightly lower temperature than the analytical temperature on the billet outer corner and somewhat higher value on the billet centre. In general numerical predictions are showing a reasonable agreement with analytical results.

4.3.2 Validation with published experimental results

The proposed model was validated against published experimental results. For this purpose a walking beam type of furnace with varying longitudinal temperature profile (constant in a particular zone) as described in Jang et al. (2010) was considered. This published literature data was chosen for validation as it includes many of the parameters considered in this study. In order to validate the billet dimensions, billet initial temperature, billet and oxide thermo physical properties, temperature conditions of the furnace and concentration distribution of CO_2 and H_2O of furnace combustion gases are taken from Jang et al. (2010).

The reheat conduction model simulated in this validation is for the walking beam furnace which has four zones: non firing, preheating, heating and soaking zones. The furnace dimension and inside pressure considered here for calculation of mean beam length are 35m×11m×5m and 1 bar respectively. Each zone has a constant gas temperature. The temperature assigned to wall is equal to the gas temperature, as they are not specified in considered literature. The emissivity of furnace wall considered is 0.8.

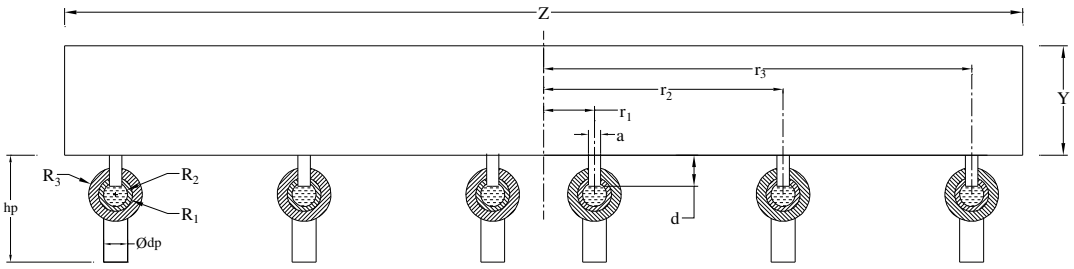

Fig. 4.7: The contact of skid considered during validation simulation

The steel billet of dimension 1100 mm× 230 mm× 8000 mm is assumed to be at uniform temperature of 298 K when charged to the furnace. This validation study also considers contact of billet with six skid beams as shown in Fig. 4.7, which is approximately (as exact data about the skid system is not reported) similar to the Jang et al. (2010) study. The skid data used here is given in Table 4.2.

Table 4.2: Skid system parameters used in validation study

Parameter	**Values (Unit)**
Skid pipe, insulation radius (R_1, R_2, R_3)	100(mm),120(mm),190(mm)
Contact width (a)	10(mm)
Height of skid button (d)	110(mm)
Distance of skids from centre of billet (r_1, r_2, r_3)	425(mm), 2000(mm), 357 (mm)
Thermal conductivity (k_{sk})	5 W/mK
Height of skid post (h_p)	2400(mm)
Diameter of skid post (ϕ_{dp})	400(mm)

In accordance with Jang et al. (2010) study, the emissivities of billet surface, skid structure and oxide scale are set to 0.5. The other parameters used as input data in this validation study, which are also taken from taken from Jang et al. (2010) are given in Table 4.3. The billet residence time in each zone and experimental centerline of the 2D billet geometry by Jang et al.(2010) are mapped from plots given in the literature. A grid spacing of 25 mm× 23 mm× 100 mm and time step of 150 seconds is used for this validation simulation.

Table 4.3: The input for validation simulation with published experimental results Data taken from Jang et al. (2010)

Thermal properties of steel billet and oxide scale			
Temperature (K)	Conductivity (W/m K)	Specific Heat (J/kg K)	Density (kg/m^3)
Steel			
303	26.89	299.0	7778
673	25.44	401.6	
873	22.70	512.0	
1073	20.89	542.8	
1273	23.69	478.9	
Oxide			
All temperature	3.20	725	7750
Furnace gas temperature conditions (K)			
Zone (residence time)	Upper	Lower	Skid
Non firing & Charging (0s-3000s)	1223	1203	1003
Preheating (3000s-5400s)	1273	1253	1053
Heating (5400s-8400s)	1473	1443	1243
Soaking (8400s-10800s)	1453	1433	1233
Concentration distribution of furnace gas			
H_2O	CO_2	O_2	N_2
0.111	0.177	0.015	0.697

The published experimental center line temperatures of the 2D billet geometry by Jang et al. (2010) are compared with the corresponding center line temperatures of present model equivalent 3D billet geometry. Here by center line we mean the direction parallel to the width along y axis at z = Z/2. Since the authors Jang et al. (2010) validated and reported a 2D model, therefore in order to compare our 3D results, we take the average value of the nodal temperature of the center line at each time.

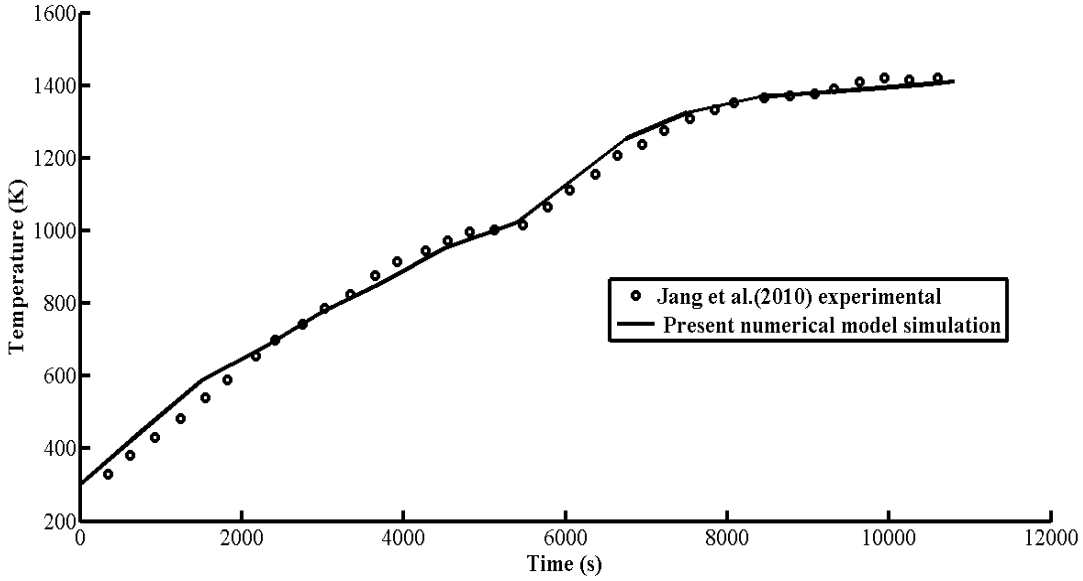

Fig. 4.8: Comparison of experimental and simulation results, temperature observed at the center line of the billet

The experimental (Jang et al., 2010) centre line temperature and present model simulated center line temperature (average value of all nodal temperatures along centre line.) are shown in Fig. 4.8. It can be observed from Fig. 4.8 that there is reasonably close agreement between the temperature profile predicted by present model and of Jang et al. (2010).

The center line plane: *x-y* plane at z = Z/2, which was used from present 3D model simulation to compare with the results reported by Jang et al. (2010) are shown in Fig. 4.9. It shows the temperature profiles in the center line plane after each zone heating.

For further clarity the 3D temperature plot of billet at the exit after 10800 seconds residence time, obtained during validation simulation is shown in Fig. 4.10. The temperatures at the billet surfaces are from 3D model were found to be in good agreement with corresponding 2D published results (Jang et al., 2010).

Figs. 4.11 & 4.12 show oxide scale layer growth on the billet top and bottom surface of the billet respectively, at the furnace exit after soaking zone. The maximum scale thickness on the billet top and bottom surfaces are 1.70 mm and 1.60 mm, respectively, The scale thickness reported by Jang et al. (2010) are on the billet top and bottom surfaces are 1.75 mm and 1.55 mm, respectively which are very close (with approximately 2.85 and 3.125 % difference) to the simulated value.

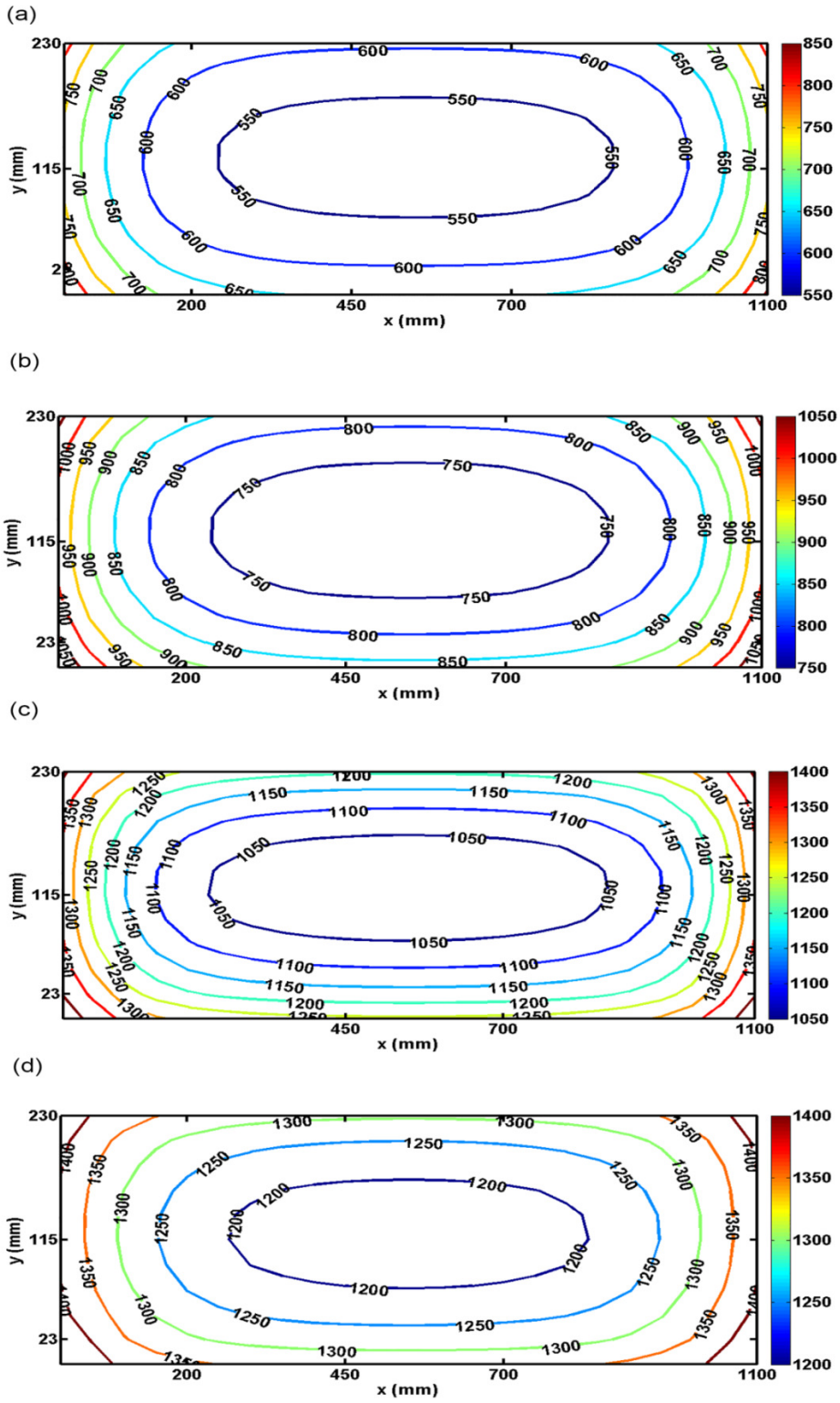

Fig. 4.9: Temperature contour of the billet plane at center line, parallel to width of billet along y axis: (a) after non firing zone, at t = 3000 seconds (b) after preheating zone, at t = 5400 seconds (c) after heating zone, at t = 8400 seconds (d) after soaking zone at 10800 seconds

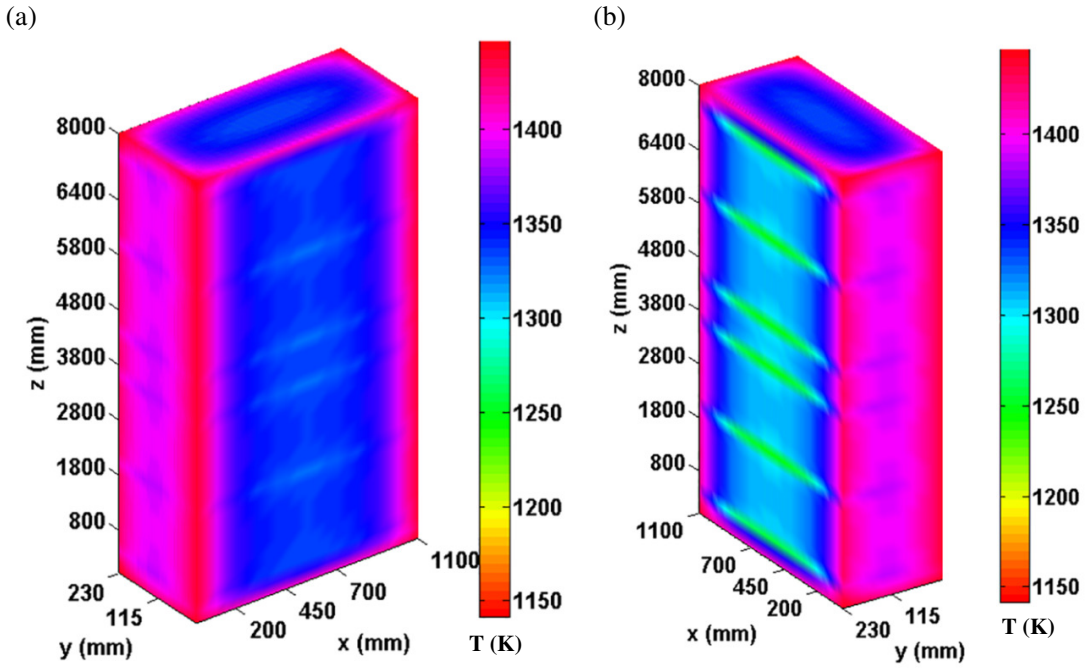

Fig. 4.10: Three dimensional temperature field of the billet after soaking zone obtained during validation study (a) at 10800 seconds view 1 (b) at 10800 seconds rotated view

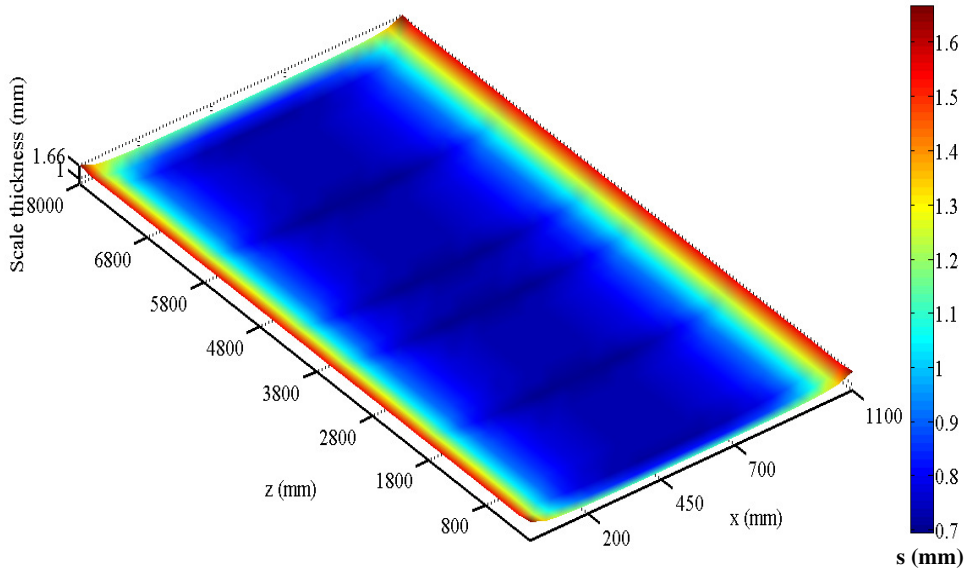

Fig. 4.11: Oxide scale thickness, surface plot after soaking zone obtained during a validation study: top surface

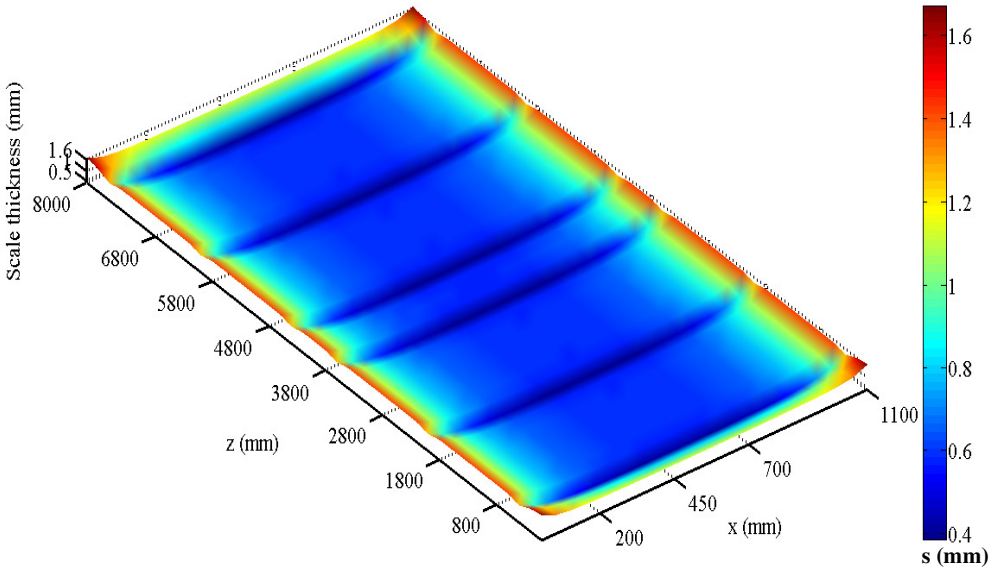

Fig. 4.12: Oxide scale thickness, surface plot after soaking zone obtained during a validation study: bottom surface

4.4 Closure

This chapter described the overall methodology; computer implementations and validation study of the developed numerical model for reheat simulation. The developed code will handle 3D transient heat conduction with the Cartesian coordinate system. The framework adopted for computer implementation was flexible enough so that the scope of modification is easy. The developed numerical model and MATLAB® code were tested during the validation study. The results of these model simulations along with conclusions thereof with supporting discussions and parametric studies will be presented in the next chapter.

Chapter 5

Reheat Model Simulation and Investigations on Zone Temperature Sensitivity

5.1 Introduction

The objectives of this chapter are to present simulation results of 3D numerical model for predicting 3D temperature and oxide scale growth; to analyze the heating characteristics in the presence of oxide scale; and, to perform parametric studies in order to investigate the effect of zone temperatures on responses of interests like maximum temperature, minimum temperature, maximum temperature difference, average temperature, maximum oxide scale thickness and average oxide scale thickness. The chapter begins with a model simulation section where input parameters used for simulations are presented. This is followed by presentation of simulation results along with conclusions drawn thereof with supporting discussions. Thereafter, reheat furnace zone temperature sensitivity study methodology, results and discussions along with the tangible evaluations of the study are presented in the subsequent sections. The chapter ends with some closure remarks.

5.2 Model Simulation for Temperature and Oxide Scale Thickness

The 3D transient heat conduction model developed for steel billet reheating was used to investigate following:

- To predict 3D temperature field in the billet and growth of oxide scale on the billet surfaces during reheating.
- To investigate steel billet heating characteristics without and with the formation and growth of oxide scale on the steel billet surfaces.
- To predict the effect of different billet cross-sections on the billet temperature field.

5.2.1 Input parameters for model simulation

The reheat conduction model simulated in this work is for the walking beam furnace which has four zones: unfired, preheating, heating and soaking zones. The furnace dimension considered here is 29 m $\times$ 3.5 m $\times$ 4 m in length, width and height. This

dimension is used to calculate mean furnace gas layer thickness. Each zone has constant gas and wall temperature. The temperatures of furnace gas in different zones of the furnace are given in Table 5.1.

Table 5.1: Furnace gas temperature conditions in different zones

Zone	**Residence time** (s)	**Temperature** (K)
Un fired	$0 \leq \text{time} \leq 3000$	1123
Preheating	$3000 \leq \text{time} \leq 5400$	1173
Heating	$5400 \leq \text{time} \leq 8400$	1448
Soaking	$8400 \leq \text{time} \leq 10800$	1428

The composition of the gas is assumed to be uniform throughout the furnace. In order to calculate radiative properties of furnace gas mixtures WSGGM was used. The WSGGM implemented for a clear plus three gray gases model corresponding to $\frac{p_{H_2o}}{P_{CO_2}} \approx 2$. The coefficients used for WSGGM implementations are given in Tables 3.1 & 3.2, which were taken from Smith et al. (1982). The results obtained from this WSGGM were included in the proposed 3D transient heat conduction model to calculate radiative exchange in the reheat furnace. The total pressure of the furnace gas chamber is assumed to be 1 bar.

In the present model simulation, assigned wall temperature is 200 K less than the gas temperatures, which are in accordance with previous study (Han et al., 2009). The temperatures of furnace wall in different zones of the furnace are given in Table 5.2. The emissivity of furnace wall considered here is 0.8.

Table 5.2: Furnace wall temperature conditions in different zones

Zone	**Residence time** (s)	**Temperature** (K)
Un fired	$0 \leq \text{time} \leq 3000$	923
Preheating	$3000 \leq \text{time} \leq 5400$	973
Heating	$5400 \leq \text{time} \leq 8400$	1248
Soaking	$8400 \leq \text{time} \leq 10800$	1228

The steel billet of dimension 140 mm × 140 mm ×1500 mm is assumed to be at uniform temperature of 298 K, when charged to the furnace. The emissivities of billet top surface and side surface are 0.7 and bottom surface is set to be 0.6. The thermo-physical properties of steel billet and oxide scale considered in this work are given in Table 5.3, which are taken from the previous study (Mogan, 1999).

Table 5.3: Thermo physical properties of steel billet and oxide scale

Material	**Specific heat** (J/kg K)	**Thermal conductivity** (W/m K)	**Density** (kg/m^3)
Steel billet	$c_{st} = 341.9 + (0.425 \times T) - (9.733 \times 10^{-6} \times T^2) - (7.05 \times 10^{-8} \times T^3)$	for $T < 1473$: $k_{st} = 92.57 - (6.36 \times 10^{-2} T) - (1.75 \times 10^{-5} \times T^2) + (2.19 \times 10^{-8} \times T^3)$ for $T < 1473$: $k_{st} = 31$	7000
Oxide scale	$c_{os} = 539.9 + (0.2795 \times T)$	$k_{os} = 1.5 + (1.5 \times 10^{-3} (T - 800))$	5000

The billet rests over water cooled skid system in the reheat furnace which reduces heat transfer to the billet bottom surface. Fig. 5.1 shows the details of skid and billet contact.

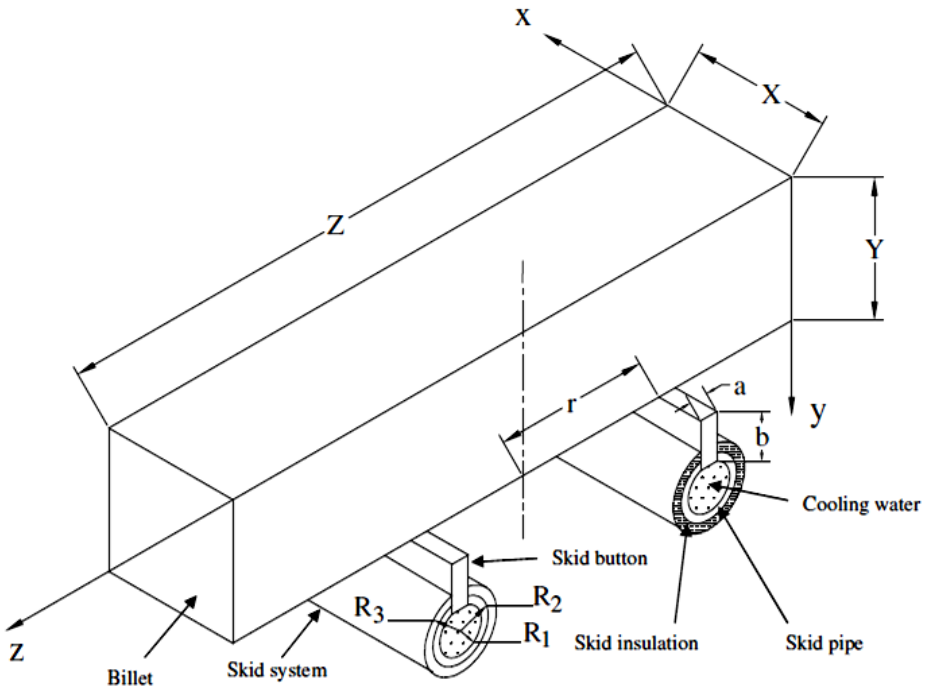

Fig. 5.1: Billet orientation and skid system

The length of skid button (d), thermal conductivity of skid button (k_{sk}) and other parameters of skid system are given in Table 5.4.

Table 5.4: Skid system parameters used in present study

Parameter	**Values** (Unit)
Skid pipe, insulation radius (R_1, R_2, R_3)	0.1 (m),0.12 (m),0.19 (m)
Contact width (a)	0.01 (m)
Height of skid button (d)	0.110(mm)
Distance of skid from center of billet (r)	0.1875 (m)
Thermal conductivity (k_{sk})	5 W/mK

Present study considers implicit scheme where stability can be maintained over much larger values of time step. This results in less simulation time. However, for very large time steps, truncation error becomes large (Anderson, 1995). The simulations are performed at different time steps, so as to identify the maximum time step that leads to minimum loss of accuracy. Based on grid independency test, the largest grid spacing and time steps at which dependent variables of interest are not varying significantly were chosen for further simulations.

5.2.2 Results and discussions

The reheat numerical model developed in this work is simulated to study the heating characteristics of billet with formation and growth of oxide scale. Results for transient temperature field and oxide scale thickness predictions are presented in this section. This is followed by the presentation and discussions on parametric study which is performed to predict the effect of different billet cross-sections on the billet temperature field.

5.2.2.1 Temperature predictions

In order to investigate the effect of oxide scale on the temperature field in the billet, simulations are carried out for two cases: with oxide scale and without oxide scale.

The 3D temperature fields in the billet with and without consideration of oxide scale are shown in Figs. 5.2 & 5.3. It shows 3D temperature fields in the billet with oxide scale and without oxide scale at the end of four zones of reheat furnace. It can be observed that rate of temperature rise in the billet is less in the presence of oxide scale. The temperature of billet with oxide scale is lower than that of billet without oxide scale. This is due to the poor thermal conductivity and large specific heat of oxide scale in comparison of the steel. However, the effect of oxide scale on the billet temperature field is more prominent in the preheating and heating zone.

It is observed that the corner and edge regions have a higher temperature. The corner of the billet is made from the intersection of three surfaces and, hence these surfaces are exposed to heat flux from three directions. In other words, it means that at the corners of the billet heat enters the billet from three directions. On the contrary, at both edges and plain surface regions, heat enters the billet from two directions and one direction, respectively. Due to this additional heat flux exposure, corners and edges get heated faster than surface regions.

Fig. 5.4 shows the rotated view of 3D temperature plot, at end of four zones of reheat furnace according to consideration and non consideration of oxide scale. At the end of 10800 seconds residence, the minimum temperature observed above the skids. It shows that the effect of skid shadowing is more pronounced at higher billet average temperature.

Fig. 5.5 shows three planes (along x-direction) of the 3D temperature field in the billet during reheat. Strong temperature differences are observed near corner, edges and near the skid contact regions of the billet. These temperature differences reduce with time, which is evident by the predicted temperature fields. The maximum temperature locations such as corner edge, surface increases in preheating and heating zone, and reduces in soaking zone (with a small magnitude). The billet center plane temperature is less than the billet outer plane temperature. It is observed that the difference between outer plane surface temperature and center plane surface temperature keeps decreasing as billet moves from preheating zone to soaking zone. The minimum temperature along the width of billet (along x-direction) is observed at center plane.

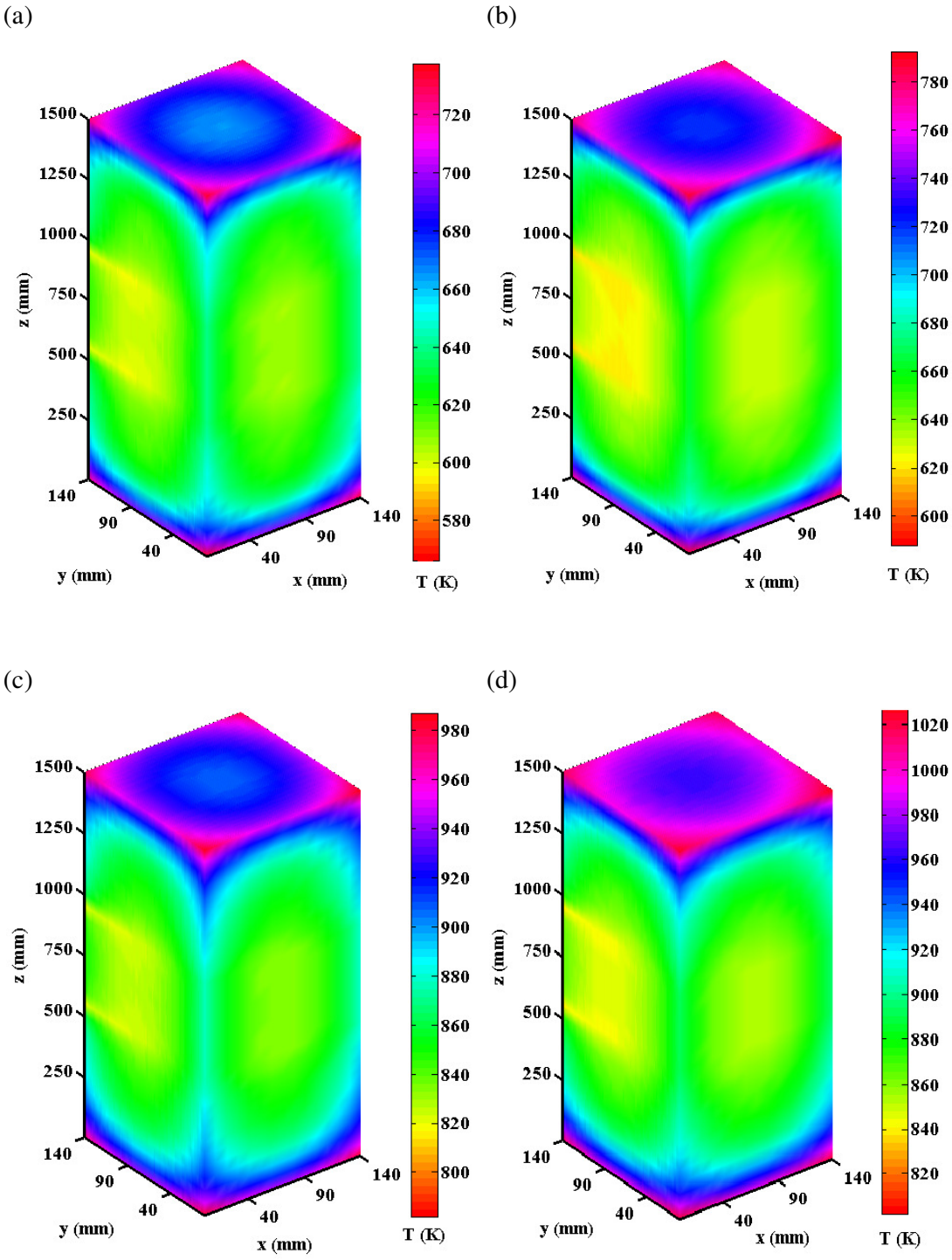

Fig. 5.2: Comparison of 3D temperature field in the billet with oxide scale and without scale: (a) with scale, at 3000 seconds (b) without scale, at 3000 seconds (c) with scale, at 5400 seconds (d) without scale, at 5400 seconds

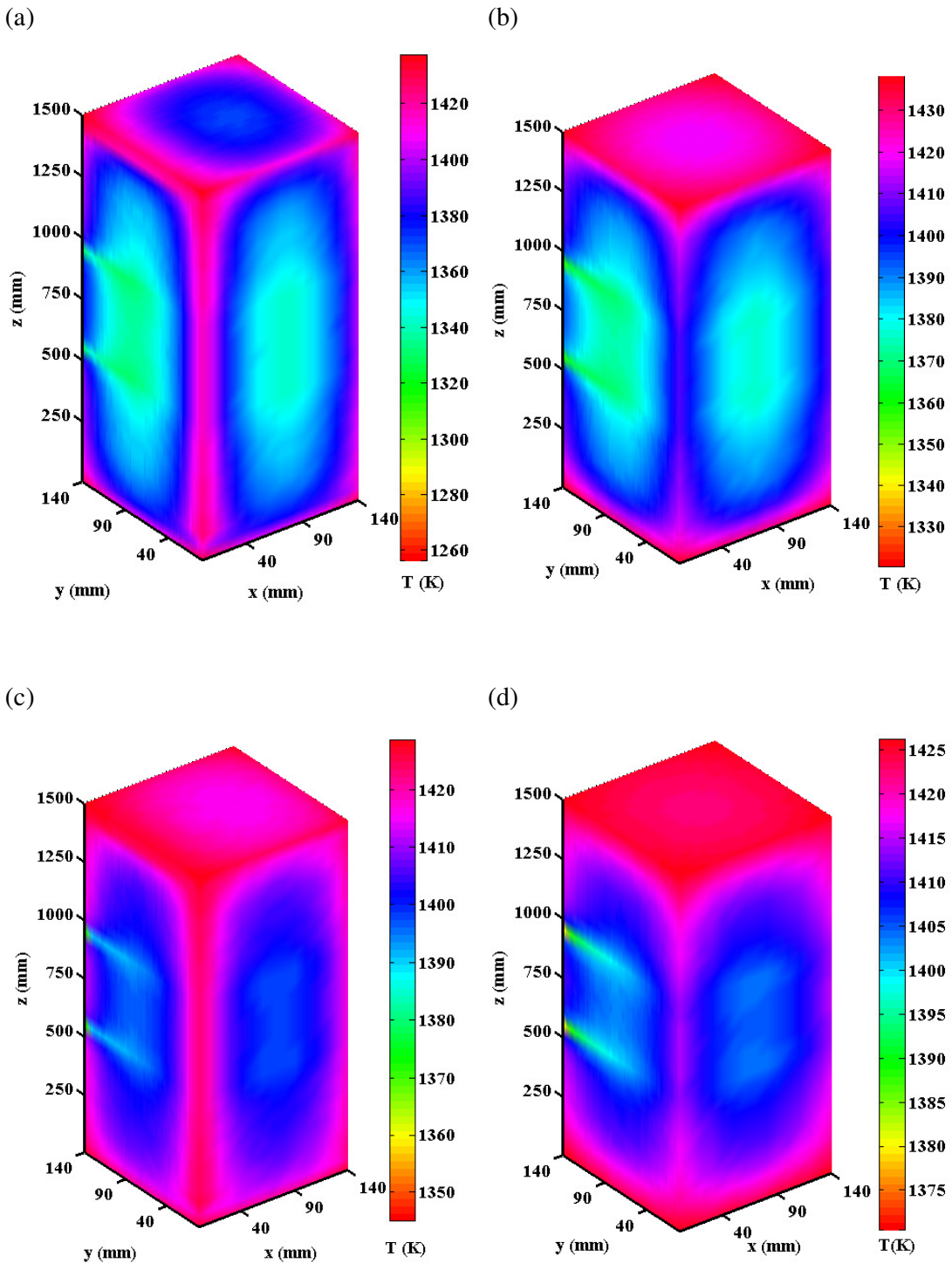

Fig. 5.3: Comparison of 3D temperature field in the billet with scale and without scale: (a) with scale, at 8400 seconds (b) without scale, at 8400 seconds (c) with scale, at 10800 seconds (d) without scale, at 10800 seconds

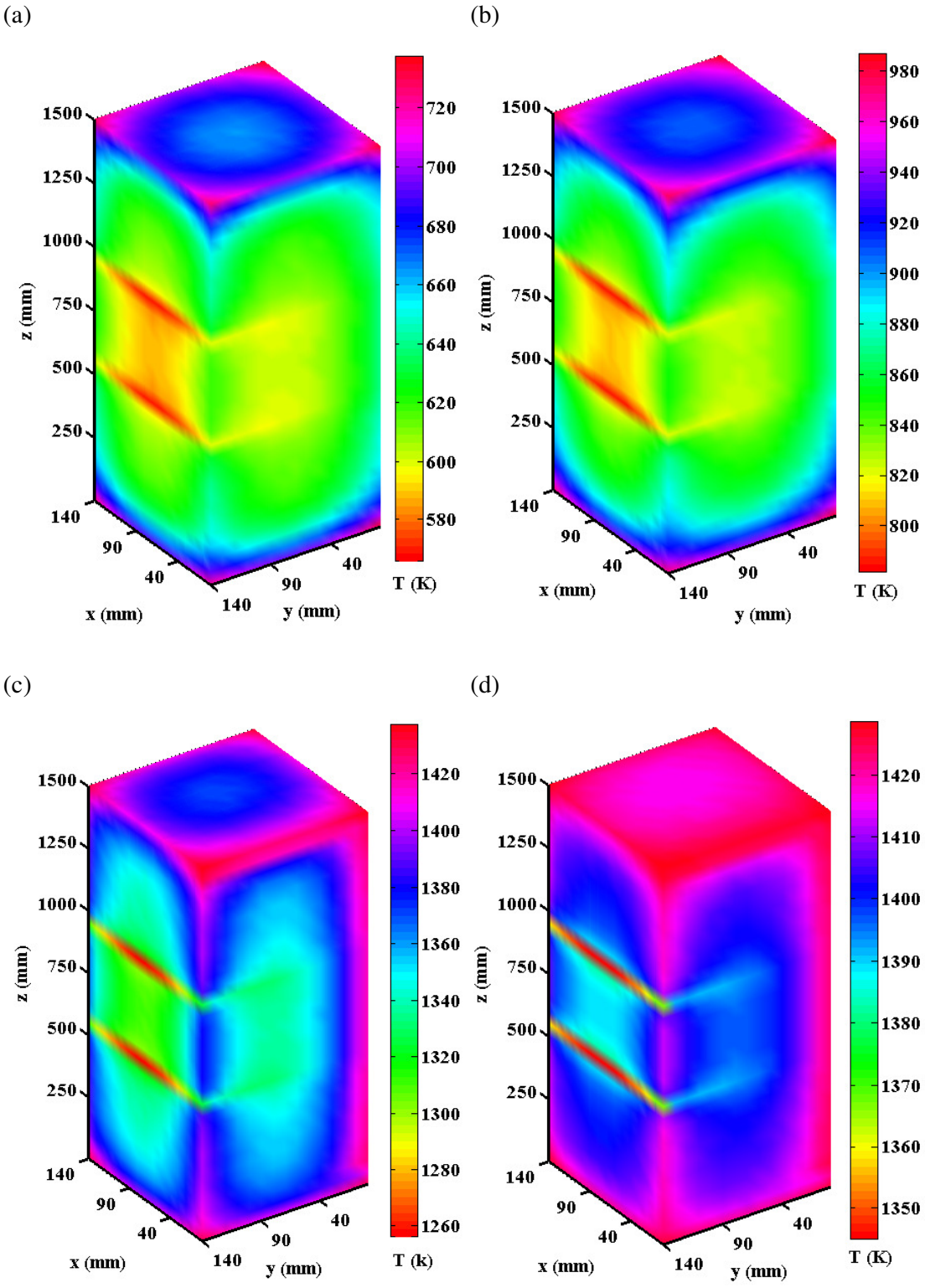

Fig. 5.4: 3D temperature field in the billet with scale (rotated view): (a) 3000 seconds, (b) 5400 seconds, (c) 8400 seconds, (d) 10800 seconds

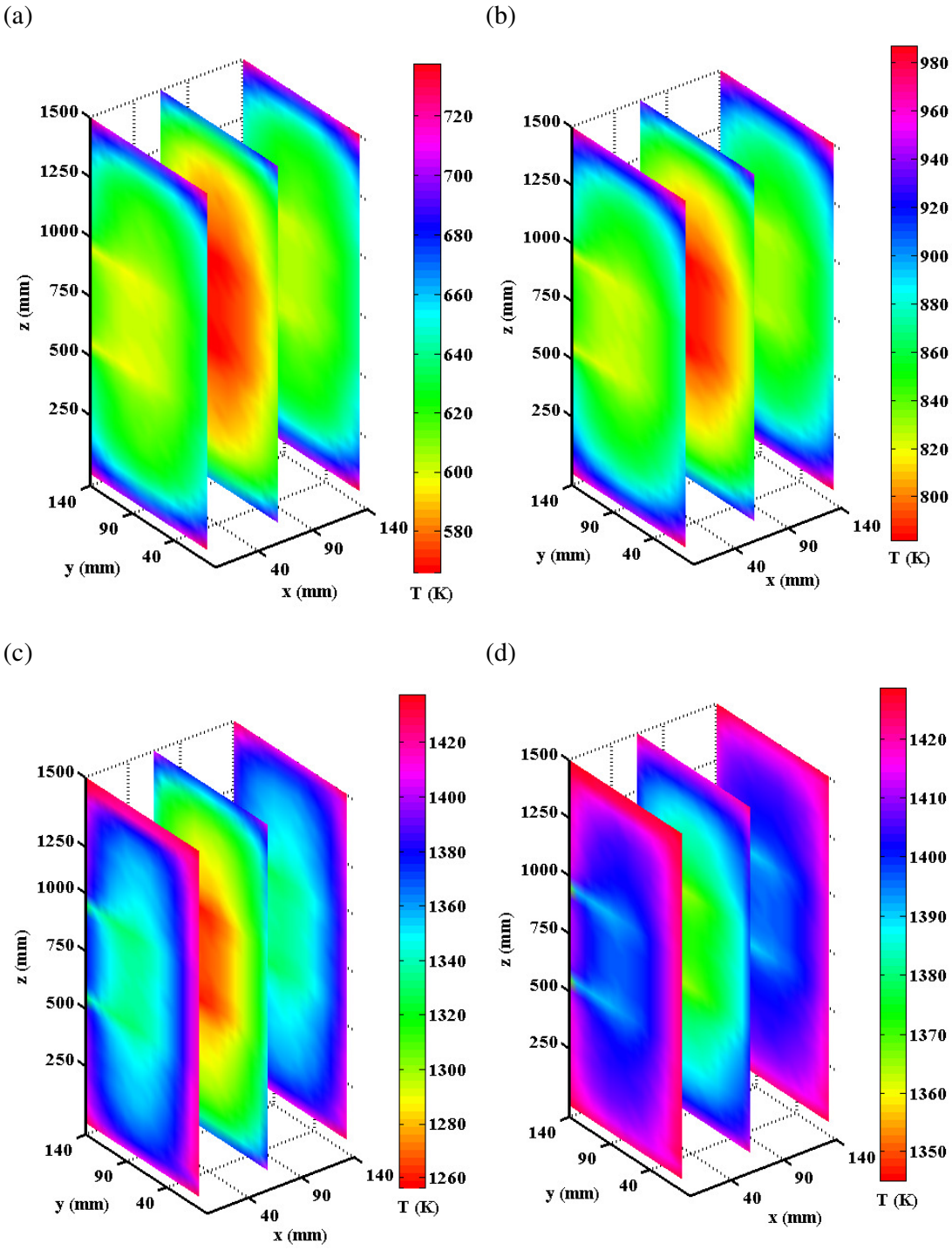

Fig. 5.5: Temperature field of the billet, three planes (along *x* direction) :(a) after non firing zone, at t = 3000 seconds (b) after preheating zone, at t = 5400 seconds (c) after heating zone, at t = 8400 seconds (d) after soaking zone at 10800 seconds

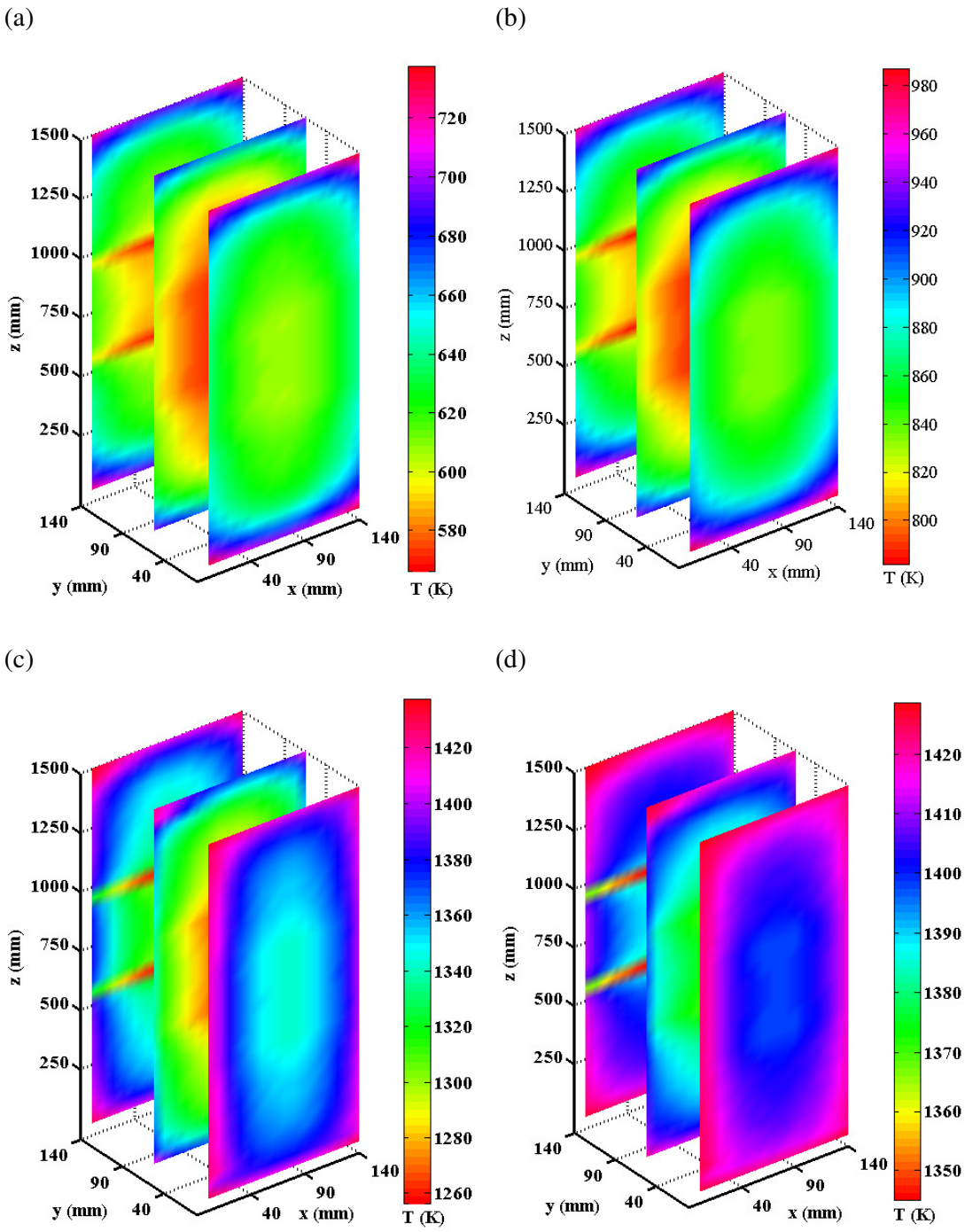

Fig. 5.6: Temperature field of the billet three planes (along *y* direction): (a) after non firing zone, at t = 3000 seconds (b) after preheating zone, at t = 5400 seconds (c) after heating zone, at t = 8400 seconds (d) after soaking zone at 10800 seconds

In order to show the effect of skid system, the three planes (along *y* direction) of 3D temperature plots are shown in Fig. 5.6. The effect of the skid system on the temperature field is very significant due to radiation shadowing at the bottom surface and energy loss because of conduction from the billet. The temperature field of the billet shows that the effect of skid system is more pronounced at the bottom surface of the billet compared to top and side surfaces. This is in agreement with the expected trend. It is observed from the predicted 3D temperature field plot and corresponding data that skid system has an effect on temperature in all the dimensions of the billet. However, the maximum influence of the skid is observed at the bottom surface of the billet. Slice wise examination of temperature plot and the data indicates that minimum temperature in the billet, during most of residence time occurs at inner node. The minimum temperature node location shifted towards bottom skids region.

Fig. 5.7 shows three planes (along *z*-direction) of the 3D temperature field in the billet during reheat. The billet center plane temperature is less than the billet outer plane temperature. It is observed that the difference between outer plane surface temperature and center plane surface temperature keeps decreasing as billet moves from preheating zone to soaking zone. The minimum temperature along the length of billet (along *z*-direction) is observed at center plane. More uniformity in the temperature center plane observed after soaking zone.

Fig. 5.8 shows the temperature variation of billet during reheating. The temperatures observed at seven representative nodes correspond to different locations in the billet. Here corner node refers to top corner of the billet on the oxide scale having nodal indices $i = 1, j = 1, k = 1$; edge node refers to top edge on the oxide scale having nodal indices $i = 3, j = 1, k = 1$; and surface nodes refer to the surface on the oxide scale having nodal indices $i = 3, j = 3, k = 1$. Among these three nodes considered here, the maximum temperature observed at the corner and a minimum at the surface node, which is also expected from the decreasing magnitude of thermal resistivity from corner nodes to surface nodes. The four internal nodes considered here are having nodal indices: $(i = 2, j = 2, k = 2)$; $(i = 3, j = 2, k = 2)$; $(i = 3, j = 3, k = 2)$ and $(i = 3, j = 3, k = 3)$ refers to internal node-1, internal node-2, internal node-3 and internal node-4 respectively. First three internal nodes are at the interface of steel and the oxide scale, whereas internal node-4 is of an interior steel control volume.

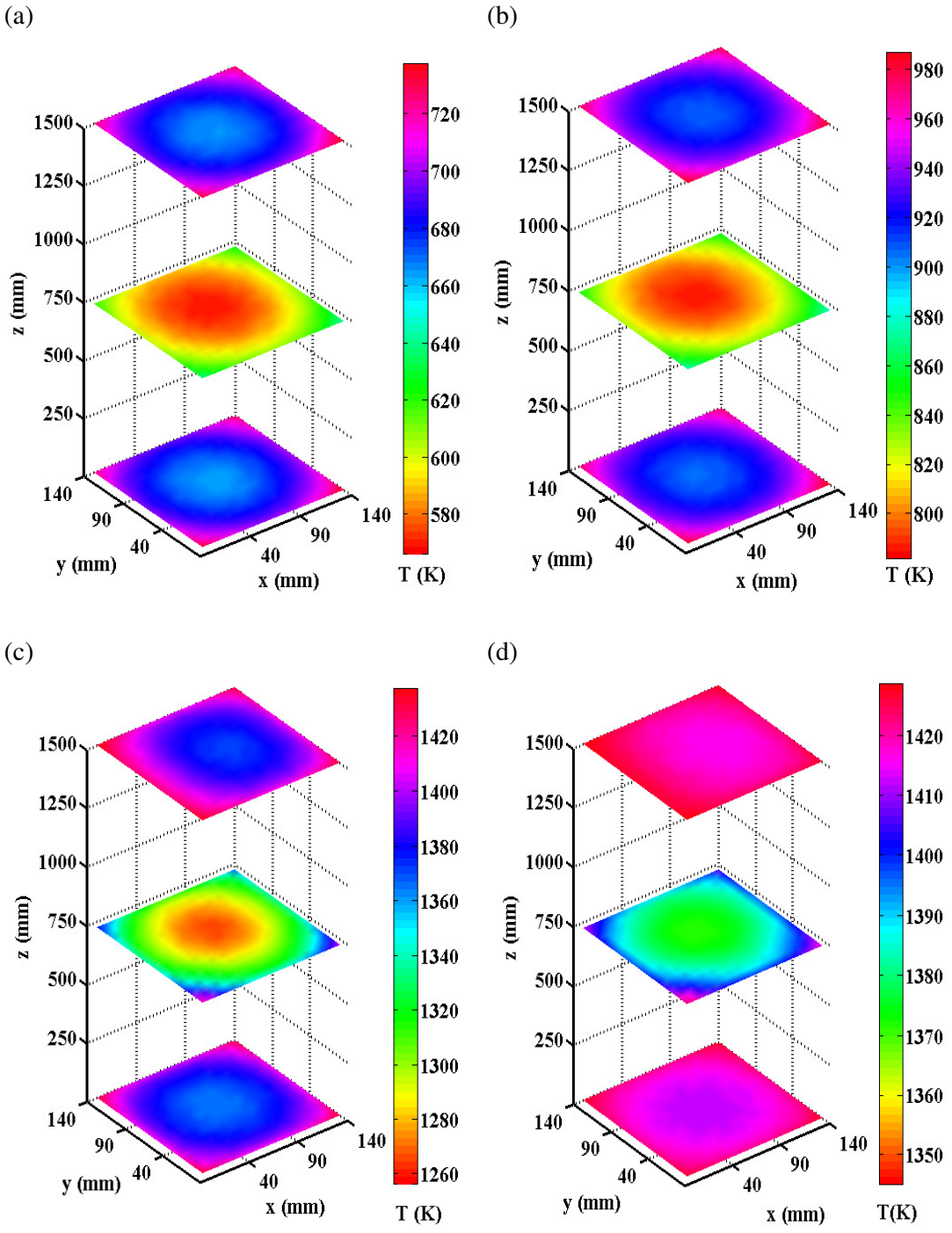

Fig. 5.7: Temperature field of the billet three planes (along *z*-direction): (a) after non firing zone, at t = 3000 seconds (b) after preheating zone, at t = 5400 seconds (c) after heating zone, at t = 8400 seconds (d) after soaking zone at 10800 seconds

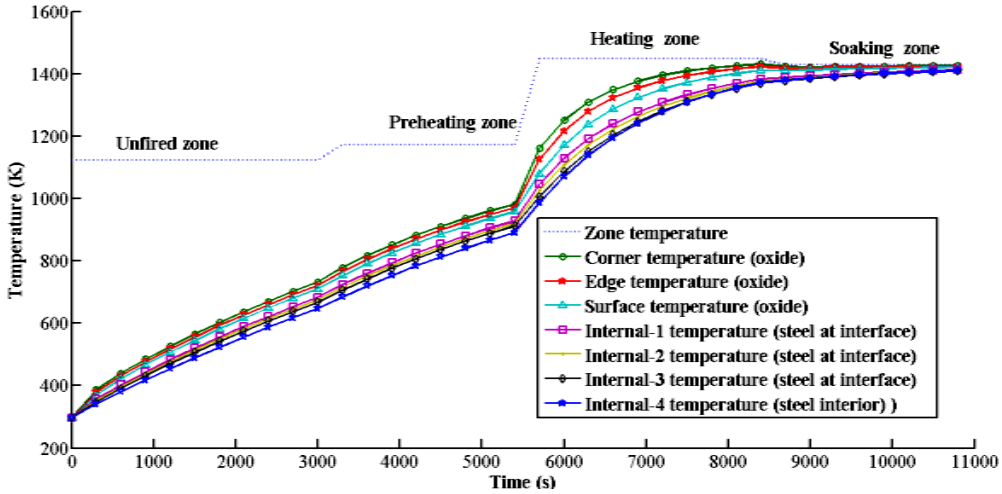

Fig. 5.8: Temperature profiles at different representative locations of the billet during reheat simulation

The effect of decreasing magnitude of thermal resistivity from internal node-1 to internal node-4 is clearly seen. The temperature difference between the nodes is reduced to a significantly lower value in the soaking zone. The temperature rise of the billet nodes is more in preheating and heating zone. The temperature rise in soaking zone is very small.

Fig. 5.9 shows local maximum temperature, average temperature, local minimum temperature and maximum temperature difference (difference of local maximum and minimum temperature) profiles of the billet. Billet maximum, minimum and average temperatures are showing a uniform trend of continuous increase. The billet average temperatures are close to billet minimum temperatures. The billet average temperature rise in preheating zone is a maximum.

Temperature profiles in soaking zone are close to each other. It means the maximum temperature difference in billet approached to a lower value. It is observed, that in later phases of preheat zone the temperature increase rate has been slow down, which is expected due reduced radiative heat flux. It can be explained by the fact that during billet reheating, the major mode of heat transfer is radiation. The radiation heat flux depends upon the difference of the fourth power of billet temperature and combustion gas temperature. As time progress in preheat zone this difference reduces which in turn reduce radiation heat flux. It is observed that the temperature profile shows step up after preheat zone. In heating zone temperature of combustion gas increases from

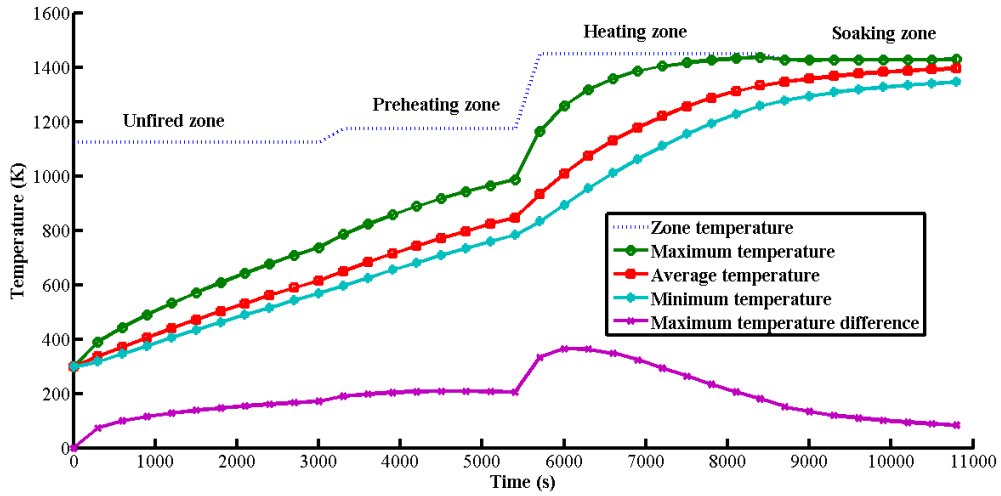

Fig. 5.9: Temperature profiles in the billet during reheat simulation

1173 K to 1448 that will cause a sudden increase in heat flux. As a result of this heat flux increase, the corner and edge have acquired higher temperature quickly due to their large thermal resistivity. As the time progressed, this difference reduces, which is clear from temperature profile change after some time elapse in heating zone. The temperature difference reduces at a faster rate in soaking zone.

Fig. 5.10 shows surface temperature plots of billet top plane surface, center plane surface and bottom plane surface at the exit of heating zone (at t = 8400 seconds). It is observed that the temperature distribution in the billet top plane surface is more uniform than that in the billet center plane surface and bottom plane surfaces. The largest temperature gradient can be seen to occur in the billet bottom plane surface, particularly near the skid region. It is also observed that minimum temperature locations are on the billet bottom surface near the skid. Fig. 5.11 shows surface temperature plots of the billet top plane, center plane and bottom plane surface at the exit of soaking zone (at t = 10800 seconds). The temperature maintained in the soaking zone of the furnace is less than the temperature of heating zone. Therefore, temperature equalization over the cross section is takes place during this zone heating. The temperature of maximum thermal resistivity locations such as corner edge reduces with a small magnitude in soaking zone, which evident from the surface plots comparisons. It is observed that the temperature difference on the entire three surfaces reduces in comparison to the previous zone temperature (shown in Fig. 5.10). It can be seen that the temperature difference values between billet surfaces in soaking goes down in comparison to the corresponding values of heating zone. The local minimum temperature in the billet at the end of soaking zone is observed at the billet bottom surface, near the skid region.

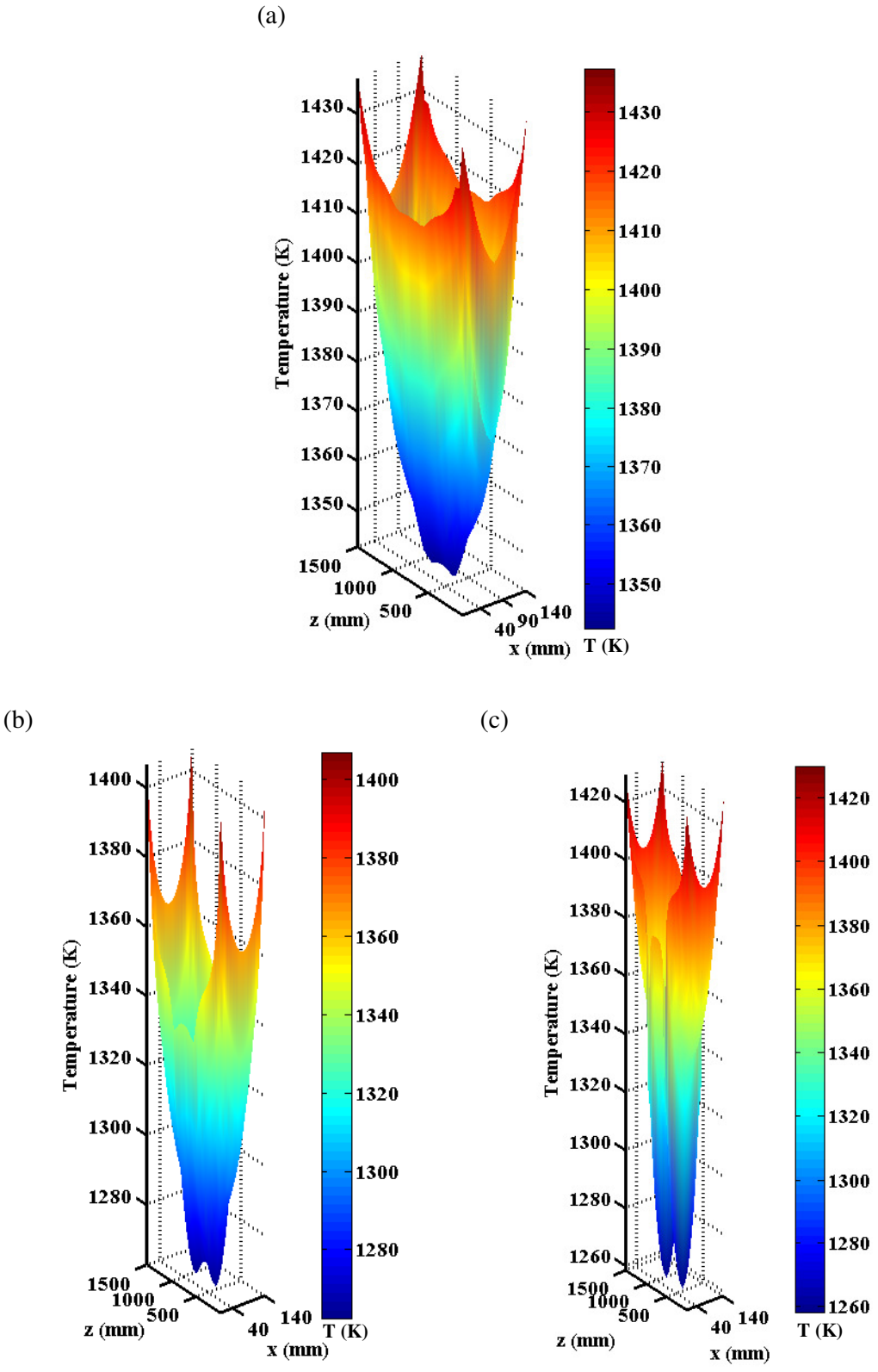

Fig. 5.10: Surface temperature plot of the billet, with scale at 8400 seconds: (a) top plane (b) center plane (c) bottom plane

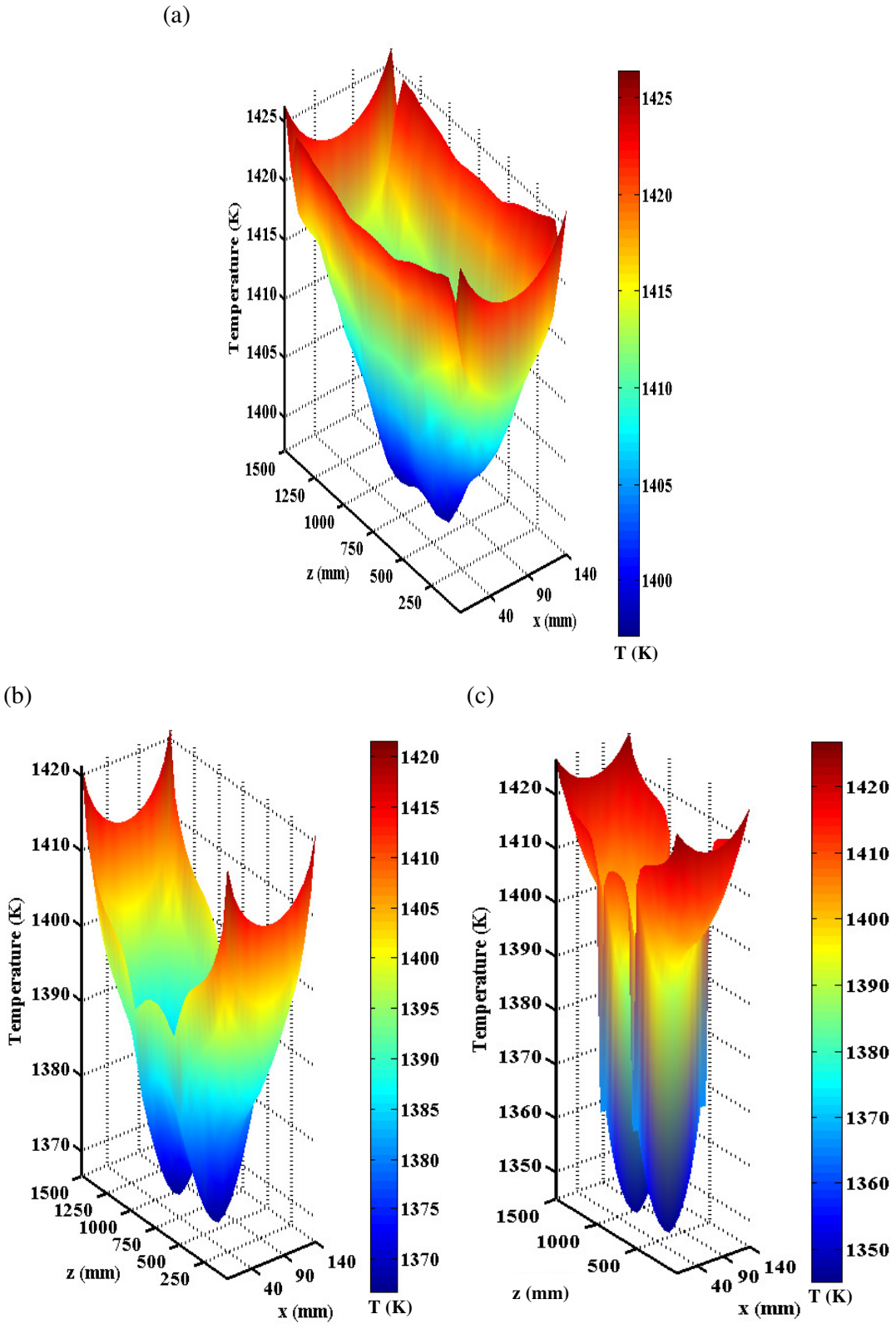

Fig. 5.11: Surface temperature plot of the billet, with scale at 10800 seconds: (a) top plane (b) center plane (c) bottom plane

Temperature contours on the billet top, center and bottom surfaces of the billet at the exit of soaking zone after 10800 seconds are shown in Fig. 5.12. The contour line has drawn at the step of 4 K temperature differences. The large number of isothermal lines appearing on the bottom surface in the skid region shows the temperature gradients.

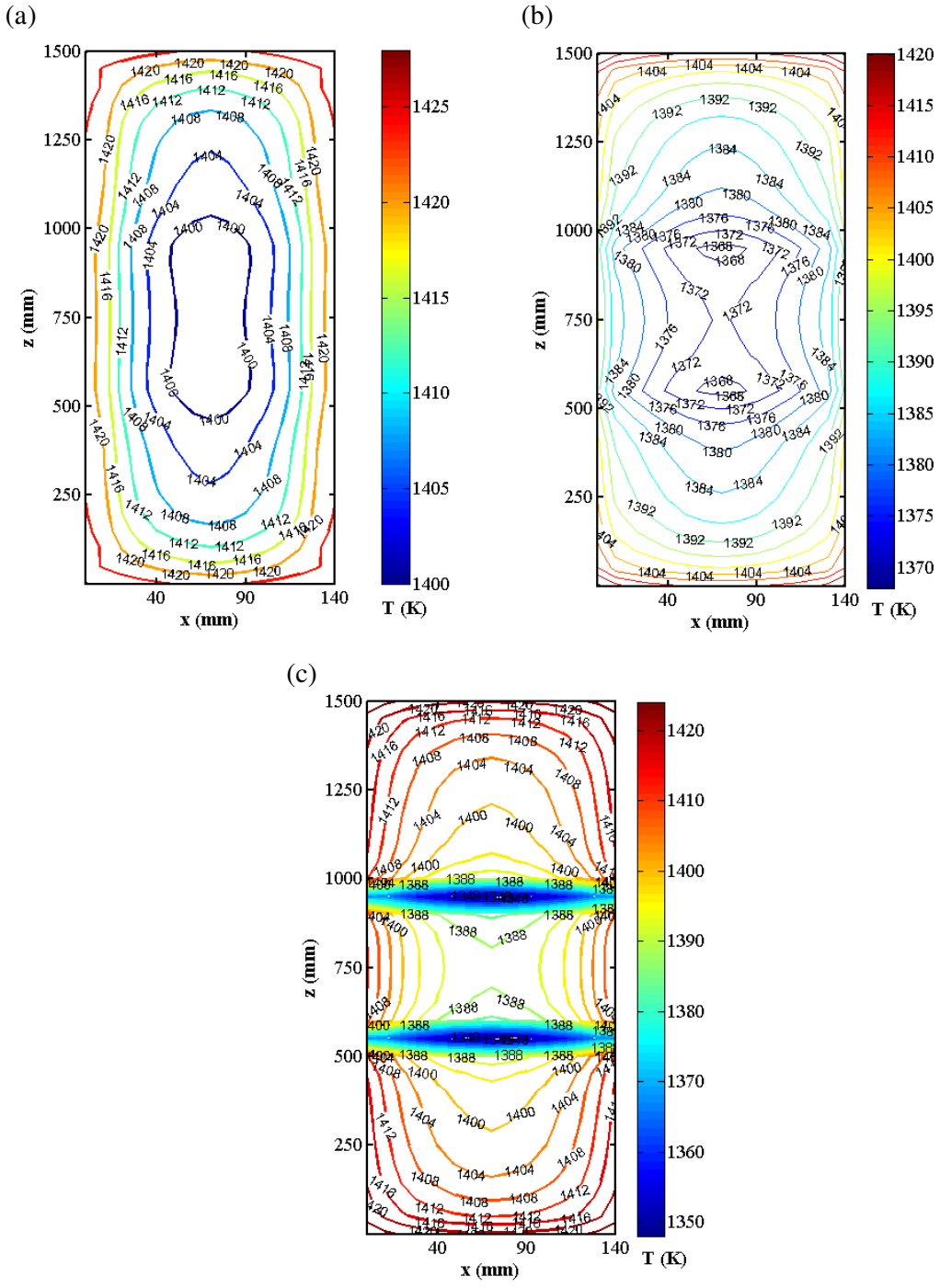

Fig. 5.12: Temperature contour plot of the billet, with scale at 10800 seconds: (a) top plane (b) center plane (c) bottom plane

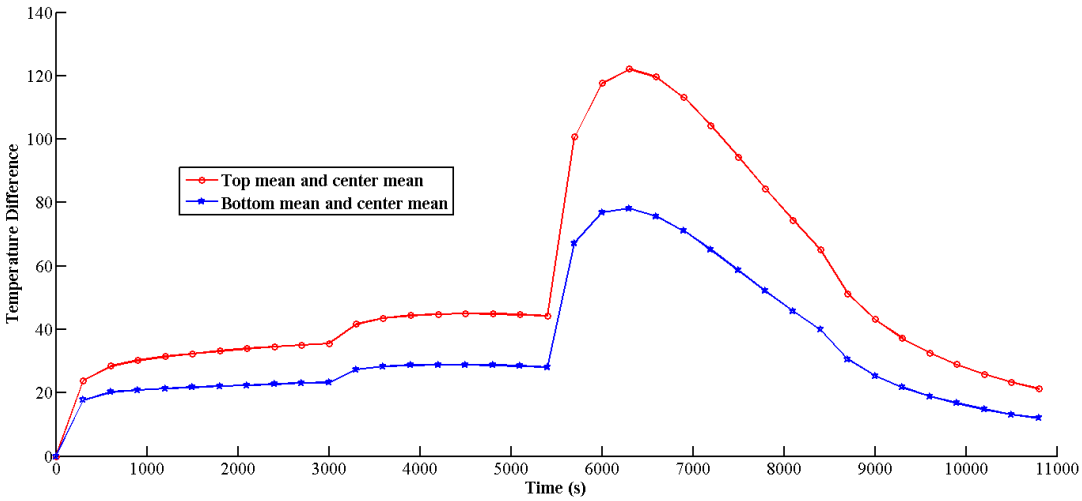

Fig. 5.13: Difference between the average temperature of billet: top plane and center plane; bottom plane and center plane during reheating

Fig. 5.13 shows the difference of area averaged temperatures of billet top plane and center plane; bottom plane and center plane. The control of average temperature difference to specified value is important for downstream activities. The temperature differences increases gradually in the unfired zone and preheating zone. The temperature difference increases at a faster rate in heating zone. In the heating zone billet exposed to a higher combustion gas temperature, which results in an increase in heat flux. As a result of this increase in the heat flux, the outer locations of the billet (having more thermal resistivity) have acquired higher temperature quickly in comparison to the inner locations of the billet. As the time progressed, this difference reduces, which is clear from temperature profile change after some time elapse in heating zone. The temperature difference reduces at a faster rate in soaking zone. It is observed that the average temperature difference reduced to a small value after soaking zone. Although, the lowest temperature at the end of heating is located at the bottom surface (as discussed earlier), the average temperature of bottom plane is always remains higher than that of center plane.

5.2.2.2 Oxide scale thickness predictions

Fig. 5.14, present oxide scale thickness, surface plots of billet top and bottom surfaces for residence time of 8400 seconds. The oxide scale growth rate equation is temperature dependent. Maximum growth of oxide scale can be seen to lie on the higher temperature locations (corner and edge) of the billet, which confirms that the numerical model exhibit

the expected behavior. It is also observed that the oxide scale growth on the billet top surface is higher than the oxide scale growth on the bottom surface of the billet. This is because of different temperature values at billet top and bottom surfaces. The oxide scale thickness at the skid contact location is lower in comparison to other locations.

(a)

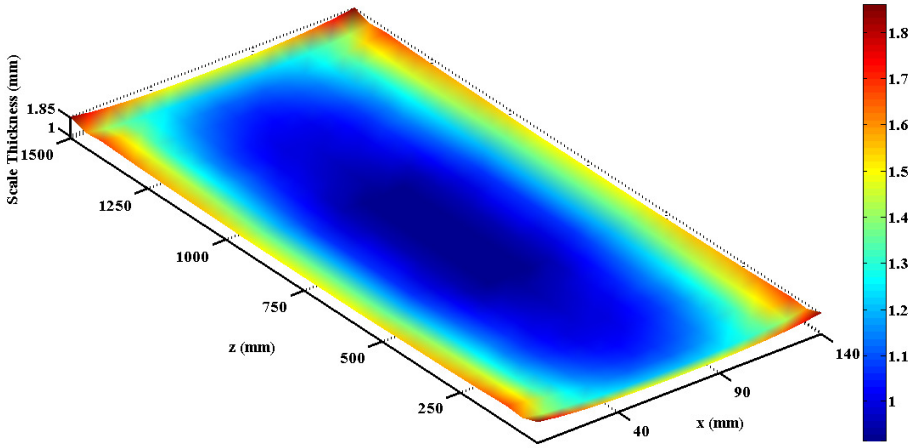

(b)

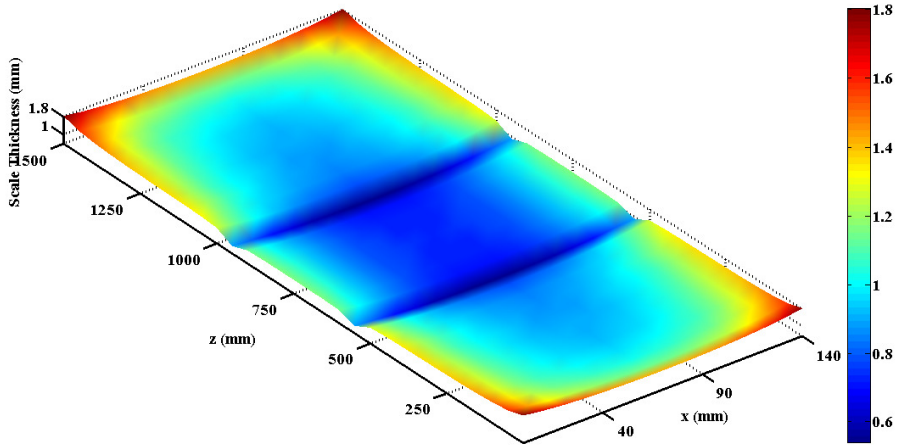

Fig. 5.14: Oxide scale thickness surface plot at 8400 seconds: (a) top surface (b) bottom surface

The surface plots of oxides scale thickness on billet side plane (*y*-*z* plane) and end plane (*x*-*y* plane) for residence time of 8400 seconds are shown in Fig. 5.15. From Fig 5.15(a), it is observed that for the region of skid contact vicinity, the oxide scale thickness growth is relatively lower in comparison to other regions. This is demonstrating clearly the effect of temperature field on oxide scale growth.

(a)

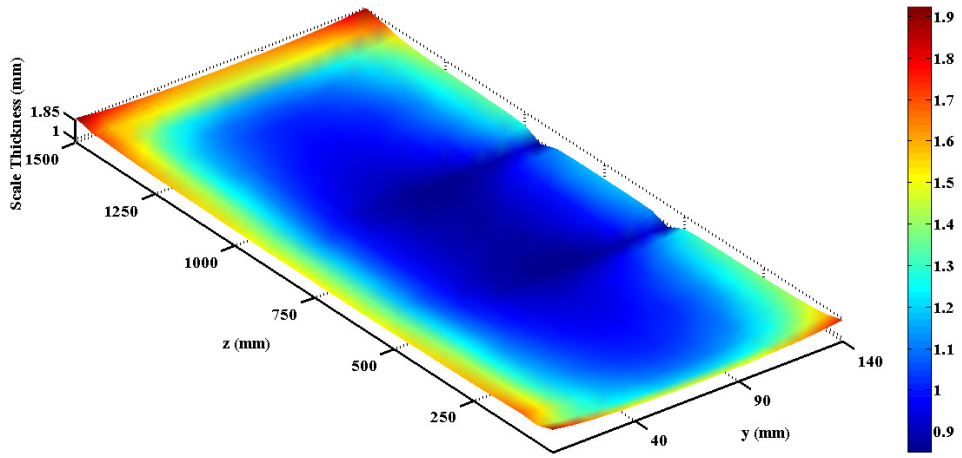

(b)

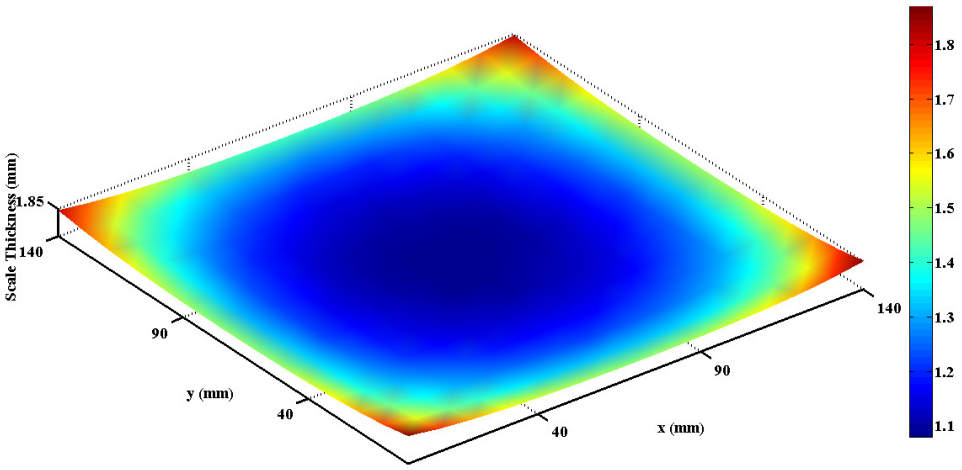

Fig. 5.15: Oxide scale thickness surface plot at 8400 seconds: (a) side surface (*y-z* plane) (b) end surface (*x-y* plane)

Fig 5.16 shows the surface plots of oxide scale thickness on the billet top and bottom surfaces after soaking zone for total residence time of 10800 seconds. It is observed from the plots that oxide scale growth in the soaking zone is more pronounced. This is demonstrating fact that higher average temperature of the billet in the soaking zone increases oxidation rate. It is observed from the plots that the oxide scale thickness on the top surface is more than the oxide scale thickness on the bottom surface. Oxide scale thickness is having minimum value at the skid contact locations. This is because of lower temperature at these locations of the billet.

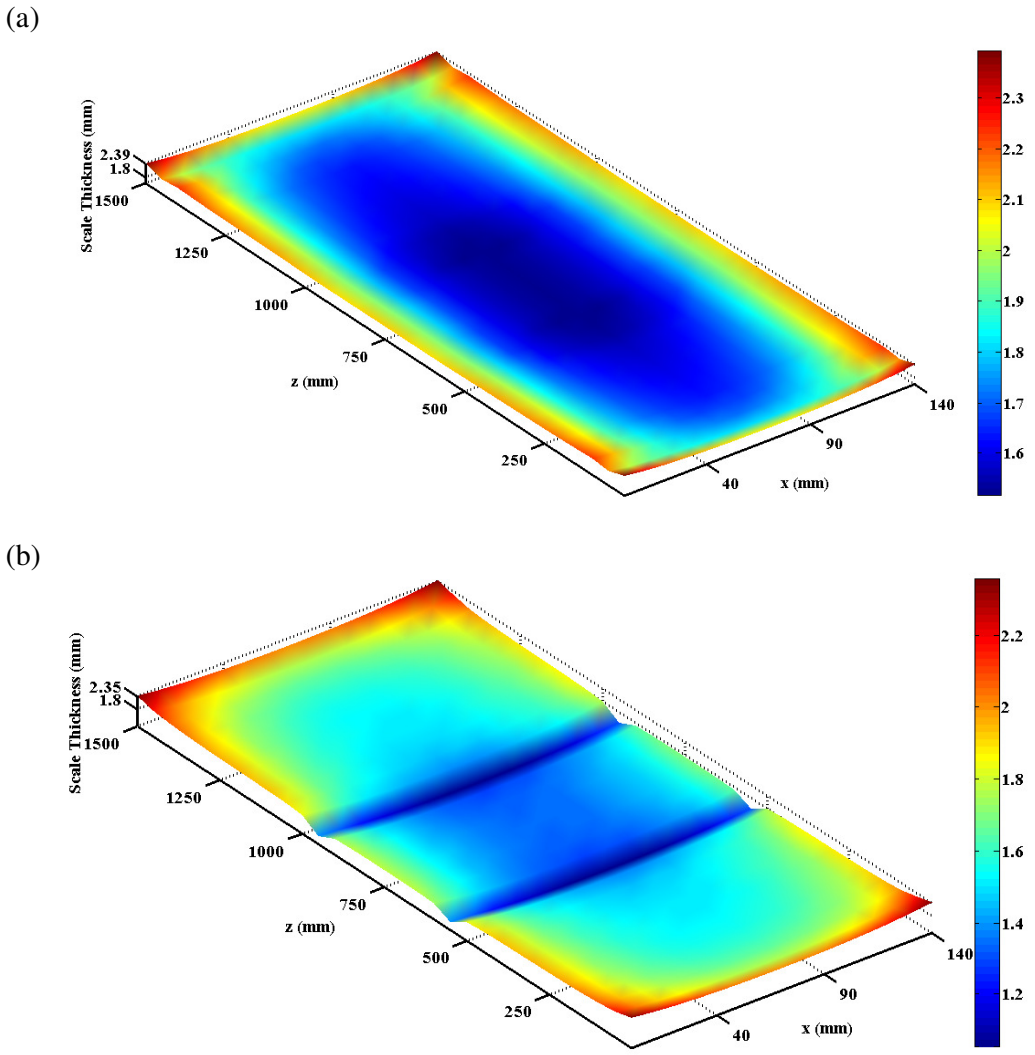

Fig. 5.16: Oxide scale thickness, surface plot at 10800 seconds: (a) top surface (b) bottom surface

The surface plots of oxides scale thickness on billet side plane (*y*-*z* plane) and end plane (*x*-*y* plane) for residence time of 10800 seconds are shown in Fig. 5.17. Plots demonstrating clearly that oxide scale thicknesses are always higher in the high temperature regions than those observed in the low temperature region. This is reinforcing the fact that elevated temperature promotes oxidation. Similar to the previous case, From Fig. 5.17(a), it is observed that for the region of skid contact vicinity, the oxide scale thickness growth is relatively lower in comparison to other regions. From these surface plots of oxide scale it can be concluded that oxide scale growth depends on the billet temperature field.

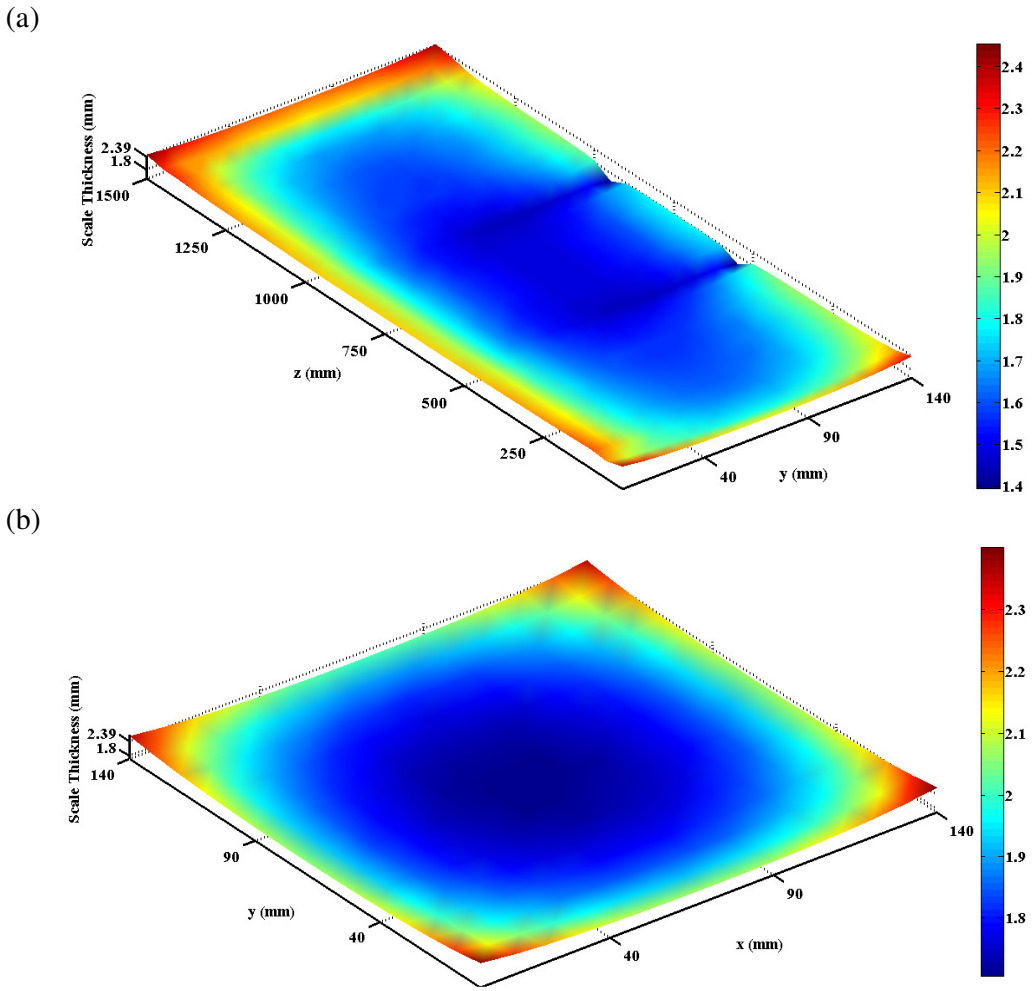

Fig. 5.17: Oxide scale thickness, surface plot at 10800 seconds: (a) side surface (*y-z* plane) (b) end surface (*x-y* plane)

5.2.2.3 Effect of billet cross section

Simulations were made for three different billets cross sectional areas to examine the effect of billet thickness on the temperature field in the billet. Here, simulations were performed; keeping with all other conditions same as used in the previous sections. The billets cross sectional areas chosen were: 100 mm × 100 mm, 140 mm × 140 mm and 180 mm × 180 mm.

Fig. 5.18 shows the comparisons of the average temperatures of billet top plane for three billet cross-sections and Figs. 5.19 & 5.20 shows the comparisons of the corresponding bottom and center plane average temperatures respectively. It is observed that the rates of average temperature rise for all the three planes are reduced with increase of billet cross-section size.

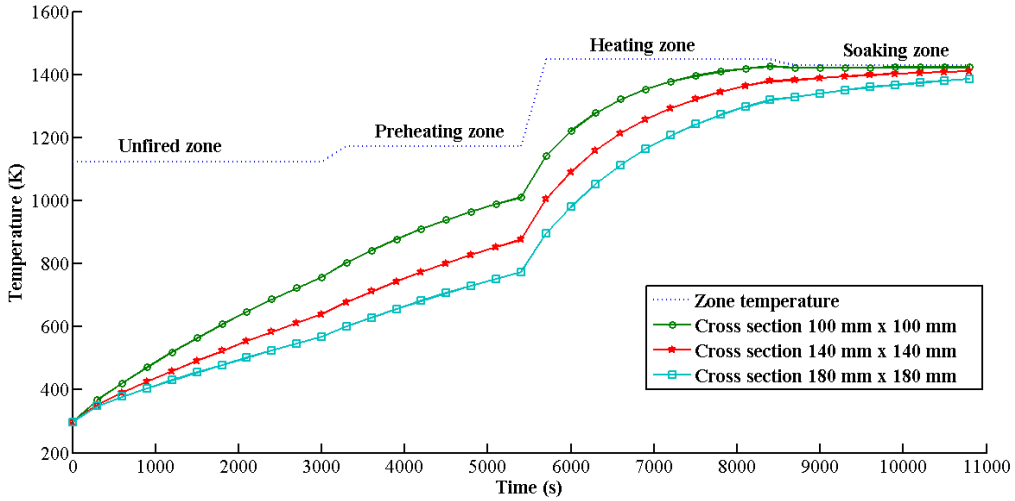

Fig. 5.18: Average temperature of the billet top plane during reheating for various billet cross-sections

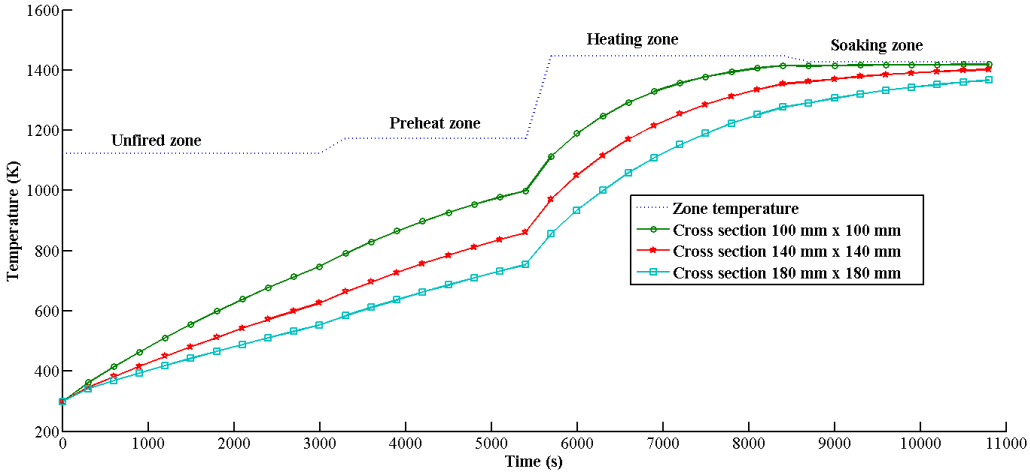

Fig. 5.19: Average temperature of the billet bottom plane during reheating for various billet cross-sections

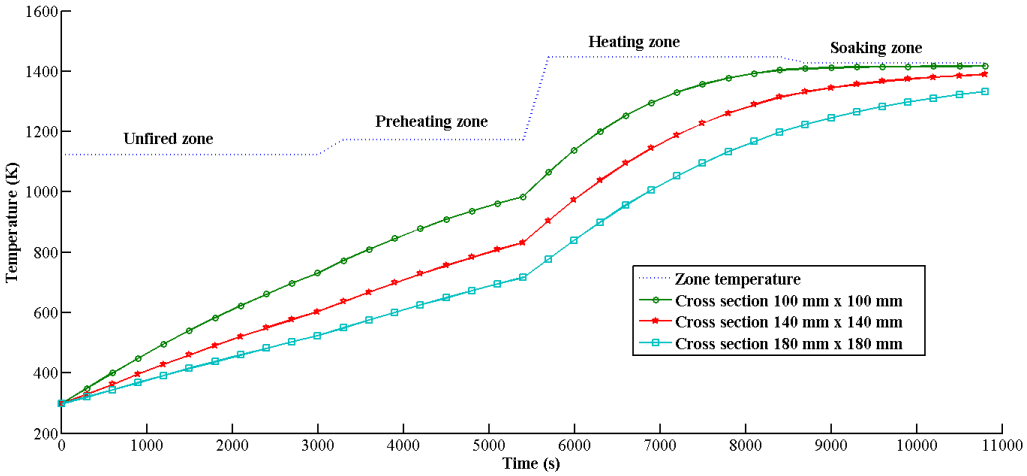

Fig. 5.20: Average temperature of the billet center plane during reheating for various billet cross-sections

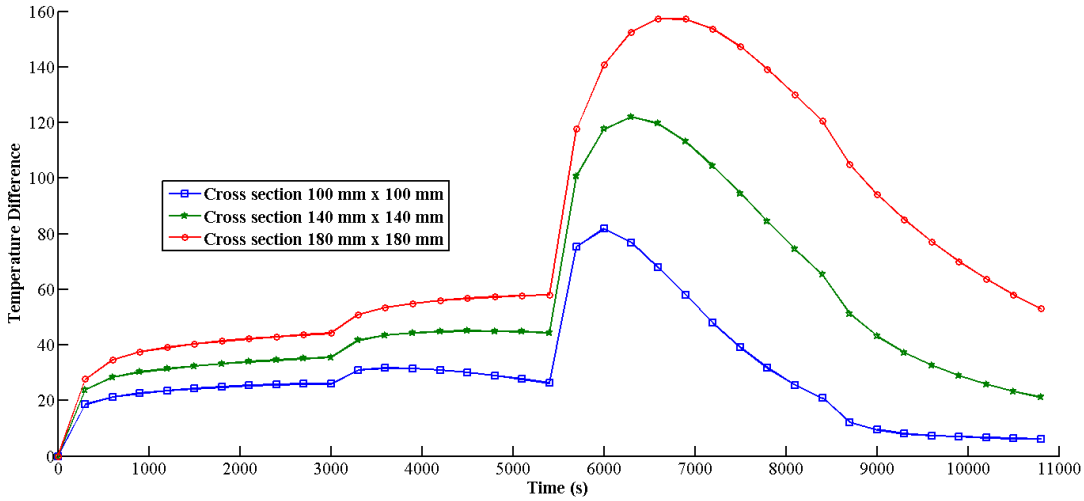

Fig. 5.21: Difference between the average temperature of billet top plane and center plane during reheating for various billet cross-sections

Fig. 5.21 shows the difference between the average temperature of billet top plane and center plane during reheating for various billet cross-sections. As expected, the billet top surface average temperatures are higher than the corresponding bottom and center plane temperatures.

Fig. 5.22 shows the difference between the average temperature of billet bottom plane and center plane during reheating for various billet cross-sections. As observed, the average temperature of the billet bottom plane is slightly higher than the corresponding center plane temperature.

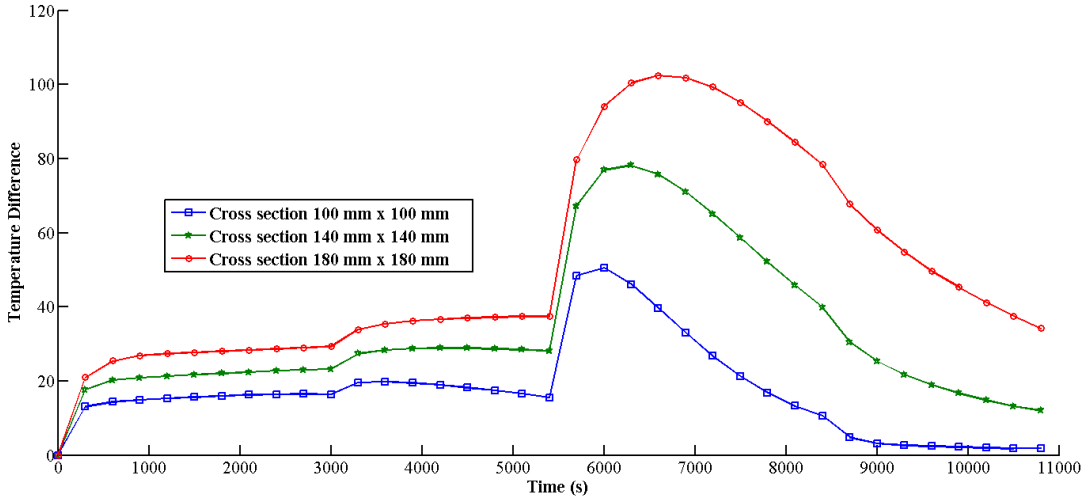

Fig. 5.22: Difference between the average temperature of billet bottom plane and center plane during reheating for various billet cross-sections

The 3D temperature field in the billet as discussed previously and shown in Fig. 5.6 indicates that the location of the minimum temperature in the billet at the later part of residence time is founds just at contact location of the billet bottom plane with skid and not at the center plane. However, here it is observed the bottom plane average temperatures are higher than the corresponding center plane average temperatures, even during later part of residence time.

5.3 Investigations on Zone Temperature Sensitivity

In order to investigate the effects of zone temperatures on responses of interest in the reheating process, simulation results are obtained for combinations. The objective of this study is to identify, which of the zone temperature values have the largest effects and to find possible interaction of zone temperature values.

5.3.1 Methodology

Design of Experiments (DOE) is a scientific approach to plan the experiments in order to collect suitable data. The collected data are analyzed by statistical methods in order to draw meaning objective conclusions. DOE based techniques are part of promising approaches for parametric investigations on real physical systems or models. These techniques have been widely studied and used in the varied field like medical, web designing, product design, manufacturing management, economics forecasts, etc. In the present study the combinations are generated through 3^k full factorial design method of DOE approach, where 3 is the number of levels used in the design and k is the number of input parameter. The further details about DOE approach can be referred from Montgomery (2014). The key steps of the methodology include:

Step 1 **Recognition of the objectives:** It is obvious that each of the reheat furnace zone temperature will have effect on the billet heating characteristics and oxide scale growth. The overall objectives considered for this theoretical experiments is to identify which zones temperature value have the most significant effect on heating responses and also to find possible interactions (if any). Additionally, this study aims to decide the effect of a level of a zone temperature, while all other zone temperatures are varying in their possible limits.

Step 2 **Selection of response of interest for billet reheating process simulation:** The response of interest chosen in this study are maximum temperature, minimum temperature, maximum temperature difference, average temperature, maximum oxide scale thickness and average oxide scale thickness.

Step 3 **Selection of input factors and their level values:** In the present study, three levels of the four zone temperature considered as input factor, and their values are given in Table 5.5. The temperatures of three level for different zones of reheat furnace are chosen in accordance with usual operating fluctuations during reheat furnace operations.

Table 5.5 Values of three levels of furnace zone temperature considered as input parameters

Level	Temperature of zone-1 (K)	Temperature of zone-2 (K)	Temperature of zone-3 (K)	Temperature of zone-4 (K)
1	1123	1223	1448	1428
2	1223	1273	1473	1453
3	1323	1323	1498	1478

Step 4 **Generation of combination set of input factors:** For this particular case of 3^4 full factorial design approach results 81 combinations of input parameters, which is given in Appendix-A1.

Step 5 **Simulation for combinations**: The 3D numerical reheating model developed in this study are simulated for each combination set of the input factor (furnace zone temperatures) using own developed MATLAB® code. The response of interests: maximum temperature, minimum temperature, maximum temperature difference, average temperature, maximum oxide scale thickness and average oxide scale thickness are obtained through simulation.

Step 6 **Analysis of results:** The model simulation results corresponding to the combination set are analyzed by statistical techniques: analysis of mean (ANOM) and analysis of variance (ANOVA).

5.3.2 Results and discussion

The chosen response of interests corresponding to each combination obtained through reheat model simulation for a residence time of 10800 seconds. The values of maximum temperature average temperature and minimum temperature of the steel billet corresponds to each combinations are shown in Fig. 5.23.

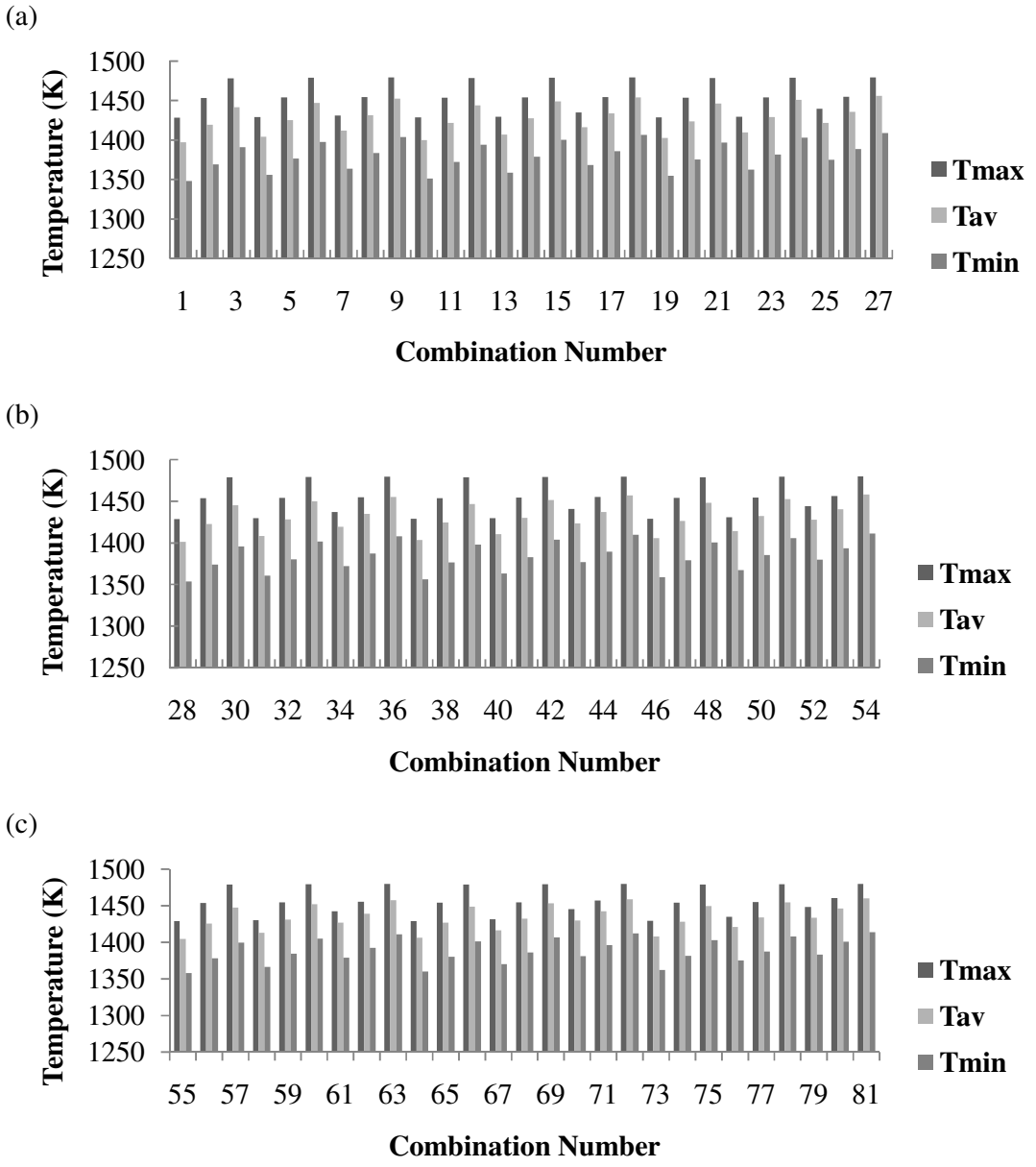

Fig. 5.23: Response of interest: Tmax, Maximum temperature of billet; Tav, Average temperature of billet; Tmin, Minimum temperature of billet for different zone temperature combinations: (a) combination number 1-27, (b) combination number 28-54, (c) combination number 55-81

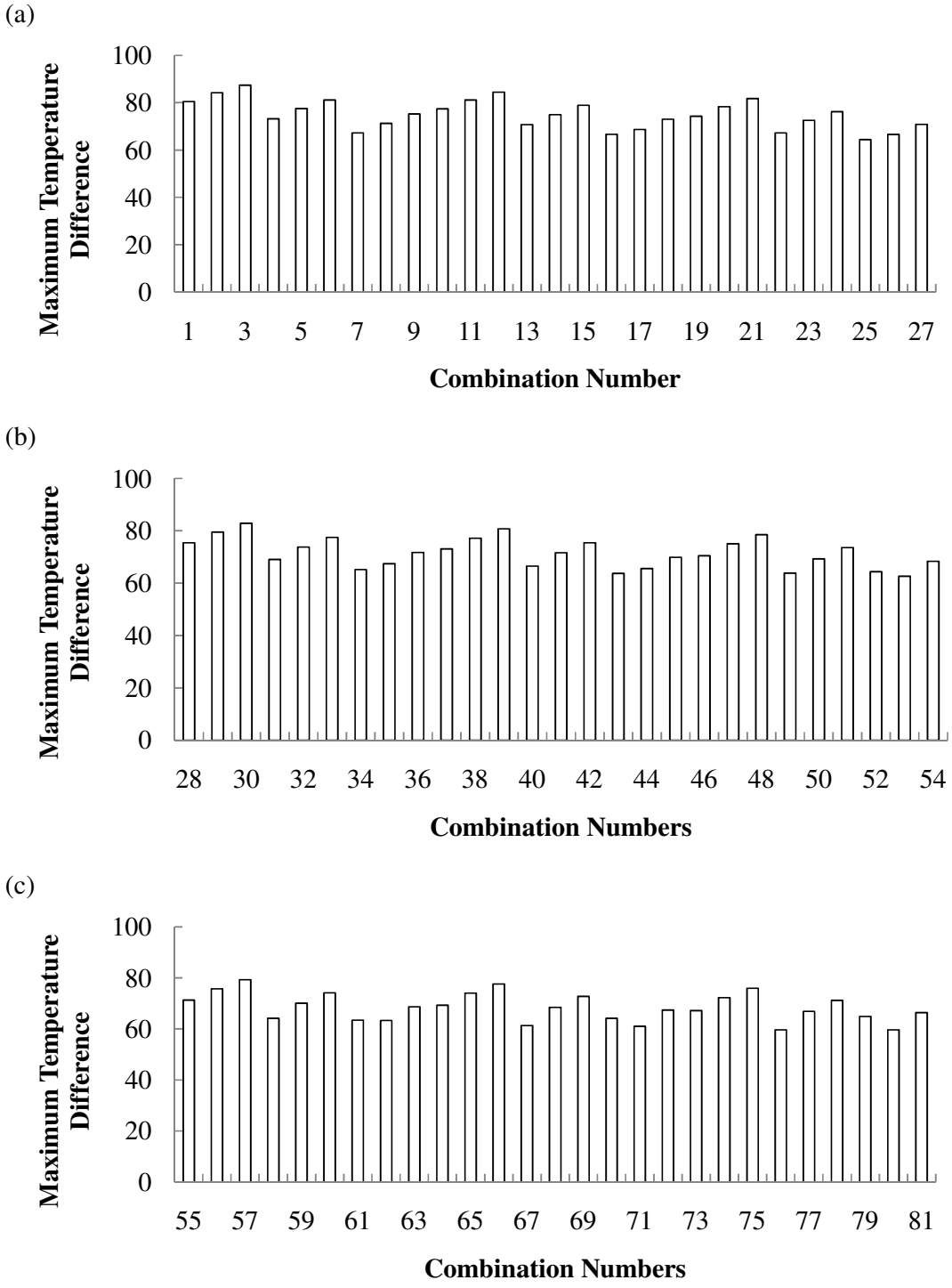

Fig. 5.24: Response of interest: Maximum temperature difference in the billet for different zone temperature combinations: (a) combination number 1-27 (b) combination number 28-54 (c) combination number 55-81

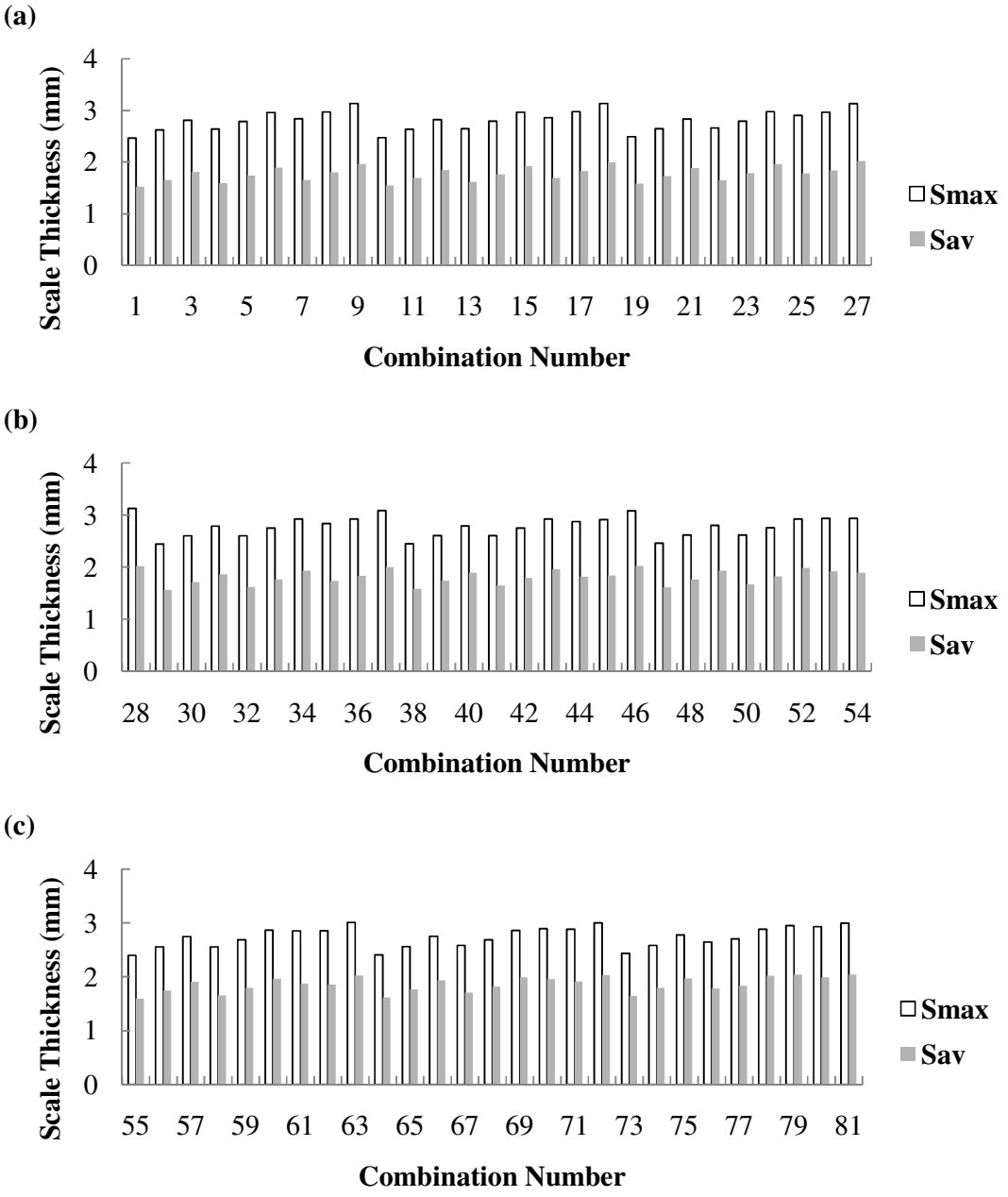

Fig. 5.25: Response of interest: Smax Maximum scale thickness; Sav Average scale thickness; for different zone temperature combinations: (a) combination number 1-27 (b) combination number 28-54 (c) combination number 55-81

Here, the maximum temperature means local maximum temperature which is observed at the corner of billet. The minimum temperature represents local minimum temperature, which is mostly observed at the billet skid contact location. Whereas average temperature of billet is representing average of all nodal temperature. Similarly maximum temperature difference, which is representing difference of maximum and minimum temperature are

shown in Fig. 5.24 The other two chosen response of interests: maximum oxide scale thicknesses and average oxide scale thicknesses are shown in Fig. 5.25.

From these values zone temperature combinations can be selected for desired values of responses of interests. These simulated results are further analyzed using statistical techniques ANOM and ANOVA. The details of procedure implementations of and analysis of the simulated results are given in the subsequent sections.

5.3.2.1 Analysis of mean

The responses of interests for combinations as presented in the previous sections are consolidated using the approach of Analysis of Mean (ANOM). ANOM is statistical technique which is very convenient for analysis of interactions among the factors and their implications (Mitra 2008; Montgomery 2014). Here, ANOM study is performed for four factors (temperature of four zone of reheat furnace) with their three levels as discussed in section 5.3.1. For each level of a factor, all corresponding responses are consolidated using the approach of ANOM. Hence, corresponding to each response for each factor three points are obtained at each level, these points are plotted as shown in Fig.5.26.

The results obtained from ANOM are given in Fig. 5.26, which shows plots for six responses of interest. It is observed that plot for all six responses of interest show strong interaction. This means that the variation of one zone temperature is related to variation of other zone temperature in terms of overall value of the response of interest.

Fig. 5.26(a) shows the combined effect of variation of zone temperatures (parameter) on the billet maximum temperature. The relative significance of each factor can also be recognized. Here, the temperature of zone-4 is highly significant and the temperature of zone -1 & zone-2 is least significant.

Fig. 5.26(b) and Fig. 5.26(d) present parameter combined effect on billet minimum temperature and billet average temperature respectively. It can be seen that billet minimum temperature and billet average temperature are most sensitive to temperature of zone-4 and least sensitive to temperature of zone-2.

Fig. 5.26(c) shows the combined effect of zone temperature on maximum temperature difference. It can be observed that in the transition from level 1 to 2, temperature of zone-3 is most significant, while for level 2 to 3, the temperature of zone-4 is most significant. The temperature of zone-2 is identified as least significant parameter.

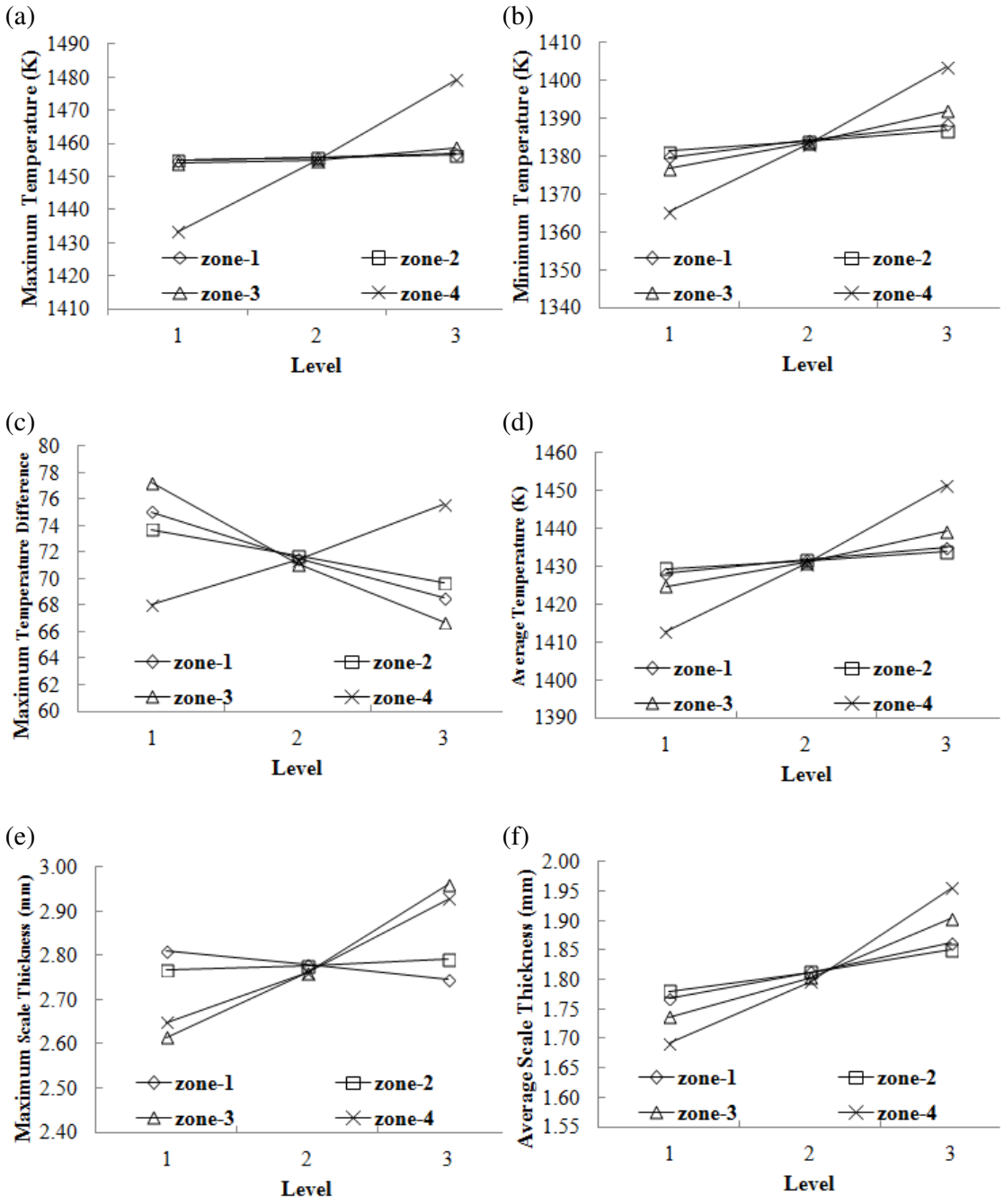

Fig. 5.26: Effect of zone temperature on the six response of interests: (a) maximum temperature (b) minimum temperature (c) maximum temperature difference (d) average temperature (e) maximum scale thickness (f) average scale thickness

Fig. 5.26(e) and Fig. 5.26(f) present parameter combined effect on the maximum scale thickness and average scale thickness respectively. It is observed that scale thickness growth is most sensitive to temperature value of zone -3 and least sensitive to the temperature value of zone-2.

This analysis is helpful to achieve a targeted value of desired response function by setting the input factors, for example, if it is desired to reduce the maximum film thickness, all factors should be kept in its first level as evident from Fig. 5.26 (e). The DOE based ANOM give more realistic results, as all the effect of a level is obtained while all other factors vary in their possible limits. This characteristic was not possible from a single parameter sensitivity analysis.

5.3.2.2 Analysis of variance

To further investigate the statistically significant zone temperatures (input factor) for the chosen responses of interests, Analysis of Variance (ANOVA) technique is used. ANOVA is useful technique in the field of statistical inference. The details of ANOVA can be referred from Montgomery (2014). The software Design- Expert (2014) is used to perform ANOVA study on the chosen responses for DOE combinations simulation runs. The Half Normal Plots (HNP) obtained during this ANOVA studies are shown in the Figs. 5.27 to Fig. 5.32.

HNP gives grouping of statically significant and insignificant factors and their interactions. It also gives their rank relative to other effects. It also gives the factors and interactions of factors that least or negligible effects. In the HNP the factors that are significant fall away to the right of the line. The factors that are statistically insignificant or have least effect on response of interest are unselected which fall along the line. The unselected insignificant terms (factors) are approximately assumed to follow a normal distribution.

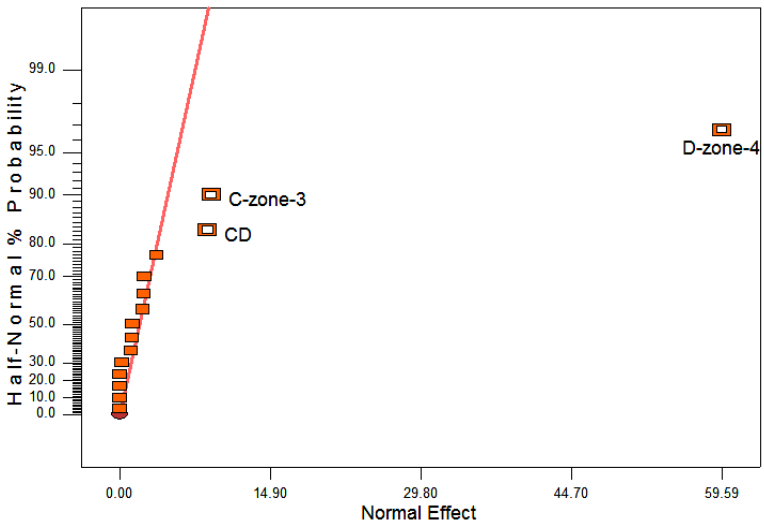

Fig. 5.27: Half-Normal plot: maximum temperature of billet

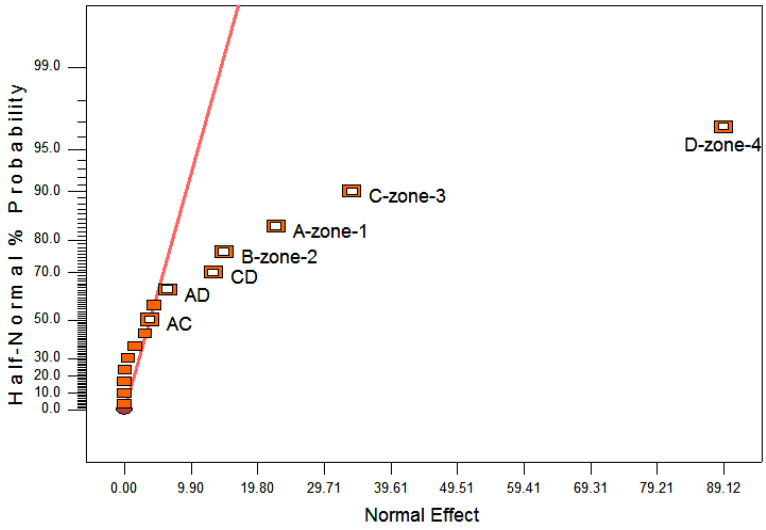

Fig. 5.28: Half-Normal plot: average temperature of billet

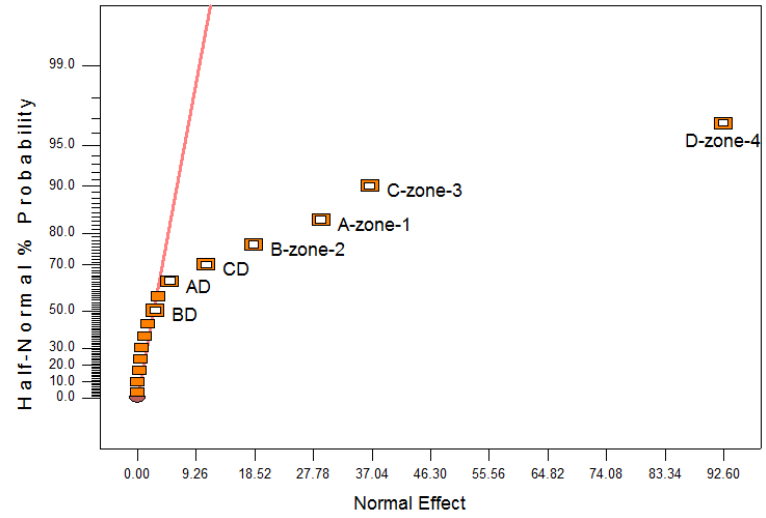

Fig. 5.29: Half-Normal Plot: minimum temperature of billet

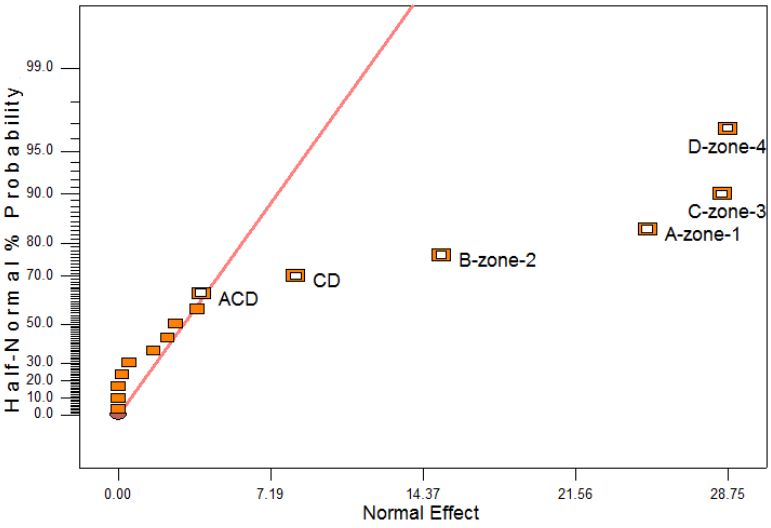

Fig. 5.30: Half-Normal Plot: maximum temperature difference in the billet

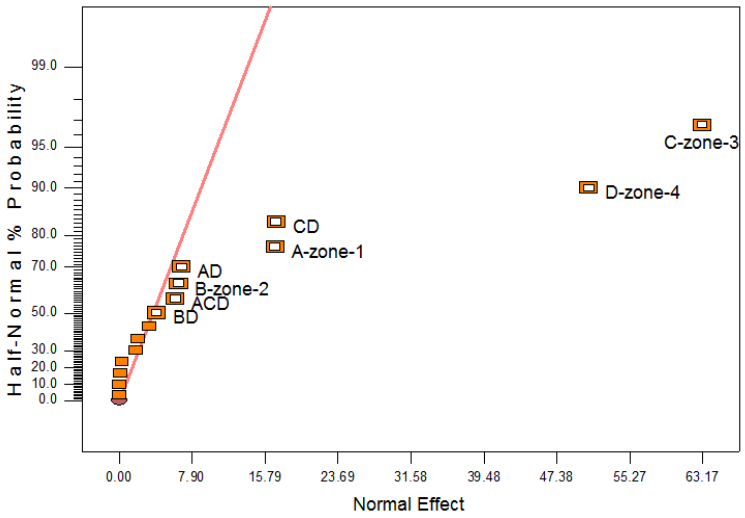

Fig. 5.31: Half-Normal Plot: maximum oxide scale thickness

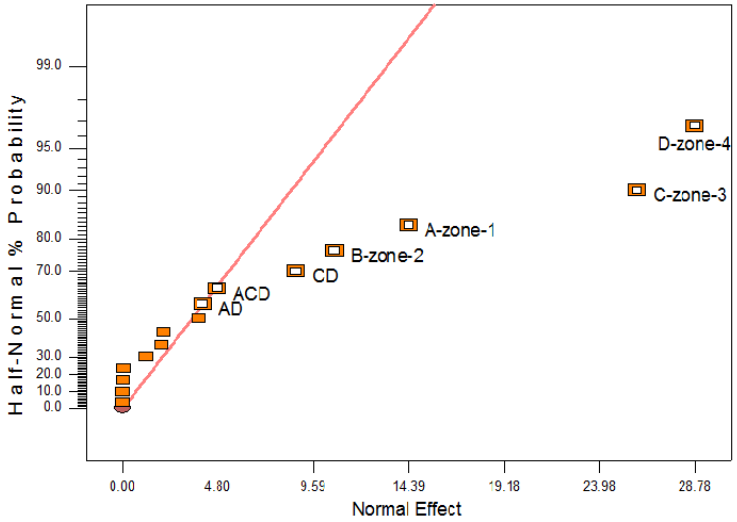

Fig. 5.32: Half-Normal Plot: average oxide scale thickness on the billet surface

The symbols A, B, C and D in ANOVA are representing zone-1, zone-2, zone-3 and zone-4 temperatures of reheat furnace respectively.

The statistically significant input factors for six responses: maximum temperature; average temperature; minimum temperature; maximum temperature difference, maximum oxide scale thickness and average oxide scale thickness obtained from this study are given in Table 5.6. Additionally, the prediction equations in terms of coded units for all six responses are given in the Tables 5.7 & 5.8. The coded values are A= [-1,0,1], B= [-1,0,1], C= [-1,0,1] and D= [-1,0,1] where -1, 0 ,1 refers to level 1, level 2 and level 3 respectively as given in Table 5.5.

Table 5.6: Statistically significant input factors (zone temperature) from ANOVA study

Response of interest	Statistically significant input factors
Maximum temperature	D, C, CD
Average Temperature	D, C, A, B, CD, AD, AC
Minimum Temperature	D, C, A, B, CD, AD, BD
Maximum temperature difference	D, C, A, B, CD, ACD
Maximum oxide scale thickness	C, D, CD, A, AD, B, ACD, BD
Average oxide scale thickness	D, C, A, B, CD, ACD, AD

Table 5.7: Functional relationship between billet temperature response values and the input factors (zone temperatures)

Response of interest	Functional relationship in terms of coded units
Maximum temperature	$Tmax = 1455.7710 - 1.8760 \times C - 1.01647 \times C^2 - 2.418 \times D - 1.0478 \times D^2 - .4446 \times CD - 1.6758 \times C^2D + 0.9733 \times CD^2 + 0.6616 \times C^2D^2$
Average temperature	$Tav = 1431.6561 - 3.4926 \times A + 0.0171 \times A^2 - 2.2714 \times B - 0.0694 \times B^2 - 6.9893 \times - 0.7062 \times C^2 - 18.866 \times D - 0.9064 \times D^2 + 0.6029 \times AC + 0.2106 \times A^2C + 0.3449 \times AC^2 - 0.12807 \times A^2C^2 - 1.4036 \times AD - 0.1087 \times A^2D + 0.25818 \times AD^2 - 0.04204 \times A^2D^2 - 2.5131 \times CD - 0.4964 \times C^2D + 0.5247 \times CD^2 - 0.0500 \times C^2D^2$
Minimum temperature	$Tmin = 1384.0643 - 4.3068 \times A + 0.0692 \times A^2 - 2.6934 \times B - 0.0553 \times B^2 - 7.3921 \times C - 0.4778 \times C^2 - 18.8070 \times D - 0.7727 \times D^2 - 1.1205 \times AD + 0.0079 \times A^2D + 0.1443 \times AD^2 - 0.1311 \times A^2D^2 - 0.6862 \times BD - 0.0654 \times B^2D + 0.0577 \times BD^2 - 0.0034 \times B^2D^2 - 2.0359 \times CD - 0.3136 \times C^2D + 0.4306 \times CD^2 - 0.1231 \times C^2D^2$
Maximum temperature difference	$MTD = 71.7067 + 3.3393 \times A - 0.1518 \times A^2 + 2.0154 \times B - .01491 \times B^2 + 5.5160 \times C - 0.5386 \times C^2 - 3.6112 \times D - 0.2751 \times D^2 - 0.4086 \times C D - 1.3622 \times C^2D + 0.5427 \times C D^2 + 0.7848 \times C^2D^2 + 0.4466 \times ACD + 0.0188 \times A^2C D + 0.7892 \times AC^2D + 0.2766 \times A^2C^2D - 0.3495 \times AC D^2 - 0.0729 \times A^2C D^2 - 0.4829 \times AC^2D^2 - 0.1732 \times A^2C^2D^2$

Table 5.8: Functional relationship between oxide scale thicknesses response values and the input factors (zone temperatures)

Response of interest	Functional relationship in terms of coded units
Maximum oxide scale thickness	$Smax = 2.7788 + 0.0328 \times A + 0.0008 \times A^2 - 0.0110 \times B - 0.0035 \times B^2 - 0.1648 \times C - 0.017 \times C^2 - 0.1300 \times D - 0.0189 \times D^2 - 0.0183 \times AD - 0.0035 \times A^2D + 0.0067 \times AD^2 - 0.00004 \times A^2D^2 - 0.0120 \times BD - 0.0020 \times B^2D + 0.0031 \times BD^2 + 0.0005 \times B^2D^2 - 0.0377 \times CD - 0.0138 \times C^2D + 0.0095 \times CD^2 + 0.0032 \times C^2D^2 + 0.0181 \times ACD + 0.0033 \times A^2CD + 0.0083 \times AC^2D - 0.0049 \times A^2C^2D - 0.0055 \times ACD^2$
Average oxide scale thickness	$Sav = 1.8145 - 0.0465 \times A - 0.00186 \times A^2 - 0.0343 \times B - 0.0021 \times B^2 - 0.0782 \times C - 0.0115 \times C^2 - 0.1230 \times D - 0.0180 \times D^2 - 0.0200 \times AD - 0.0045 \times A^2D + 0.0092 \times AD^2 - 0.0001 \times A^2D^2 - 0.0290 \times CD - 0.0202 \times C^2D + 0.0137 \times CD^2 + 0.0060 \times C^2D^2 + 0.02492 \times ACD + 0.0047 \times A^2CD + 0.0134 \times AC^2D - 0.0065 \times A^2C^2D - 0.0085 \times ACD^2 + 0.0007 \times A^2CD^2 - 0.0020 \times AC^2D^2$

5.4 Closure

The developed model was simulated using code developed in MATLAB® for predictions of 3D field in the billet and growth of oxide scale on the billet surfaces. The model was used to study the heating characteristics of steel billet in the presence and growth of oxide scale. It was found that the effect of oxide scale formation and growth on billet heating is significant. The effect of the skid on the billet temperature field is significant. It was also observed that due to skid rail local minimum temperature location in the billet changes during reheat when billet moves from preheat zone to soaking zone. The effects of skid cannot be modeled properly in 2D and 1D models. Hence, it becomes imperative to consider 3D heat conduction modelling for better observations of temperature field. A study was carried out to investigate the effect of zone temperature on responses of interest during the reheating process. The statistical methodology employed in the study is useful to decide the zone temperature variations that have more effect on particular response of interest. The interactions of different zone temperatures were also observed. Notwithstanding that the results presented in this study are for specific input parameters, the same methodology may be

applicable to other reheating process. The developed 3D model will be in general, useful to steel industry, for the effective development of reheating process control system and control strategy. The next chapter presents heat transfer simulation during transport of billet from reheat furnace to the rolling mills.

Chapter 6

Heat Transfer Simulation during Transport of Steel Billet

6.1 Introduction

The work discussed in the previous chapters resulted in the development, validation and simulation of numerical heat transfer model with growth of oxide scale for the prediction of 3D temperature in the billet during reheat. In steel industries the billets coming out from the reheat furnace are transported to the rolling mills. Predictions of billet temperature during transport are vital for several reasons, especially for downstream activities like rolling force calculation and microstructure study of rolled product. Inadequate temperature measuring instruments demands suitable model for billet temperature field predictions. This chapter presents heat transfer simulation for predictions of 3D temperature field in the billet during transport from the reheat furnace to the rolling mills. The chapter begins with the presentation of the model development approach. The remainder of this chapter is devoted for the validation study and model simulations. In order to validate the proposed model, the numerical model simulation results are compared with analytical solutions results subjected to limited conditions. This is followed by a presentation of simulation results along with conclusions drawn from the study of billet cooling characteristics. Finally, some closure remarks are presented.

6.2 Problem Descriptions & Overall Methodology

The temperature field in the steel billet developed during reheating is further changed when heated billets from the reheat furnace are transported to the rolling mills. As discussed in the previous chapters, during reheating an oxide scale layer grows on the billet surfaces. The presence of oxide layer modifies the cooling rate of steel billet during transport. After getting discharged from the furnace the billets are descaled using descaler which is kept at a distance from the furnace, further it is transported to the rolling mills. The descaler is using high pressure water jets to remove the oxide scale layer developed on the billet surfaces. All these processes affect the heat loss from the billet during transport significantly, which in turn influences the temperature field in the billet. The predictions of the temperature field will be of immense help to downstream activities of rolling mills such as roll force

calculations, product quality and micro structural control of the product. Previous reported work (Jaklic et al., 2002) FDM explicit numerical model for steel billet transport, assumes the billet at uniform initial temperature and having constant uniform oxide scale thickness throughout the billet surfaces. However, uniform initial temperature assumption makes temperature predictions erroneous because in actual situations, the billets coming out from the furnace by and large have a certain temperature gradient within the material. Additionally, growth of oxide scale layer on the billet surfaces is not uniform as observed and discussed in the previous chapters. Hence, it is essential for the model to capture the actual temperature field of the billet and oxide scale thickness after reheat as initial conditions for heat transfer simulation during transport. Here an attempt was made to develop a model to simulate the heat transfer during transport of the billet.

The proposed numerical model for heat transfer simulation during steel billet transport considers actual non-uniform temperature and oxide scale thickness as initial conditions. To facilitate this, the time dependent boundary conditions are assigned. While change of boundary conditions, the temperature and oxide scale history is carried forward. The numerical model is very much similar to the reheating model as discussed in the previous chapters. In the reheating model the surrounding environment is the combustion gases whereas in transport model, the surrounding environment is atmospheric air. The radiation heat transfer is included in reheat model as heat flux on the steel billet surfaces, where the emissive and absorptive behavior of combustion gases was approximated by WSGGM (Hottel and Sarofim, 1967; Smith et al., 1982) as detailed in chapter 3. Whereas the radiation heat transfer is included in transport model as heat flux on the steel billet surfaces using Stefan Boltzmann law, where thermo-physical properties of surrounding air at nodal mean film temperature is obtained by NIST Database 23 REFPROP® Version 9.0 (2010). The convection heat transfer is included as heat flux on the steel billet surfaces, assuming the case flow of air over a flat plate.

6.3 Model Development Approach

The model development focuses on a single billet and follows its movement when it is transported through conveyor from the reheat furnace to the rolling mill. The temperature history of the billet is carried forward. In the 3D transient conduction model of billet: x, y and z directions are considered as billet width, billet height and billet length directions respectively, similar to reheat model conditions. The billets are transported by the roller

conveyor. The billet is assumed to be placed longitudinally along the displacement direction on the roller conveyor such as shown in Fig. 6.1.

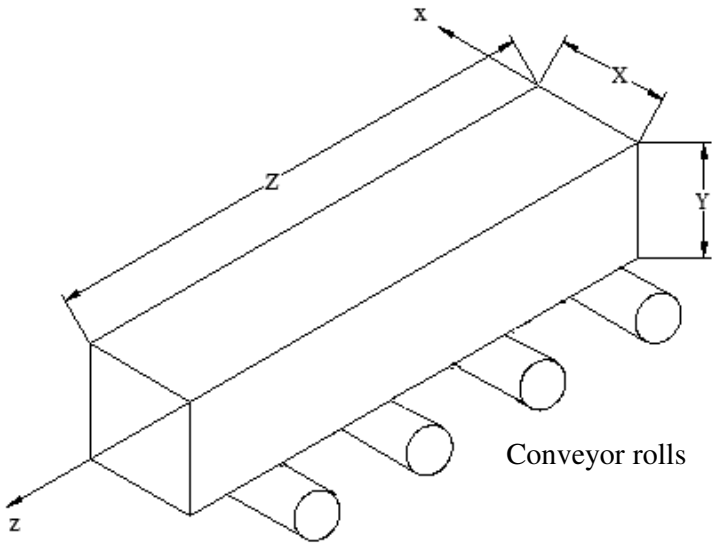

Fig. 6.1: Orientation of billet considered in numerical modelling and heat transfer simulation during billet transport

The following assumptions are made for present study: (i) Oxide scale is assumed to be single layer of wustite. (ii) It is assumed that the oxide layer remains attached to the steel outer surface. (iii) The contact resistance between oxide scale and steel is neglected. (iv) The heat exchanged between the billet and transport rolls uniformly distributed on the bottom surface. This assumption is reasonably justified as the billet move fast during transport. (v) The descaling process removes the oxide scale completely from the billet surfaces and no further oxidation takes place.

6.3.1 Governing equation & boundary conditions

The phenomenon of transient heat conduction in the steel for 3D problem is governed by

$$\frac{\partial}{\partial x}\left(k\frac{\partial T}{\partial x}\right)+\frac{\partial}{\partial y}\left(k\frac{\partial T}{\partial y}\right)+\frac{\partial}{\partial z}\left(k\frac{\partial T}{\partial z}\right)=\rho c\frac{\partial T}{\partial t} \qquad (6.1)$$

The boundary conditions used here to solve 3D transient heat condition in the billet are adopted from Jaklic et al. (2002). The top, side and end surfaces of the steel billet are exposed to the surrounding air. During transport of billet, it exchanges heat with the surrounding air by convection and radiation modes of heat transfer. The total heat transfer coefficient accounts for both convection and radiation can be expressed as:

$$h_t = h_c + \varepsilon\sigma(T_\infty^2 + T^2)(T_\infty + T) \tag{6.2}$$

where h_c is convective heat transfer coefficient, ε is the emissivity of billet surface, σ Stefan Boltzmann constant, T_∞ is the surrounding air temperature and T refers to billet surface temperature.

In order to calculate the convection heat transfer coefficient, the flow of surrounding air over billet surface is assumed to be a case of laminar flow along a flat plate (Holman, 2002) and accordingly the convective heat transfer coefficient is given as:

$$h_c = 0.332 \frac{k_a}{x_b} \mathrm{Pr}^{1/3} \mathrm{Re}_x^{1/2} \tag{6.3}$$

where h_c is local convective heat transfer coefficient, k_a is surrounding air thermal conductivity, $\boldsymbol{x_b}$ is the length scale, the distance measured from leading edge, Pr is Prandtl number and Re_x is the local Reynolds number.

The Reynolds number Re_x is given by

$$\mathrm{Re}_x = \frac{\rho_a v_b x_b}{\mu_a} \tag{6.4}$$

where ρ_a is the density of the surrounding air, v_b billet velocity (surrounding air velocity) and μ_a is the dynamic coefficient of viscosity of air. All the above discussed air thermo-physical properties are evaluated at billet surface & air mean film temperature.

The radiation and convection heat loss from surfaces which are exposed to surrounding is given by

$$-k \left.\frac{\partial T}{\partial x}\right|_{\text{surface}} = h_t (T_\infty - T) \tag{6.5}$$

Billet exchange heat with the conveyor rolls, the heat loss from small contact surface of the billet to conveyor rolls is given by

$$-k \left.\frac{\partial T}{\partial x}\right|_{\text{contact surface}} = h_{ct} (T_r - T) \tag{6.6}$$

where h_{ct} is the contact coefficient for billet and transport rolls and T_r is the conveyor transport roll temperature. The heat exchanged between billet and transport rolls is assumed to be uniformly distributed on the billet bottom surface. In order to calculate the heat flux on the billet bottom surface, the heat flux given by Eq. (6.6) is multiplied by the ratio of contact area to total bottom area of the billet.

The high pressure water jet is used for the removal of oxide scale from the billet surfaces. Ceuller et al., 2004 established and suggests water jet conditions such as flow rate, velocity and pressure of water jets for the removal of the oxide scale layer from the steel billet surfaces. The heat transfer from the billet surface for water spray can be characterized by a quench heat transfer coefficient (Jaklic et al. (2002). The heat exchange by the billet during the descaling is given as:

$$-k\left.\frac{\partial T}{\partial x}\right|_{surfaces} = h_q\,(T_{water} - T\,) \tag{6.7}$$

where h_q is the quench heat transfer coefficient and T_w is temperature of water spray. The quench heat transfer coefficient values depend upon the jet conditions and steel surface temperature. The further details about the range and experimentally measured heat transfer coefficients for different alloy of steel quenching in water can be referred from literature (Metals Hand Book, 1981; Hasan et al., 2011).

6.3.2 Discretization approach

The numerical model for heat transfer simulation during billet transport builds on the 3D transient heat conduction numerical model with the growth of oxide scale as proposed in the previous chapters for steel billet reheating simulations. Similar to the previous reheat model this model also consider oxide scale layer on the billet surfaces for the first few seconds of transport before billets pass through the descaler. As discussed in chapter 3, the oxide scale layer is modeled as one separate finite volume with node at the outer surface. Separate mesh for oxide scale and steel are considered during model development. The oxide scale layer is modeled as one separate finite volume in thickness with node at the outer surface. The details of the 3D nodal system and control volumes used for 3D transient heat conduction model are already discussed in the previous chapter 3 and 4. The heat exchange between the oxide control volume and steel control volume is through the conduction. The nodal schemes selected for modelling of oxide scale do not affect the nodal scheme and control volumes of the steel billet. In other words the nodal scheme and control volumes selected for steel billet remains identical for with and without oxide scale. This facilitates the use of the same numerical model of steel with the changed boundary conditions for the case, where oxide scale is not present: such as heat transfer simulation of the billet transport after descaling.

As discussed in chapter 3, implicit scheme is chosen for discretization, which makes the model unconditionally stable and provides flexibility in the selection of time steps. The present study considers two different time dependent values of time step. The larger value of the time step is selected for reheat simulation, where calculations are to be performed over a large time period. A smaller value of the time step is selected for transport simulation, where calculations are to be performed over a small time period. Although, the explicit scheme solution procedure is less computationally involved than that of the implicit; but the maximum size of the time step restricted by stability criterion (Ozisik, 1993), makes it inappropriate for reheat and combined reheat and transport simulation with thin oxide layer. Hence, the fully implicit 3D transient heat conduction model detailed in the chapter 3 can be easily extended for combined reheat and transport simulation with thin oxide layer.

For transport simulation, discretization equations for each node are obtained by using a control volume approach of FDM as discussed in the chapter 3, with an appropriate change in the terms contributed by new boundary conditions. For instance, for a given inner oxide surface cell, the implicit finite difference equation corresponds to the typical three stages of heat transfer simulation during billet transport are given as:

Simulation with oxide scale: When the billet is coming out of the reheat furnace the oxide scale layer surrounds and attached to steel surface. The inner surface cell which is exposed to the surroundings will be an inner oxide surface cell such as those shown in Fig. 3.4(f). The discretized equation for this inner oxide surface cell with the transport simulation boundary condition is given as:

$$\begin{aligned}\rho_{os}\, c_{os}\ \Delta x\Delta y\ s_{i,j,k}\frac{T_{i\,j,k}^{m+1}-T_{i,j,k}^{m}}{\Delta t} &= (k_{os})_{i+1/2,\ j,\ k}\ \Delta y\ s_{i,j,k}\frac{T_{i+1,jk}^{m+1}-T_{i,j,k}^{m+1}}{\Delta x}\\ &+(k_{os})_{i-1/2,\ j,\ k}\ \Delta y\ s_{i,j,k}\frac{T_{i-1,j,k}^{m+1}-T_{i,j,k}^{m+1}}{\Delta x}\\ &+(k_{os})_{i,\ j+1/2,\ k}\ \Delta x\ s_{i,j,k}\frac{T_{i,j+1,k}^{m+1}-T_{i,j,k}^{m+1}}{\Delta y}\\ &+(k_{os})_{i,\ j-1/2,k}\ \Delta x\ s_{i,j,k}\frac{T_{i,j-1,k}^{m+1}-T_{i,j,k}^{m+1}}{\Delta y}\\ &+(k_{os})_{i,j,k}\ \Delta x\Delta y\frac{T_{i,j,k-1}^{m+1}-T_{i,j,k}^{m+1}}{s_{i,j,k}}\\ &+(h_t)\Delta x\Delta y(T_\infty-T_{i,j,k}^{m+1})\end{aligned} \tag{6.8}$$

In the Eq. (6.8), the LHS represents change in internal energy within model cell volume. The first four terms of RHS are conduction into the model cell volume from surrounding oxide cells and the fifth term represents conduction into the model cell volume from surrounding steel cell. The sixth term represents convection and radiation across the one cell face from the surrounding air. In the above equation [Eq.(6.8)], density of oxide scale is assumed constant, whereas oxide scale thermal conductivity (k_{os}) specific heat (c_{os}) and oxide scale thickness (s) are functions of the nodal temperature, which are evaluated at the temperature corresponding to the previous iteration. As discussed in the chapter 3, the thermal conductivities at the interfaces are calculated using the harmonic mean approach (Patankar, 1980).

Simulation of water jet spray: When the billet passes through the descaler, the high pressure water jet used for removal of oxide scale from the billet surfaces. The heat lost from the billet surfaces during this process is accounted by a quench heat transfer coefficient. The discretized equation for this inner oxide surface cell with the transport simulation boundary condition is given as:

$$\begin{aligned}\rho_{os}\, c_{os}\ \Delta x\Delta y\ s_{i,j,k}\frac{T_{i\,j,k}^{m+1}-T_{i,j,k}^{m}}{\Delta t} &= (k_{os})_{i+1/2,\ j,\ k}\ \Delta y\ s_{i,j,k}\frac{T_{i+1,j\,k}^{m+1}-T_{i,j,k}^{m+1}}{\Delta x}\\ &+(k_{os})_{i-1/2,\ j,\ k}\ \Delta y\ s_{i,j,k}\frac{T_{i-1,j,k}^{m+1}-T_{i,j,k}^{m+1}}{\Delta x}\\ &+(k_{os})_{i,\ j+1/2,\ k}\ \Delta x\ s_{i,j,k}\frac{T_{i,j+1,k}^{m+1}-T_{i,j,k}^{m+1}}{\Delta y}\\ &+(k_{os})_{i,\ j-1/2,k}\ \Delta x\ s_{i,j,k}\frac{T_{i,j-1,k}^{m+1}-T_{i,j,k}^{m+1}}{\Delta y}\\ &+(k_{os})_{i,j,k}\ \Delta x\Delta y\frac{T_{i,j,k-1}^{m+1}-T_{i,j,k}^{m+1}}{s_{i,j,k}}\\ &+(h_q)\Delta x\Delta y(T_{water}-T_{i,j,k}^{m+1})\end{aligned} \tag{6.9}$$

In the above Eq. (6.9), h_q the quench heat transfer coefficient. A constant value of the quenching heat transfer coefficient is selected for the simulation.

Simulation without oxide scale: After descaling process the oxide layer is removed and exposing the steel billet material to the surrounding air. The steel surface cell such as those shown in Fig. 3.6(c), is exposed to the surrounding air. The discretized equation with the transport simulation boundary condition for this steel inner surface cell is given as:

$$\rho_{st}\, c_{st}\ \Delta x \Delta y \frac{\Delta z}{2} \frac{T_{i,\,j,\,k}^{m+1} - T_{i,j,k}^{m}}{\Delta t} = (k_{st})_{i+1/2,\,j,k} \Delta y \frac{\Delta z}{2} \frac{T_{i+1,jk}^{m+1} - T_{i,j,k}^{m+1}}{\Delta x}$$
$$+ (k_{st})_{i-1/2,\,j,\,k}\ \Delta y \frac{\Delta z}{2} \frac{T_{i-1,j,k}^{m+1} - T_{i,j,k}^{m+1}}{\Delta x}$$
$$+ (k_{st})_{i,\,j+1/2,\,k}\ \Delta x \frac{\Delta z}{2} \frac{T_{i,j+1,k}^{m+1} - T_{i,j,k}^{m+1}}{\Delta y} \qquad (6.10)$$
$$+ (k_{st})_{i,\,j-1/2,k}\ \Delta x \frac{\Delta z}{2} \frac{T_{i,j-1,k}^{m+1} - T_{i,j,k}^{m+1}}{\Delta y}$$
$$+ (h_t) \Delta x \Delta y (T_{\infty} - T_{i,j,k}^{m+1})$$
$$+ (k_{st})_{i,j,k-1/2}\ \Delta x \Delta y \frac{T_{i,j,k-1}^{m+1} - T_{i,j,k}^{m+1}}{\Delta z}$$

6.3.3 Numerical solution

Similar to reheat simulation model, all the discretized equations are assembled in a system of matrices as given by

$$\mathrm{A}\,T = b \qquad (6.11)$$

where, **A** is (N x N) matrix, **T** and **b** are (N x1), where N is total number nodes, which is equals to nx x ny x nz as discussed in chapter 4. To solve the system of matrices modified Gauss-Seidel iterations were implemented. The temperatures are calculated by visiting each nodal point in an order. The details of Gauss-Seidel method and their implementation for 3D transient heat conduction model with temperature dependent steel and the oxide thermo-physical properties are already mentioned in the chapter 4. The boundary conditions used here are time dependent, which were calculated before each new time step.

6.4 Model Validation for Billet Cooling

The developed numerical model was validated with analytical results. However, the analytical results are available for simple cases and limited conditions. In order to validate the proposed model, the simulations are carried out in the conditions, for which analytical methods are available. The analytical results obtained here through the variable separation method which is applied for one dimensional heat conduction with constant heat flux and constant surrounding temperature as boundary conditions. The analytical solutions available in the form of series of infinite terms as expressed as:

$$\frac{T(x,t)-T_\infty}{T_i-T_\infty}=\sum_{n=1}^{\infty}a_n\exp^{-d_n{}^2Fo}\cos\left(d_n\frac{x}{L}\right) \tag{6.12}$$

where Fo is Fourier number, dimensionless time ($Fo=\alpha t/L^2$) and coefficient a_n is expressed as:

$$a_n=\frac{4\sin d_n}{2d_n+\sin(2d_n)} \tag{6.13}$$

where eigenvalues d_n are the roots of characteristic equation or eigenfunction, expressed as

$$d_n\tan d_n=Bi \tag{6.14}$$

where, Bi is Biot number, dimensionless heat transfer coefficient ($Bi=hL/k$). The same procedure is applied to other two directions and 3D solution is obtained by using a product solution approach (Ozisik, 1993; Cengel and Ghajar, 2011). In the validation study the following parameters are used: billet dimension 140mm × 140mm × 140mm, constant heat transfer coefficient equal to 150 W/m^{2}K applied to all sides of the billet.

Fig. 6.2 shows comparison between numerical model simulation results and analytical solution results, temperature observed at the top corner of the billet. A good agreement between numerical model simulation results and analytical solution results is observed.

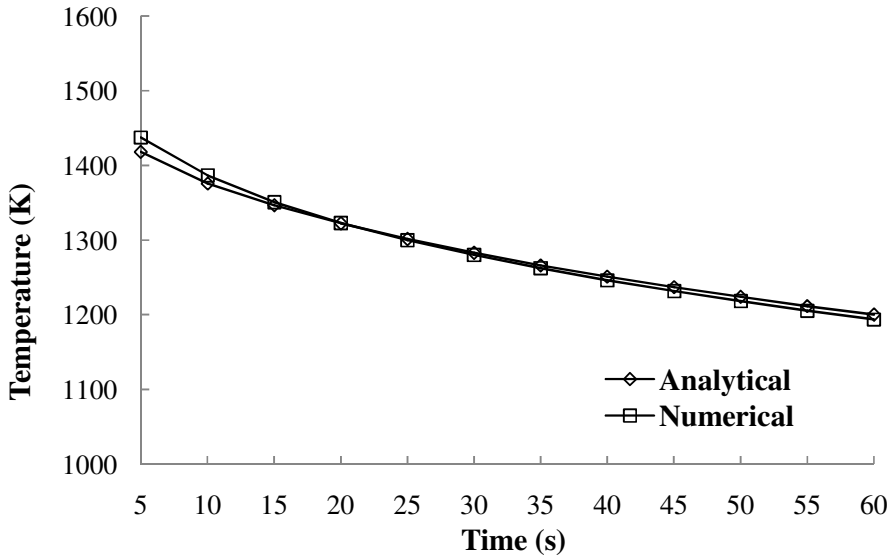

Fig. 6.2: Comparison between numerical model simulation and analytical solution results, temperature observed at the top corner of the billet

6.5 Model Simulation

The 3D transient numerical model developed in this work for steel billet transport was simulated to predict the 3D temperature field in the billet and to study the cooling characteristics of the steel billet during transport.

6.5.1 Input parameters

The steel billet of dimension $140\,\text{mm} \times 140\,\text{mm} \times 1500\,\text{mm}$ assumed to have a non-uniform temperature field when discharged from the furnace. The thermo-physical properties: density, temperature dependent specific heat and thermal conductivity for steel billet and oxide scale considered for the present transport simulation are similar to the reheat simulation. These values and expressions are already given in the Table 5.3. During billet transport simulation NIST Database 23 REFPROP® Version 9.0 (2010) is called in MATLAB® code for calculation of surrounding air thermo physical properties corresponding to local cell mean film temperature. The surrounding air temperature is set to 298 K. A grid spacing of $10\,\text{mm} \times 10\,\text{mm} \times 50\,\text{mm}$ and time step of 01 second is used for simulations.

6.5.2 Results and discussions

The developed numerical model simulation results are presented and discussed in this section. Simulations are performed for two different conditions. The details of these conditions and simulation results along with discussions are presented in the following sections.

6.5.2.1 With uniform initial temperature and oxide scale thickness

Simulations are performed with the model conditions: uniform initial temperature of 1423 K and a 2 mm uniform oxide scale thickness over the billet surfaces. It is assumed that the billets are transported at the speed of 2 m/s. The effect of oxide scale is considered for the first 10 seconds of transport time. After 10 seconds of transport, billet passes through the descaler; billet cooling under this condition is simulated through consideration of a quenching heat transfer coefficient of 2 $\text{kW/m}^2\text{K}$ for 01 second. After descaling the billet cooling is simulated without consideration of oxide scale.

The 3D temperature fields predicted during the cooling simulations with above conditions are shown in Fig. 6.3. From 3D temperature plots, it is observed that the corner and edge regions have lower temperature.

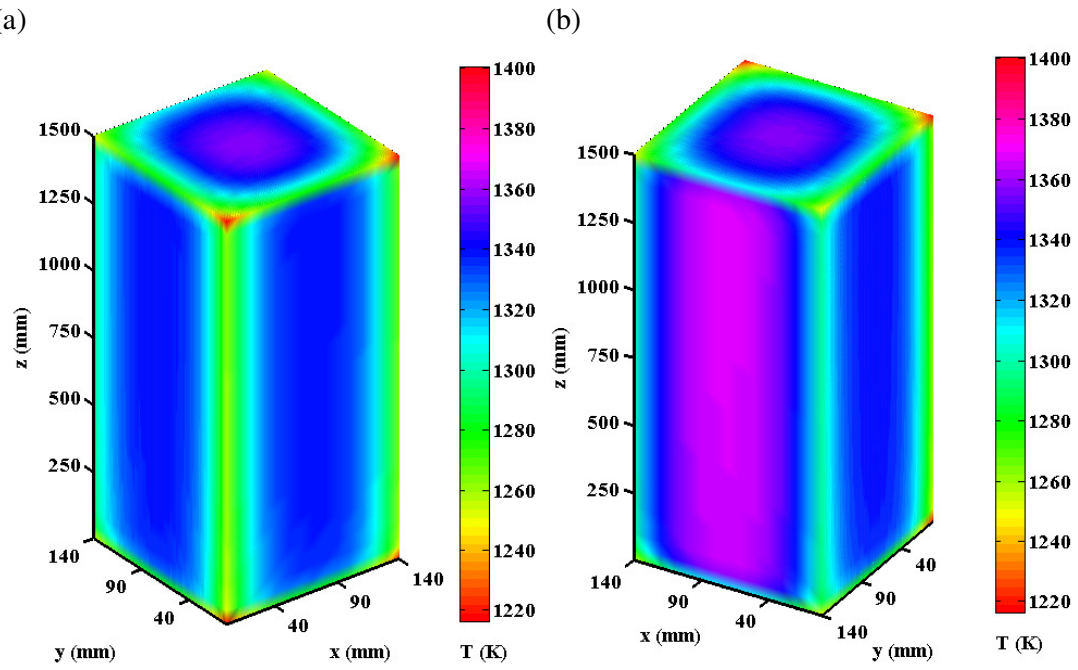

Fig. 6.3: 3D temperature field in the billet, simulation results considering uniform initial temperature of 1423 K and uniform oxide scale thickness of 2mm: (a) 120 seconds of transport time, (b) 120 seconds of transport time-rotated view

The corner of the billet is made from the intersection of three surfaces and, hence these surfaces are exposed to surrounding cooling from three directions. In other words, it means that at the corners heat come out from three directions. On the contrary, at both edges and plain surface regions, heat come out from two directions and one direction, respectively. Due to this, corners and edges get cooled faster than surface regions. Hence, predicted results exhibit the expected behavior. Fig. 6.3(b) shows the rotated view of 3D temperature plot, after 120 seconds. It shows that the effect of transport rolls on the bottom surface. It is observed that the billet bottom surface have higher temperature than the top and side surfaces. This is because of transport rolls contact with billet bottom surface which reduce heat loss from the bottom of billet.

Fig. 6.4 shows temperature surface plots of billet top plane surface, bottom plane surface and center plane surface. A significant temperature difference is seen between the top surface and the center surface of the billet. The control of temperature difference is important for many metallurgical phenomena; especially the temperature difference affects the dynamic recrystallization and the dynamic recovery mechanism during the rolling of billet resulting in microstructure changes (Sheikh, 2009).

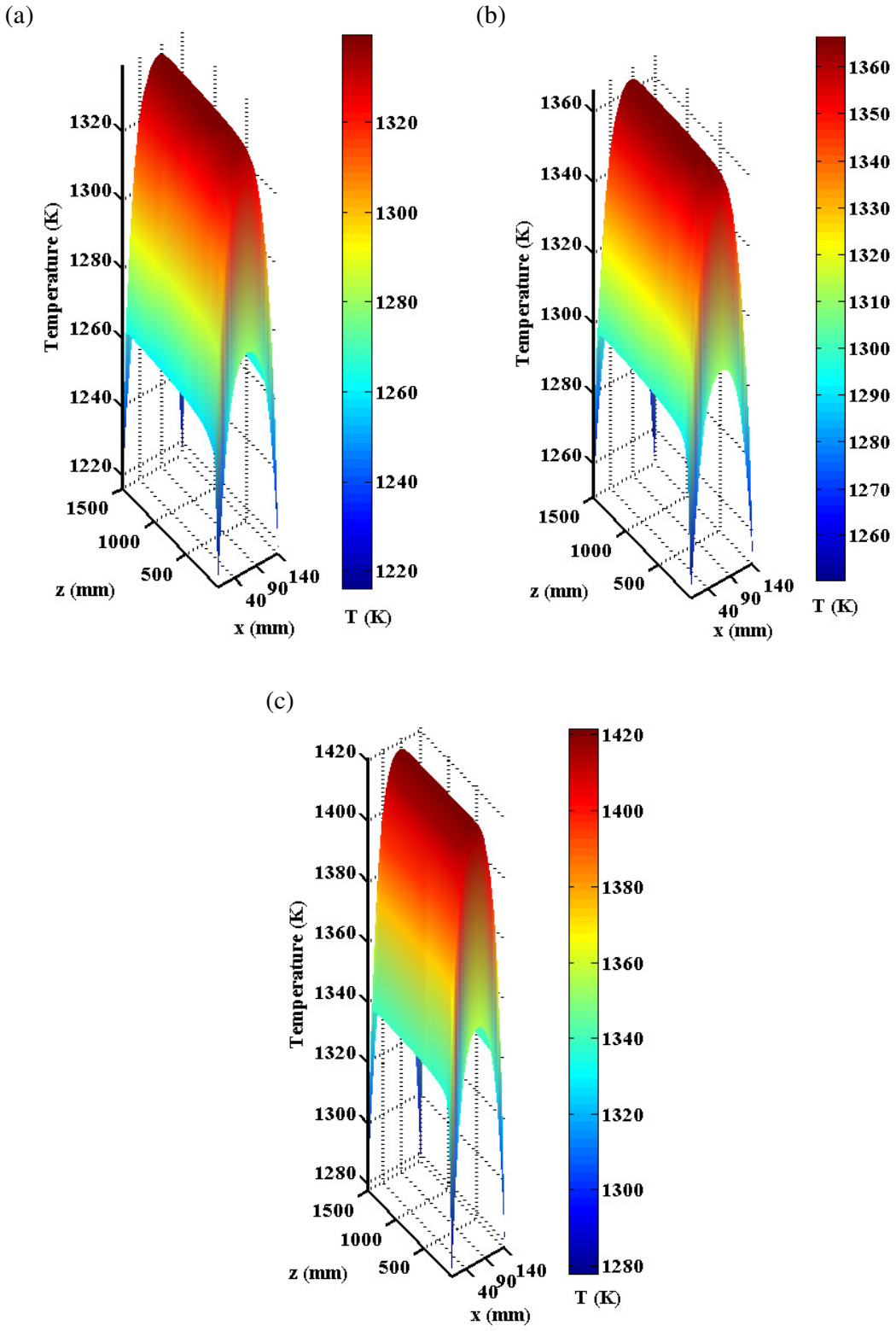

Fig. 6.4: Surface temperature plot of the billet, simulation results considering uniform initial temperature of 1423 K and uniform oxide scale thickness of 2mm, after 120 seconds of transport: (a) top plane, (b) bottom plane, (c) center plane

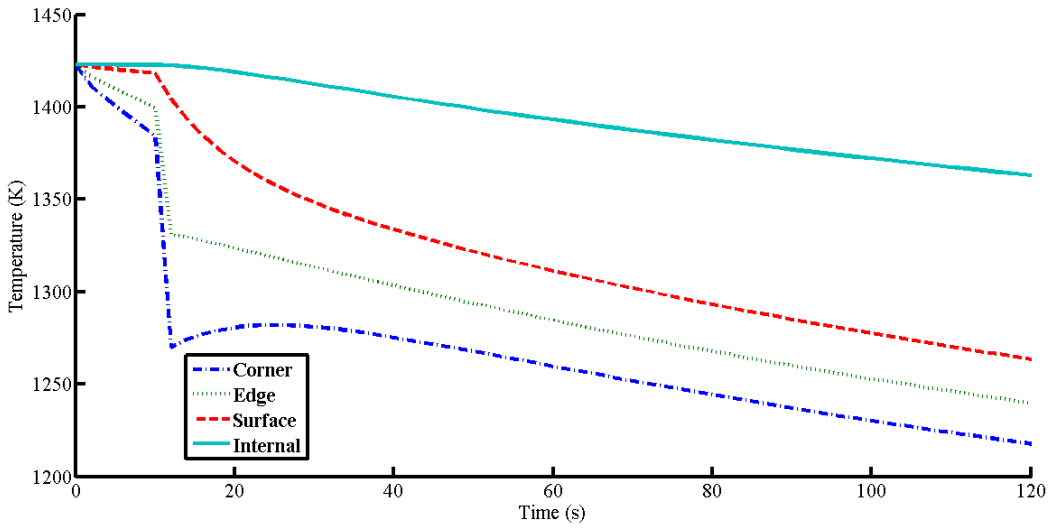

Fig. 6.5: Temperature profiles in the billet, simulation results considering uniform initial temperature of 1423 K and uniform oxide scale thickness of 2mm

Fig. 6.5 shows the temperature variation of billet during transport. The temperatures observed at four representative nodes correspond to the different locations in the billet. Here corner node refers to top corner of the billet on the oxide scale having nodal indices $i=1, j=1, k=1$; edge node refers to top edge on the oxide scale having nodal indices $i=3, j=1, k=1$; surface nodes refers to the surface on the oxide scale having nodal indices $i=3, j=3, k=1$ and internal node refers to the steel cell node having nodal indices $i=4, j=4, k=4$. Among all the nodes considered, the maximum temperature drop is observed for the corner and a minimum for internal node. It is observed that the corner, surface and edge nodes undergo a sudden temperature drop after descaling. However, the temperature of interior nodes is not affected significantly. The temperature of exterior nodes (corner, edge & surface) decreases more rapidly in comparison to the internal node. This is because, for small time period of water spray, the exterior location cools faster and there is not enough time for heat diffusion to take place from the interior. It is also observed that the corner nodes temperature, which has observed significant drop of temperature, rebounds marginally by taking the heat from surrounding nodes which are at a higher temperature. This phenomenon can be observed till heat transfer to the model cell node by conduction from the immediate surrounding node is greater than the heat loss from the cell by radiation and convection.

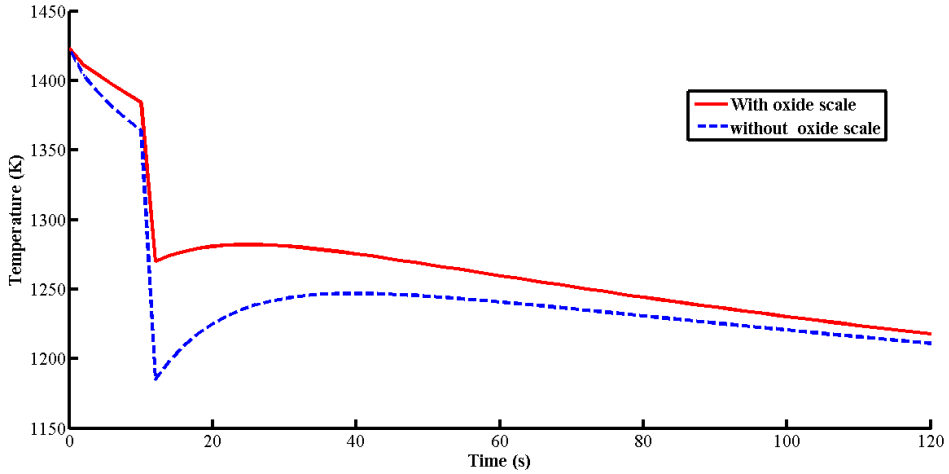

Fig. 6.6: Billet corner temperature profiles, simulation results considering the oxide scale thickness of 2 mm and without oxide scale

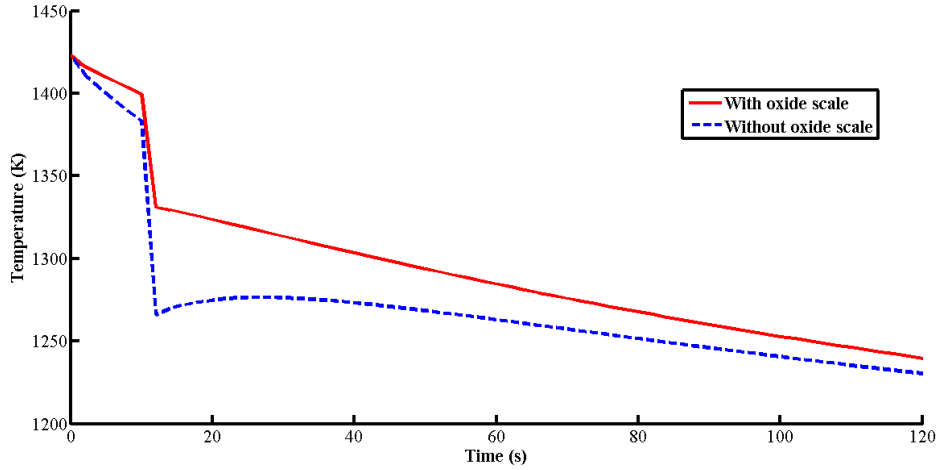

Fig. 6.7: Billet edge temperature profiles, simulation results considering the oxide scale thickness of 2 mm and without oxide scale

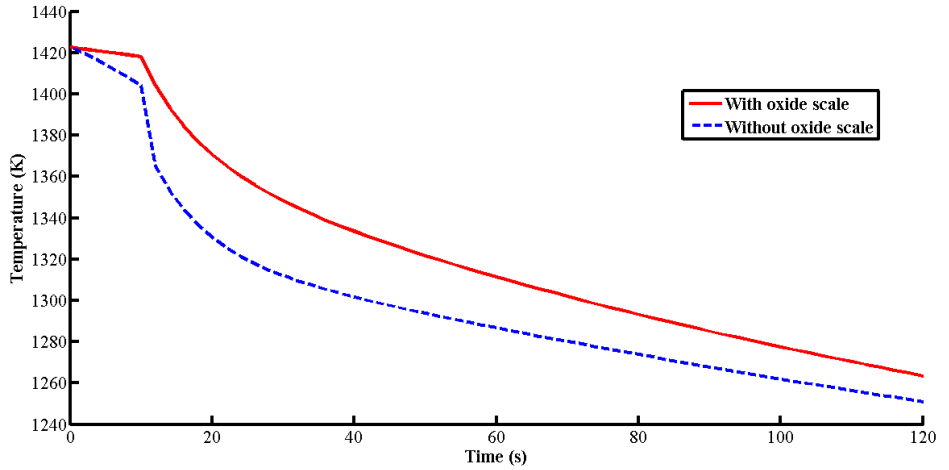

Fig. 6.8: Billet surface temperature profiles, simulation results considering the oxide scale thickness of 2 mm and without oxide scale

In order to examine the effect of oxide scale on the billet temperature field, simulations were performed with consideration of oxide scale and without oxide scale. Figs. 6.6, 6.7 & 6.8 shows the simulation results considering the oxide scale thickness of 2 mm and without an oxide scale for corner, edge and surface of the billet respectively. After descaling (first 10 seconds of transport) the billet cooling is simulated without consideration of oxide scale. Although, the simulation carried out after descaling is same for both the cases, the final temperature field at the end of transport have significant difference. Hence, it can be concluded that the of oxide scale affects billet temperature field significantly.

6.5.2.2 With non-uniform initial temperature and oxide scale thickness

The 3D temperature field of the billet after 10800 seconds reheat which shown in Fig. 6.9(a) is obtained from reheat simulation presented in the chapter 5. This temperature field is used as an initial temperature field in the billet for the transport simulation. The oxide scale layer on the billet surface after 10800 seconds reheating obtained from reheat simulation as presented in chapter 5, is also considered during the transport simulation. The simulation was done by keeping all other conditions similar to the previous section

The 3D temperature fields predicted during the cooling simulations with above conditions are shown in Fig. 6.9. The temperature field in the billet after first seconds (just before descaling) is shown in Fig. 6.9(b), which indicate some drop in temperature of corner, edge and surface of the billet. Fig. 6.9(c) shows the temperature field in the billet just after descaling. Considerable change in the temperature of corner edge and surface of the billet is observed even for small time duration of descaling process.

For transport time of 120 seconds, the 3D temperature field in the billet predicted by the model simulation is shown in Fig. 6.10(a). The rotated view of 3D temperature plot, after 120 seconds is shown in Fig. 6.10(b). It shows the effect of transport rolls on the billet bottom surface temperature. From 3D temperature plots, it is observed that the corner and edge regions have lower temperature. Hence, predicted results, trends are in agreement with the expectations.

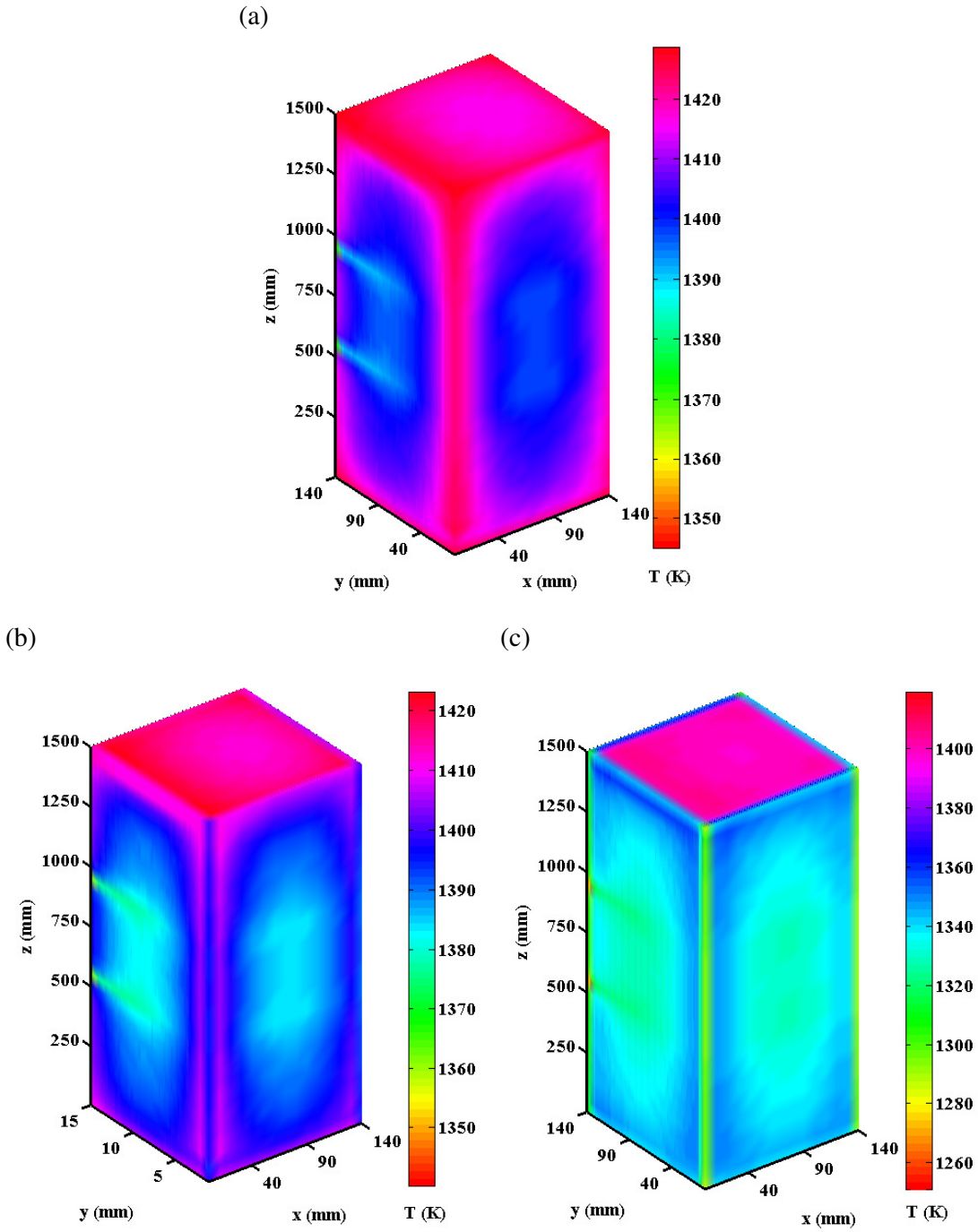

Fig. 6.9: 3D temperature field in the billet, simulation results considering non-uniform temperature and oxide scale: (a) after 10800 seconds reheat (initial condition for transport cooling simulation) (b) after first 10 seconds of transport time (before descaling) (c) after first 11 seconds of transport time (after descaling)

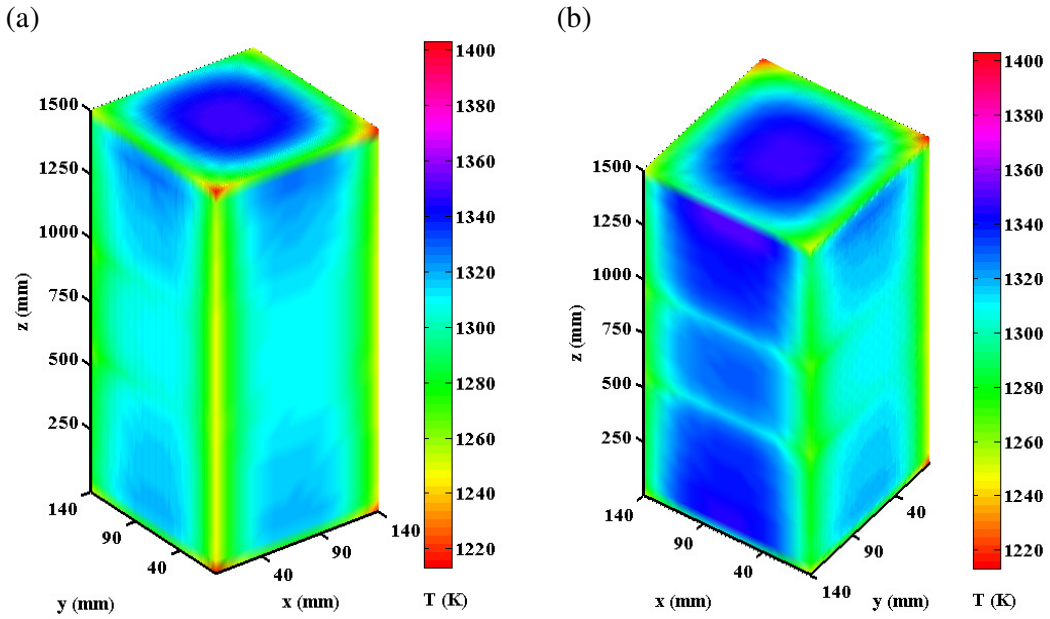

Fig. 6.10: 3D temperature field in the billet, simulation results considering non-uniform temperature and oxide scale (10800 seconds reheat taken as initial condition) (a) after 120 seconds of transport time (b) after 120 seconds of transport time-rotated view

Fig. 6.11 shows the temperature variation of billet during transport. The temperatures observed at four representative nodes correspond to the different locations in the billet as discussed earlier. Among all the nodes considered, the maximum temperature drop observed at the corner and a minimum at the internal node. The overall trends of nodal temperature profiles shown in Fig. 6.11 are similar to those presented in Fig. 6.5.

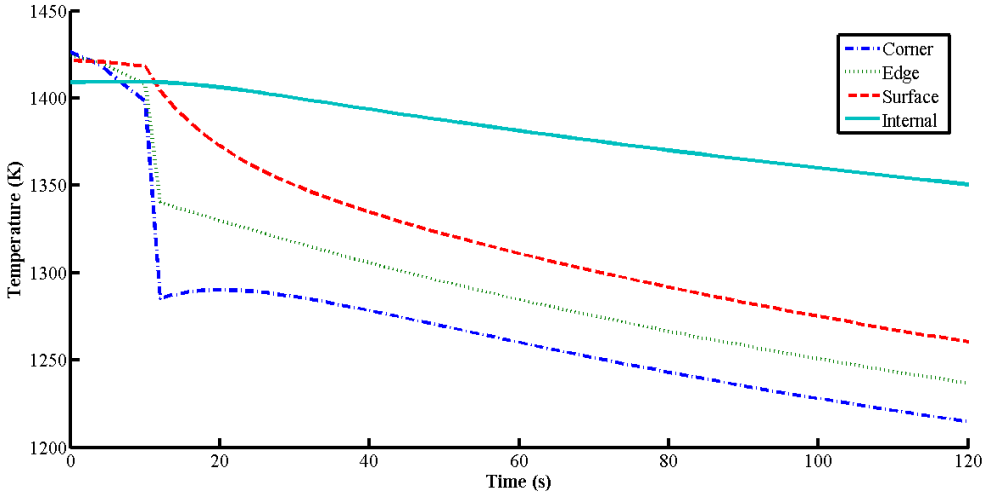

Fig. 6.11: Temperature profiles in the billet predicted form heat transfer simulation during transport after 10800 seconds reheat

Some interesting observations are made in the temperature field during the billet transport simulation. It is observed that internal node of the billet undergoes heating and increase in temperature. This is because; the heat from exterior node is transferred to the interior nodes due to the initial temperature difference existing between them at the beginning of transport. In the early duration of transport where the temperature of exterior nodes of the billet are higher than the temperature of interior nodes. This leads to heat conduction, resulting in small rise in the internal node temperature which is evident from the internal node temperature profile. It is also observed that this rise in temperature for internal node is only for sufficiently short time period, it is mainly because during such short time heat flux(cooling condition) applied at the surface did not penetrate far enough into the billet. However, such phenomenon is not observed when the billet is assumed to have a uniform initial temperature. These observations are further demonstrated in the Figs. 6.12 & 6.13.

In order to examine the effect of the initial temperature field of billet on the cooling characteristics of billet during transport simulations were performed for two different initial temperature field of the billet. The two different non-uniform initial temperature fields assigned to transport model are corresponding to the billet temperature field after residence time of 8400 seconds and 5400 seconds in reheat furnace. The nodal temperature variations for the above said initial conditions are shown in Figs. 6.12 & 6.13.

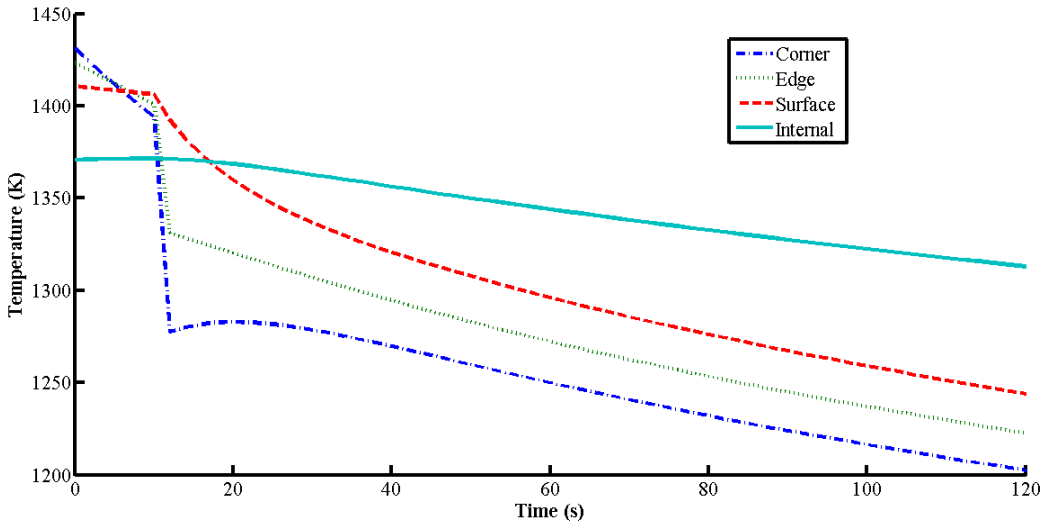

Fig. 6.12: Temperature profiles in the billet predicted form heat transfer simulation during transport after 8400 seconds reheat

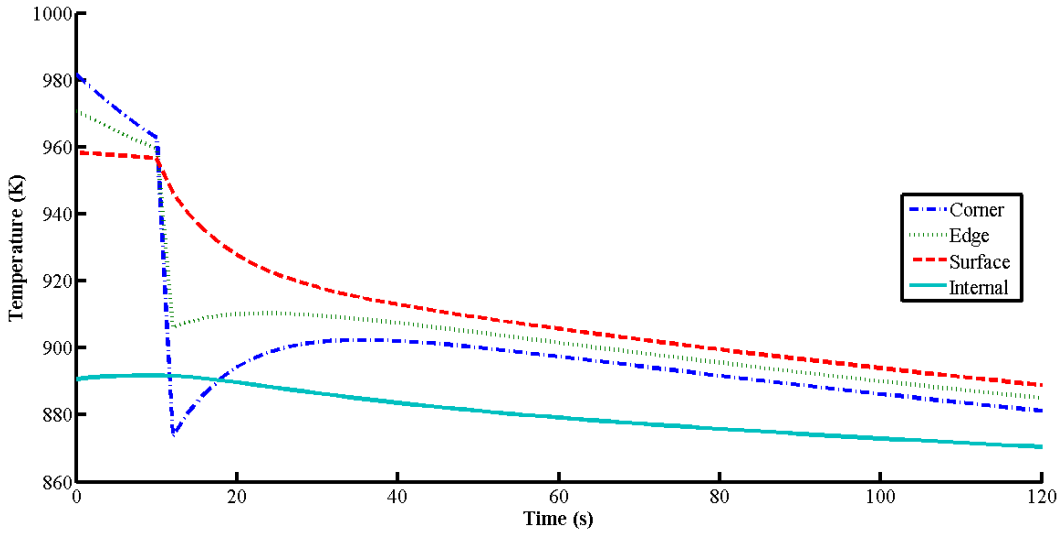

Fig. 6.13: Temperature profiles in the billet predicted form heat transfer simulation during transport after 5400 seconds reheat

It is apparent that the nodes far below the surface undergo more temperature increase and rise is more for larger temperature non-uniformity at the beginning of transport. These observations justifies the need for taking the actual temperature field of the billet after reheating instead of assuming the uniform temperature of the billet at the beginning of the transport.

6.6 Closure

A 3D transient heat conduction numerical modelling with oxide scale and simulations of billet transport cooling has been presented in this chapter. The FDM with an implicit scheme was used to model transient heat conduction in steel billet and oxide scale. It was found that the oxide scale and initial temperature field significantly affects the final temperature field in the billet. The developed 3D numerical model will be useful to the steel industry billet transport system study, design and for downstream activities. The next chapter is devoted to conclusions and future scope, based on the analysis and findings of all chapters.

Chapter 7

Conclusions and Future Scope

7.1 Conclusions

The development of numerical model, its validation and heat transfer simulations with the formation and growth of oxide scale during the steel billet reheating and transport are presented in this thesis. The present work is aimed at prediction of 3D temperature field, oxide scale thickness and study of thermal characteristics. The developed 3D numerical model and procedures discussed in the thesis are beneficial and relevant to the steel industry. The model development with computer implementation and its applications presented in this thesis is going to be a promising tool to predict 3D temperature field in the billet and oxide scale growth on the billet surfaces. The major contributions and conclusions drawn on the analysis and findings of all chapters are as given below:

Chapter 1: Central theme of research along with motivation, need, and overall objectives of the research were discussed, and the philosophy of this thesis work was outlined.

Chapter 2: The first part of chapter constitutes the preparatory phase, here a preliminary description of reheat furnace, heat transfer in the reheat furnace, oxidation during reheat and phase change behavior were included to provide the necessary basis of the subject matter. In the second part of the chapter, a comprehensive literature review on numerical modelling and heat transfer simulation during steel billet reheating and transport was carried out. The main observations from the current literature review on numerical modelling and heat transfer simulation during steel billet reheating are given below:

- There is some numerical modelling and simulation works were performed with CFD and combustion models. These models are mainly limited to 1D or 2D temperature field predictions without consideration of oxide scale. These categories of numerical model simulations require high computational resources and complex in nature.
- The numerical modelling and simulation works were performed with simplified heat transfer conditions, which only consider steady state radiation and 1D or 2D transient conduction in the billet. The advantages of these models are that the

simulations can be performed with lower computational facilities within reasonable time. Hence, it is more convenient for industrial control use. These models also give reasonably accurate predictions of billet temperature field.

- The numerical modelling and simulation for the prediction of 3D temperature field with growth of oxide scale is not available in the literature.

The second part of the literature review was about numerical modelling and heat transfer simulation during transport of steel billet from the reheat furnace to the rolling mills. The main observations are:

- The reported transient heat conduction models for heat transfer simulation during billet transport are based on explicit scheme of FDM which assumes uniform initial temperature of the billet. However, the assumption of uniform initial temperature makes temperature predictions erroneous because in actual situations billet coming out from the furnace by and large have a certain temperature gradient within the material.

The review of the current literature on the numerical models for the steel billet temperature predictions suggested need of a 3D transient heat conduction model with growth of oxide scale for steel billet reheat and transport. Additionally, it is essential to take up an approach, where the actual non-uniform temperature fields of billet after reheat is assigned as initial conditions for the modelling of transport simulation. This thesis therefore makes an attempt to address above needs.

Chapter 3: The development procedures of numerical heat transfer modelling for steel billet reheat application was presented. The control volume based FDM with implicit scheme was used to model 3D transient conduction heat transfer in the steel billet and oxide scale. The numerical heat transfer model developed in this work accounts for the growth of oxide scale, variation of thermo-physical properties of steel and oxide scale with temperature, oxidation reaction heat and skid contact with the billet. The salient features of the developed model are enumerated as follows.

- Development of a generalized discretization procedure for modelling of 3D transient heat conduction in the rectangular billet with formation and growth of oxide scale.

- The model is based on the control volume approach of FDM and capable of taking into account for radiation heat transfer from furnace wall, gases, contact and shadowing effect of the water cooled skid system.
- The use of implicit scheme for 3D transient heat conduction in steel and oxide, this selection makes the model unconditionally stable and suitable for heat transfer simulation during steel billet reheating with thin oxide scale layer where calculations are to be performed over a large time period.
- Modelling of furnace gas mixtures temperature dependent radiative properties using WSGGM for calculations of radiative fluxes on the billet surfaces.

Chapter 4: The overall methodology, computer implementations and validation study of the developed numerical model for heat transfer simulation during reheating of steel billet were presented. To perform temperature field and oxide scale thickness computations, the developed numerical model was implemented through an own developed MATLAB® computer program. The developed computer program is flexible enough to accommodate and simulate various aspects of steel billet reheating. The following salient features are considered in the numerical model computer implementations and solution methodology.

- The developed MATLAB® computer program handles three dimensions in the Cartesian coordinates, different dimension of the billet, different number of skid beam contacts with a billet, different grids for oxide and steel, transient conduction in steel and oxide scale and variable thermo-physical properties of steel and the oxide scale.
- The developed program and computer implementations have a flexible framework so that the scope of the program can be easily changed.
- To enhance computation efficiency the nodal values are stored in 1D array using natural ordering scheme where data of 3D grid are mapped to 1D array. The dependent variable nodal data like temperature and oxide scale thicknesses mapped back from 1D array to 3D array as and when required.
- The Gauss-Seidel iteration algorithm in modified form is successfully implemented.

The second part of the chapter 4 presents validation study of developed model. The developed 3D numerical model is simulated at conditions for which analytical solutions are available. The analytical solutions are used to verify the numerical model results.

Finally the published experimental results were used to validate the numerical model predictions. Validation study shows:

- Numerical predictions are in good agreement with analytical results.
- The experimental (Jang et al., 2010) center line temperature and present model simulated center line temperature are found to be in reasonably close agreement.
- The maximum scale thickness on the billet top and bottom surfaces after 10800 seconds which is predicted by numerical model simulation are in close agreement (with approximately 2.85 and 3.12 % difference) with the 2D numerical simulation results reported by Jang et al. (2010).

Chapter 5: Heat transfer simulations for steel billet reheating were performed using the developed numerical model. The following conclusions can be drawn from the simulation results.

- The developed numerical model is capable of predicting 3D temperature field in the billet with the formation and growth of oxide scale.
- Numerical model results exhibit expected trends such as, 3D temperature field of the billet shows anticipated symmetry and higher temperatures are observed at the corner and edge regions.
- The temperature of billet with oxide scale is lower than that of billet without oxide scale. The effect of oxide scale on the billet temperature field is more prominent in the early zones of reheat furnace.
- The effect of the skid system on the temperature field is very significant due to radiation shadowing at the bottom surface and energy loss because of conduction from the billet. It is observed that the skid system influences the entire temperature field. However, the maximum influence of the skid is observed at the bottom surface of the billet. Slice wise examination of temperature plot and the data indicates that minimum temperature in the billet, during most of residence time occurs at inner node and this location shifted towards bottom skids region in the later part of residence time.
- It is observed that the temperature distribution in the billet top plane surface is more uniform than that in the billet center plane surface and bottom plane surfaces. The largest temperature gradient can be seen in the billet bottom plane surface, particularly near the skid regions.

- The temperature rise of the billet nodes is more in preheating and heating zone. The temperature rise in soaking zone is very small. The temperature difference between the nodes is reduced to a significantly lower value in the soaking zone.
- Billet maximum, minimum and average temperatures are showing a uniform trend of continuous increase. The billet average temperatures are close to billet minimum temperatures. The billet average temperature rise in preheating zone is a maximum. Temperature profiles in soaking zone are close to each other. It means the maximum temperature difference in billet approached to a lower value.
- It is observed that the growth rate of scale is low in preheating zone. The scale growth rate increases in heating and soaking zone. It can be seen that the locations of maximum value of scale thickness are coinciding with locations of maximum temperature, which is obvious from scale thickness function selected in the present model.
- It is observed that the rate of the average temperature rise of the billet reduced with an increase of billet cross-section size.
- The minimum temperature in the billet at the later part of residence time, founds just at contact location on the billet bottom plane and not at the center plane. However, the bottom plane average temperatures remain higher than the corresponding center plane average temperatures, even in the later part of residence time.

The second part of chapter 5, an investigation on zone temperature sensitivity was performed. The objective of this study was to identify, which of the zone temperature values have the largest effects on the responses of interest and to find the possible interaction of zone temperature values. The responses of interest chosen in this study are: maximum temperature, minimum temperature, maximum temperature difference, average temperature, maximum oxide scale thickness and average oxide scale thickness. The zone temperature combinations were generated through 3^k full factorial design method of DOE approach. The developed numerical model was simulated for zone temperature combinations. The model simulation results corresponding to the combination set were analyzed with statistical techniques: ANOM ANOVA. The main conclusions from this analysis are:

- It is observed from ANOM analysis that all six responses of interest show strong interaction. This means that the variation of one zone temperature is related to the

variation of other zone temperature in terms of overall value of the response of interest.

- The temperature of zone-4 (soaking zone) is highly significant and the temperature of zone-1 & zone-2 is least significant for maximum temperature of the billet
- It is observed that billet minimum temperature and billet average temperature are most sensitive to temperature of zone-4 and least sensitive to temperature of zone-2.
- It can be concluded that in the transition from level 1 to 2, temperature of zone-3 is most significant, while for level 2 to 3, the temperature of zone-4 is most significant. The temperature of zone-2 is identified as least significant parameter for maximum temperature difference of billet.
- It is evident from the analysis that scale thickness growth is most sensitive to the temperature value of zone -3 and least sensitive to the temperature value of zone-2.

Chapter 6: This chapter presents the methodology employed for the development of FDM implicit scheme numerical model for heat transfer simulation during billet transport. The numerical model simulation results have been compared with analytical solution results. The model simulation results have been found to be in good agreement with the analytical solution results. The salient features of the developed numerical model are enumerated as follows.

- The generalized discretization procedure used for modelling of 3D transient heat conduction billet with the formation and growth of oxide scale used for billet reheating simulation successfully extended to billet cooling during transport.
- The developed model is based on the control volume approach of FDM and capable of capturing non-uniform initial temperature and oxide scale conditions obtained from reheat simulations.
- The model also accounts for the descaling process during transport.
- The use of implicit scheme for 3D transient heat conduction in steel and oxide, this selection makes the model unconditionally stable and suitable for both heat transfer simulations during steel billet reheating and transport.

Heat transfer simulations for steel billet cooling were performed using the developed numerical model. The following conclusions can be drawn from the simulation results.

- Numerical model results for billet cooling also exhibit expected trends, such as a 3D temperature field of the billet shows anticipated symmetry and lower temperatures at the corner and edge regions.
- The water spray during the descaling process produces a sudden temperature drop in the exterior nodes: corner, edge and surface locations of the billet. The temperature of exterior nodes decreases more rapidly in comparison to internal nodes. This is because, for small time period of water spray, the only exterior location cools and there in not enough time for heat diffusion to take place from the interior. It is also observed that the corner nodes temperature, which has observed significant drop, rebounds marginally by taking heat from surrounding nodes which are at higher temperatures.
- It can be concluded that the oxide scale affects the billet temperature field significantly.
- From the simulation results considering non-uniform temperature, as initial condition, it was observed that, the heat from the exterior nodes is transferred to interior nodes due to temperature difference existing between them. This cause temperature rise of interior node. However, such phenomenon is not observed when the billet is assumed to have uniform temperature as initial condition.

7.2 Future Scope

The development of numerical model with growth of oxide scale for heat transfer simulation during steel reheating and transport is presented in this thesis work. This is one of the first attempts to predict 3D temperature field in the billet with the growth of oxide scale. Although many complexities involved in reheating and transport process have been accounted in the present work, there are some issues that can be considered for future research work. The present work can be extended as follows:

- Experimental analysis may be carried out for the proper selection and refinement of input data for the simulation such as billet and oxide scale emissivities, contact resistance between billet and skids.
- The model can be implemented for online monitoring of 3D temperature field during reheating. The model can be connected to reheat furnace zone temperature measurement system, to ensure real time input of the furnace gas temperature

profile. Present model can very well incorporate such furnace gas temperature inputs.

- The steel surface at elevated temperature during reheating is subjected to decarburization. The billet surface properties change considerably with decarburization. Hence, this effect may be considered for future studies.
- The current form of model predicts 3D temperature field of billet with reasonable accuracy and does not cost huge computation. This makes the present model more suitable for online monitoring and control. However, to make it more accurate numerical model future work may be carried out to link our present model with combustion model, so that the current model can use furnace gas temperature profile according to the fuel firing conditions. This will lead to large computation time, but such model may be suitable offline model for study and design of the system.

Abuluwefa, H. (1992). *Scale Formation in a Walking-Beam Steel Reheat Furnace.* M. E. Thesis, McGill University, Canada.

Abuluwefa, H. (1996). *Characterization of Oxides (Scale) Growth of Low Carbon Steel During Reheating.* Ph.D Thesis, McGill University, Montreal, Canada.

Abuluwefa, H. T., Guthrie, R. I., & Ajersch, F. (1997). Oxidation of Low Carbon Steel in Multicomponent Gases: Part II. Reaction Mechanisms during Reheating. *Metallurgical and Materials Transactions A, 28* (A), 1643-1651.

Anderson Jr., J. D. (2012). *Computational Fluid Dynamics.* Delhi, India: Tata McGraw-Hill.

Barr, P. V. (1995). The Development, Verification, and Application of a Steady-State Thermal Model for the Pusher-Type Reheat Furnace. *Metallurgical and Materials Transactions B, 26*(B), 851-869.

Birks, N., & Meier, G. H. (1983). *Introduction to High Temperature Oxidation of Metals.* London: Edward Arnold Ltd.

Brittain, C. P., & Dales, M. (1988). A Modern Walking Beam Slab Reheating Furnaces. *Metallurgical Plant and Technology, 1*, 77-80.

Callister, W. D., & Balasuramaniam, R. (2014). *Material Science & Engineering* (2nd ed.). Wiley.

Cengel, Y. A., & Ghajar, A. J. (2011). *Heat and Mass Transfer* (4th ed.). New Delhi, India: Tata McGraw Hill.

Chapman, K. S., Ramadhyani, S., & Viskanta, R. (1990). Modeling and Parametric Studies of Heat Transfer in a Direct-Fired Batch Reheating Furnace. *Journal of Heat Treating, 8*(2), 137-146.

Chapman, K. S., Ramadhyani, S., & Viskanta, R. (1991). Modeling and Parametric Studies of Heat Transferin a Direct-Fired Continuous Reheating Furnace. *Metallurgical Transactions B, 22*(B), 514-521.

Chapman, K. S., Ramadhyani, S., & Viskanta, R. (1994). Two-Dimensional Modeling and Parametric Studies of Heat Transfer in a Direct-Fired Furnace with Impinging Jets. *Combustion Science and Technology, 97*, 99-120.

Chen, R. Y., & Yuen, W. Y. (2003). Review of the High-Temperature Oxidation of Iron and Carbon Steel in Air or Oxygen. *Oxidation of Metals, 59*(5), 433-468.

Chen, S., Abraham, S., & Poshard, D. (2008). Modification of Reheat Furnace Practices Through Comprehensive Process Modeling. *Iron and Steel Technology Conference and Exposition* (pp. 68-79). Indianapolis: AISTech.

Chen, W. H., Lin, M. R., & Leu, T. S. (2010). Optimal Heating and Energy Management for Slabs in a Reheating Furnace. *Journal of Marine Science and Technology, 18*(1), 24-31.

Cuellar, J. R., Mata, M. P., Leduc, L. A., & Colas, R. (2004). Modelling Descaling During Hot Rolling of Steel. *2nd International Conference on Thermal Process Modelling and Computer Simulation. 120*, pp. 209-215. Nancy, France: Journal de Physique IV.

Design-Expert Software. (2014, August). Retrieved from http://www.statease.com

Edwards, D. K. (1976). Moleculer Gas Band Radiation. *Advances in Heat Transfer, 12*, 115-193.

Emadi, A., Saboonchi, A., Taheri, M., & Hassanpour, S. (2014). Heating Characteristics of Billet in a Walking Hearth Type Reheating Furnace. *Applied Thermal Engineering, 63*, 396-405.

Farag, I. H., & Allam, K. A. (1981). Gray Gas Approximation of Carbon Dioxide Standard Emissivities. *Journal of Heat Transfer, 103*, 403-405.

Fitzgerald, F., & Sherdan, A. T. (1970). Heating of the Slab in the Furnace. *Journal of Iron and Steel Institute, 208*, 18-28.

Fontana, P. G., Boggiano, A., Furinghetti, A., & Pastorino, B. (1984). Optimizing Heat Distribution in Continous Furnace Using a Dynamic Mathematical Model. *BTF-Special issue*, 9-14.

Ford, R., Suryanarayana, R., & Johnson, J. H. (1980). Heat Transfer Model for Solid Slab Water-Cooled Skid Pipe in Reheating Furnace. *Ironmaking and Steel Making, 7*(3), 140-146.

Gerasimov, S. P., Efroimovich, S. Y., Klimovitskii, M. D., & Khloponin, V. N. (1984). Stastical Modelling of Heating of Metal in Conveyor Furnaces Taking into Account Heating Atmosphere Temperature Profile. *Steel in the USSR, 14*, 461-462.

Ghannam, B., Nemer, M., Khoury, K. E., & Yuen, W. (2010). Experimental Validation of the Multiple Absorption Coefficient Zonal Method (MACZM) in a Dynamic Modeling of a Steel Reheating Furnace. *Numerical Heat Transfer, Part A: Applications, 58*, 545–563.

Golub, G., & Ortega, J. M. (1993). *Scientific Computing: An Introduction with Parallel Computing*. Boston, USA: Academic Press.

Han, S. H., & Chang, D. (2012 a). Optimum Residence Time Analysis for a Walking Beam Type Reheating Furnace. *International Journal of Heat and Mass Transfer, 55*, 4079–4087.

Han, S. H., & Chang, D. (2012 b). Radiative Slab Heating Analysis for Various Fuel Gas Compositions in an Axial-Fired Reheating Furnace. *International Journal of Heat and Mass Transfer, 55*, 4029-4036.

Han, S. H., Baek, S. W., & Kim, M. Y. (2009). Transient Radiative Heating Characteristics of Slabs in a Walking Beam Type Reheating Furnace. *International Journal of Heat and Mass Transfer, 52*, 1005–1011.

Han, S. H., Baek, S. W., Kang, S. H., & Kim, C. Y. (2007). Numerical Analysis of Heating Characteristics of a Slab in a Bench Scale Reheating Furnace. *International Journal of Heat and Mass Transfer, 50*, 2019-2023.

Han, S. H., Chang, D., & Huh, C. (2011). Efficiency Analysis of Radiative Slab Heating in a Walking-Beam-Type Reheating Furnace. *Energy, 36* , 1265-1272.

Han, S. H., Chang, D., & Kim, C. Y. (2010). A Numerical Analysis of Slab Heating Characteristics in a Walking Beam Type Reheating Furnace. *International Journal of Heat and Mass Transfer, 53*, 3855–3861.

Hanselman, D., & L., B. (2011). *Mastering MATLAB 7* (5th ed.). India: Pearson Education.

Harish, J., & Dutta, P. (2005). Heat Transfer Analysis of Pusher type Reheat Furnace. *Ironmaking and Steelmaking, 32*(2), 151-158.

Hasan, H. S., Peet, M. J., Jalil, J. M., & Bhadeshia, H. K. (2011). Heat Transfer Coefficients During Quenching of Steels. *Heat Mass Transfer, 47*, 315–321.

Hollander, F. (1983). Reheating Processes and Modifications to Rolling Mill Operations for Energy Savings. *Iron and Steel Engineer, 60*(6), 55-62.

Holman, J. P. (2002). *Heat Transfer* (9th ed.). New York, USA: McGraw-Hill Education.

Hottel, H. C., & Sarofim, A. F. (1965). The Effect of Gas Flow Pattern on Radiative Transfer in Cylindrical Enclosures. *International Journal of Heat and Mass Transfer, 8*, 1153-1169.

Hottel, H. C., & Sarofim, A. F. (1967). *Radiative Transfer.* New York, USA: McGraw-Hill.

Howells, R. I., Ward, J., & Probert, S. D. (1972). Influence of Skid Design on Skid Mark Formation,. *Journal of the Iron and Steel Institute*, 10-15.

Hsieh, C. T., Huang, M. J., Lee, S. T., & Wang, C. H. (2008 a). A Coupled Numerical Study of Slab Temperature and Gas Temperature in the Walking Beam Type Slab Reheating Furnace. *6th International Conference on CFD in Oil & Gas, Metallurgical and Process Industries*, (pp. CFD08-084). Trondheim, Norway.

Hsieh, C. T., Huang, M. J., Lee, S. T., & Wang, C. H. (2008 b). Numerical Modeling of a Walking-Beam-Type Slab Reheating Furnace. *Numerical Heat Transfer, Part A: Applications, 53*, 966–981.

Hsieh, C. T., Huang, M. J., Lee, S. T., & Wang, C. H. (2010). A Numerical Study of Skid Marks on the Slabs in a Walking-Beam Type Slab Reheating Furnace. *Numerical Heat Transfer, Part A: Applications, 57*, 1-17.

Huang, M. J., Hsieh, C. T., Lee, S. T., & Wang, C. H. (2008). A Coupled Numerical Study of Slab Temperature and Gas Temperature in the Walking-Beam-Type Slab Reheating Furnace. *Numerical Heat Transfer, Part A: Applications, 54*, 625–646.

Ishii, T., Zhang, C., & Hino, Y. (2002). Numerical Study of the Performance of Regenerative Furnace. *Heat Transfer Engineering, 23*, 23-33.

Jaklic, A., Glogovac, B., Kolenko, T., Zupancic, B., & Tezak, B. (2002). A Simulation of Heat Transfer during Billet Transport. *Applied Thermal Engineering, 22*, 873–883.

Jaklic, A., Kolenko, T., & Zupancic, B. (2005). The Influence of the Space Between the Billets on the Productivity of a Continuous Walking Beam Furnace. *Applied Thermal Engineering, 25*, 783-795.

Jang, H. J., Lee, D. E., Kim, M. Y., & Kim, H. G. (2010). Investigation of the Slab Heating Characteristics in a Reheating Furnace with the Formation and Growth of Scale on the Slab Surface. *International Journal of Heat and Mass Transfer, 53*, 4326–4332.

Jang, Y. J., & Kim, S. W. (2007). An Estimation of a Billet Temperature during Reheating Furnace Operation. *International Journal of Control, Automation, and Systems, 5*(1), 43-50.

Jiang, Q., Zhang, C., & Jiang, J. (2004). An Industrial Reheating Furnace with Flue Gas Recirculation Modeled by Linear Transfer Functions. *Combustion Science and Technology, 176*, 1437-1464.

Jiang, Q., Zhang, C., & Jiang, J. (2007). A CFD Assisted Control System Design with Applications to NOx Control in a FGR Furnace. *Combustion Theory and Modelling, 11*(3), 469-481.

Kalman, R. E. (1960). A New Approach to Linear Filtering and Prediction Problems. *Transactions ASME, Series D, Journal of Basic Engineering, 82*, 35-45.

Kim, J. G., & Huh, K. Y. (2000). Prediction of Transient Slab Temperature Distribution inthe Re-heating Furnace of a Walking-beam Type for Rolling of Steel Slabs. *ISIJ International, 40*(11), 1115-1123.

Kim, J. G., Huh, K. Y., & Kim, I. T. (2000). Three-Dimensional Analysis of the Walking-Beam-Type Slab Reheating Furnace in Hot Strip Mills. *Numerical Heat Transfer, Part A: Applications, 38*, 589-609.

Kim, J. W., & Kim, S. W. (2005). Parameter Identification of Induction Motors Using Dynamic Encoding Algorithm for Searches (DEAS). *IEEE Transactions on Energy Conversion, 20*(1), 16-24.

Kim, M. Y. (2007). A Heat Transfer Model for the Analysis of transient Heating of the Slab in a Direct-Fired Walking Beam Type Reating Furnace. *International Journal of Heat and Mass Transfer, 50*, 3740-3748.

Ko, H. S., Kim, J. S., Yoon, T. W., Lim, M., Yang, D., & Jun, I. S. (2000). Modeling and Predictive Control of a Reheating Furnace. *American Control Conference* (pp. 2725-2729). Chicago, USA: IEEE.

Kofstad, P. (1966). *High Temperature Oxidation of Metals.* Nework: Wiley.

Krivandin, V. A., & Markov, B. L. (1980). *Metallurgical Furnaces.* Moscow: Mir Publishers.

Lawson, D. A., & Ziesler, C. D. (1996). An Accurate Program for Radiation Modelling in the Design of High-Temperature Furnaces. *Journal of Management Mathematics, 7*(2), 109-116.

Leckner, B. (1972). Spectral and Total Emissivity of Water Vapor and Carbon Dioxide. *Combustion and Flame, 19*, 33-48.

Leden, B. (1986). STEELTEMP- A Program for Temperature Analysis. *Scandinavian Journal of Metallurgy, 15*, 215—223.

Leden, B. T. (1985). Mathematical Reheating Furnace Models in STEELTEMP. *International Conference, SCANHEATING- 85.* Lulea, Sweden.

Lee, D. E., & Kim, M. Y. (2013). Optimum Residence Time for Steel Productivity and Energy Saving in a Hot Rolled Reheating Furnace. *Journal of Mechanical Science and Technology, 27* (9), 2869-2877.

Lee, V. H., Gleeson, B., & Young, D. J. (2005). Scaling of Carbon Steel in Simulated Reheat Furnace Atmospheres. *Oxidation of Metals, 63*(1), 15-31.

Li, Z., Barr, P. V., & Brimancombe, J. K. (1988). Computer Simulation of the Slab Reheating Furnace. *Canadian Metallurgical Quarterly, 27*(3), 187-196.

Lindholm, D., & Leden, B. (1999). A Finite Element Method for Solution of the Three Dimensional Time Dependent Heat Conduction Equation with Application for Heating of Steels in Reheating Furnaces. *Numerical Heat Transfer, Part A: Applications, 35*, 155-172.

Ludwig, C. B., Malkmus, W., Reardon, J. E., & Thomson, J. A. (1973). *Handbook of Infrared Radiation from Combustion Gases.* NASA.

Madsen, E. E. (1994). STEELTEMP- A Program for Temperature Analysis in Steel Plants. *Journal of Material Processing Technology, 42*, 187-195.

Marino, P., Pignotti, A., & Solis, D. (2002). Numerical Model of Steel Slab Reheating in Pusher Furnaces. *Latin American Applied Research, 32*, 257-261.

Marlow, D. O. (1996). Modelling Direct-Fired Annealing Furnaces for Transient Operations. *Appllied Mathematical Modelling , 20*, 34-40.

Marston, H. F., Bolt, P. H., Leprince, G., Roder, M., Klima, R., Niska, J., & Jarl, M. (2004). Challenges in the Modelling of Scale Formation and Decarburisation of High Carbon,Special and General Steels. *Ironmaking and Steelmaking, 31*(1), 57-65.

Metals Hand Book (9th ed., Vol. 4). (1981). American Society for Metals.

Mitra, A. (2008). *Fundamentals of quality control and improvement* (3rd ed.). New Jersy, USA.

Modak, A. T. (1978). Radiation from Products of Combustion. *Fire Research, 1*, 339-361.

Modak, A. T. (1979). Exponential Wide Band Parameters for Pure Rotational Band of Water Vapor. *Journal of Quantitative Spectroscopy and Radiative Tranasfer, 21*, 131-142.

Modest, M. F. (1991). The Weighted- Sum- of Gray- Gases Model for Arbitary Solution Methods in Radiative Transfer. *Journal of Heat Transfer, 113*, 650-656.

Mogan, J. L. (1999). *Tranasient Billet Heating Model for Steel Reheat Furnace.* M. S. Thesis, Queen's University, Kingston Ontario, Canada.

Montgomery, D. C. (2014). *Design of Experiments* (8th ed.). Delhi: Wiley.

NIST Standard Reference Database 23, Reference Fluid Thermodynamic and Transport Properties- REFPROP, Version 9.0. (2010). National Institute of Standards and Technology, Department of Commerce, Government of USA.

Ozisik, M. N. (1993). *Heat Conduction* (2nd ed.). New York, U S A: Wiley Interscience Publication.

Patankar, S. V. (1980). *Numerical Heat Transfer and Fluid Flow*. Leittown , USA: Hemisphere Publishing Corporation .

Pike, H. E., & Citron, S. J. (1970). Optimization Studies of a Slab Reheating Furnace. *Automatica, 6*, 41-50.

Price, J. C. (1980). Temperature Control of Slab Reheating Furnace. *Iron and Steel Engineer*, 59-64.

Roth, J., Sierpinski, H., Chabanier, J., & Germe, J. (1986). Computer Control of Slab Furnace Based on Physical Models. *Iron and Steel Engineer, 63*(8), 41-47.

Rubini, P., & Pollard, A. (1990). Three Dimensional Modelling of a Steel Reheat Furnace. *International Symposium on Steel Reheat Furnace Technolgy.* Hamilton, Ontario, Canada.

Sheikh, H. (2009). Thermal Analysis of Hot Strip Rolling Using Finite Element and Upper Bound Methods. *Applied Mathematical Modeling, 33*, 2187-2195.

Singh, V. K., & Talukdar, P. (2013). Comparisons of Different Heat Transfer Models of a Walking Beam Type Reheat Furnace. *International Communications in Heat and Mass Transfer, 47*, 20–26.

Sinha, G. P., Bagchi, D. K., & Mukharjee, U. C. (2006). Emerging Trends in Iron and Steel-making Technology and its Relevance to the Indian Steel Industry. *Institution of Engineers (India), 87*, 14-24.

Smith, T. F., Shen, Z. F., & Friedman, J. N. (1982). Evaluation of Coefficients for the Weighted Sum of Gray Gases Model. *Journal of Heat Transfer, 104*, 602-608.

Tan, C. K., Jenkins, J., Ward, J., Broughton, J., & Heeley, A. (2013). Zone Modelling of the Thermal Performances of a Large-Scale Bloom Reheating Furnace. *Applied Thermal Engineering, 50* , 1111-1118.

Venturino, M., & Rubini, P. (1995). Coupled Fluid Flow and Heat Transfer Analysis of Steel Reheat Furnaces. *3rd Europian Conference on Industrial Furnaces and Boilers.* Lisbon, Portugal.

Wick, H. J. (1987). Estimation of Temperature Profiles within Slabs of a Simulated Reheat Furnace using the Extended Kalman Filter. *American Control Conference* (pp. 1040 - 1045). Minneapolis, MN, USA: IEEE.

Wick, H. J. (1990). Estimation of Average Slab Temperatures of a Simulated Reheat Furnace using the Extended Kalman Filter. *American Control Conference* (pp. 2953 - 2954). San Diego, CA, USA: IEEE.

Wild, D., Meurer, T., & Kugi, A. (2009). Modelling and Eexperimental Model Validation for a Pusher-Type Reheating Furnace. *Mathematical and Computer Modelling of Dynamical Systems, 15*(3), 209–232.

Yang, Y. Y., & Lu, Y. Z. (1988). Dynamic Model Based Optimization Control for Reheating. *Computers in Industry, 10*(1), 11-20.

Zhang, C., Ishii, T., & Sugiyama, S. (1997). Numerical Modeling of the Thermal Performance of Regenerative Slab Reheat Furnace. *Numerical Heat Transfer, Part A: Applications, 32*, 613-631.

Table A1: Data for combinations for 3^4 factorial design

Combination number	Zone-1 temperature	Zone-2 temperature	Zone-3 temperature	Zone-4 temperature
1	1123	1223	1448	1428
2	1123	1223	1448	1453
3	1123	1223	1448	1478
4	1123	1223	1473	1428
5	1123	1223	1473	1453
6	1123	1223	1473	1478
7	1123	1223	1498	1428
8	1123	1223	1498	1453
9	1123	1223	1498	1478
10	1123	1273	1448	1428
11	1123	1273	1448	1453
12	1123	1273	1448	1478
13	1123	1273	1473	1428
14	1123	1273	1473	1453
15	1123	1273	1473	1478
16	1123	1273	1498	1428
17	1123	1273	1498	1453
18	1123	1273	1498	1478
19	1123	1323	1448	1428
20	1123	1323	1448	1453
21	1123	1323	1448	1478
22	1123	1323	1473	1428
23	1123	1323	1473	1453
24	1123	1323	1473	1478
25	1123	1323	1498	1428
26	1123	1323	1498	1453
27	1123	1323	1498	1478

Combination number	Zone-1 temperature	Zone-2 temperature	Zone-3 temperature	Zone-4 temperature
28	1223	1223	1448	1428
29	1223	1223	1448	1453
30	1223	1223	1448	1478
31	1223	1223	1473	1428
32	1223	1223	1473	1453
33	1223	1223	1473	1478
34	1223	1223	1498	1428
35	1223	1223	1498	1453
36	1223	1223	1498	1478
37	1223	1273	1448	1428
38	1223	1273	1448	1453
39	1223	1273	1448	1478
40	1223	1273	1473	1428
41	1223	1273	1473	1453
42	1223	1273	1473	1478
43	1223	1273	1498	1428
44	1223	1273	1498	1453
45	1223	1273	1498	1478
46	1223	1323	1448	1428
47	1223	1323	1448	1453
48	1223	1323	1448	1478
49	1223	1323	1473	1428
50	1223	1323	1473	1453
51	1223	1323	1473	1478
52	1223	1323	1498	1428
53	1223	1323	1498	1453
54	1223	1323	1498	1478
55	1323	1223	1448	1428
56	1323	1223	1448	1453
57	1323	1223	1448	1478
58	1323	1223	1473	1428

Combination number	Zone-1 temperature	Zone-2 temperature	Zone-3 temperature	Zone-4 temperature
59	1323	1223	1473	1453
60	1323	1223	1473	1478
61	1323	1223	1498	1428
62	1323	1223	1498	1453
63	1323	1223	1498	1478
64	1323	1273	1448	1428
65	1323	1273	1448	1453
66	1323	1273	1448	1478
67	1323	1273	1473	1428
68	1323	1273	1473	1453
69	1323	1273	1473	1478
70	1323	1273	1498	1428
71	1323	1273	1498	1453
72	1323	1273	1498	1478
73	1323	1323	1448	1428
74	1323	1323	1448	1453
75	1323	1323	1448	1478
76	1323	1323	1473	1428
77	1323	1323	1473	1453
78	1323	1323	1473	1478
79	1323	1323	1498	1428
80	1323	1323	1498	1453
81	1323	1323	1498	1478

List of Publications

Peer Reviewed International Journal:

[1] Dubey, S. K., & Srinivasan, P. (2014). Development of Three Dimensional Transient Numerical Heat Conduction Model with Growth of Oxide Scale for Steel Billet Reheat Simulation. *International Journal of Thermal Sciences, 84*, 214-227.(**Elsevier)**

[2] Dubey, S. K., & Srinivasan, P. (2014). Steel Billet Reheat Simulation with Growth of Oxide Layer and Investigation on Zone Temperature Sensitivity. *Journal of Mechanical Science and Technology, 28*(3), 1113-1124. (**Springer)**

[3] Dubey, S. K., & Srinivasan, P. (2013). Three Dimensional Transient Explicit Finite Difference Heat Transfer Modeling of Billet Transport. *International Journal of Thermal & Environmental Engineering, 6*(2), 95-100. (**IASKS)**

Peer Reviewed International Conference Proceedings:

[1] Dubey, S. K., & Srinivasan, P. (2013). Transient Heat Conduction Model and its Application to Billet Transport Simulation with Oxide Scale. *Proceedings of 22nd National and 11th International ISHMT- ASME Heat and Mass Transfer Conference* (HMTC1300139). IIT Kharagpur, India: **ISHMT-ASME**

[2] Dubey, S. K., Agarwal, N., & Srinivasan, P. (2012). Three Dimensional Transient Heat Transfer Model for Steel Billet Heating in Reheat Furnace. *Proceeding of the ASME Summer Heat Transfer Conference. 2*, pp. 963-967. Rio Grande, Purto Rico, USA: **ASME**. doi:10.1115/HT201258151

[3] Dubey, S. K., & Srinivasan, P. (2011). Transient Heat Transfer Modeling and Simulation of Hot Billet Transport for Temperature Predictions and Energy Efficiency. *Proceedings of 21st National and 10th International ISHMT- ASME Heat and Mass Transfer Conference* (pp. 251-256.). IIT, Madras, India: **ISHMT-ASME**

National Conference:

[1] Dubey, S. K., & Srinivasan, P. (2012). Heat Transfer Simulation of Pusher Reheat Furnace. *National Conference on Modelling, Computational Fluid Dynamics & Operations Research.* BITS, Pilani, India

Brief Biography of the Candidate

Mr. Satish Kumar Dubey did his B.E. in Mechanical Engineering from Pt. Ravi Shankar Shukla University, Raipur (CG) and M.Tech. in Thermal Engineering from Maulana Azad National Institute of Technology (MANIT), Bhopal (MP). He is presently pursuing Ph.D. at Birla Institute of Technology & Science, Pilani (BITS, Pilani) and working as a Lecturer with Department of Mechanical Engineering, BITS-Pilani, Pilani Campus. He has fourteen years of teaching experience at under graduate and postgraduate levels. His areas of research interest are computational heat transfer, modeling and simulation of thermal systems.

Brief Biography of the Supervisor

Prof. P. Srinivasan is presently an Associate Professor, Mechanical Engineering Department, and Associate Dean, Practice School Division at Birla Institute of Technology & Science, Pilani (BITS Pilani) India. He has been working with BITS Pilani for past eight years in various capacities and has a total of twenty five years of experience in academics. He obtained his B. E., Degree from Regional Engineering College, Srinagar, and M. E. and Ph.D degrees from Regional Engineering College, Trichirapalli, India. His research interest include: heat transfer modelling and simulation, fracture mechanics, failure analysis and residual life assessment of thermal power plant. He has published several papers in various national and international journals, and conferences. He has extensively delivered invited lectures at many industries He was also instrumental in the successful conduct of several workshops and training programs for industry and academia. He is actively involved in teaching and consultancy of subjects related to thermal engineering, materials and fracture mechanics. He is a member of Indian Society for Heat and Mass Transfer (ISHMT) and Indian Welding Society (IWS).